

**MINISTRY OF EDUCATION AND SCIENCE OF THE
RUSSIAN FEDERATION
NATIONAL RESEARCH TOMSK STATE UNIVERSITY**

**Victor Cherepanov, Alexander Eliseev, Ekaterina Karlovets,
Alexander Lugovskoi, Yulia Morozova, Dmitriy Petrov, Leonid
Sinitsa, Oxana Zharkova**

Optical methods in biomedicine

Study Guide

**Tomsk
2016**

Content

Part 1. Introduction to emission-atomic absorption spectroscopy	5
Lecture 1. Introduction to atomic spectroscopy	5
Lecture 2. Basic elements of spectroscopic technique: Light sources and detectors, optical elements, basic principles of spectroscopic devices	14
Part 2. Application of vibrational-rotational molecular spectroscopy in medicine	19
Lecture 3. General concepts of molecular absorption spectroscopy	19
Lecture 4. High-resolution molecular spectroscopy	30
Lecture 5. Structures and spectra of water absorption	46
Lecture 6. Dynamic registration of water clusters In nanopores and bio-objects	54
Part 3. Methods of electronic spectroscopy for biomedicine	59
Lecture 7. General scheme of photo physical processes	59
Lecture 8. Spectral-luminescent prophesies of molecules and intermolecular interactions	64
Lecture 9. Solvation of molecules and its spectral manifestation	71
Part 4. Raman spectroscopy for analytical diagnostics	89
Lecture 10. Physical foundation of raman spectroscopy	89
Lecture 11. Raman instrumentation	100
Part 5. Practicum manual	110
Laboratory work 1. Qualitative elemental analysis of substance	110
Laboratory work 2. Studying the spectroscopy databases. Modelling ch4 gas- analyser in exhaled air	112
Laboratory work 3. Studying water absorption spectra in nanopores	114
Laboratory work 4. Determination of characteristics of the electronic bands of absorption and electronic states as exemplified for amino-acid residues contained in proteins (phenylalanine, tryptophan, tyrosine)	116
Laboratory work 5. Solvatofluorochromism of fluorescent probes in biophysics and medicine	117
Laboratory work 6. Application of uv and visible regions in the analysis of vitamins	118
Laboratory work 7. Fundamentals of the qualitative analysis by means of raman spectroscopy	119
Laboratory work 8. Fundamentals of the qualitative analysis by means of raman spectroscopy	121
References	123

PART 1. INTRODUCTION TO EMISSION-ATOMIC ABSORPTION SPECTROSCOPY

LECTURE 1. INTRODUCTION TO ATOMIC SPECTROSCOPY

Modern understanding of substance is the result of the work of scientists during more than 2.5 thousand years. The earliest statements about the existence of atoms belong to Democritus (~ 460 BC) who believed that they are indivisible particles. Spectroscopy plays a fundamental role in the development of the viewpoint about the structure of substance. Virtually, spectroscopy development can be divided into two periods: the first period (from I. Newton to N. Bohr: 1666 – 1931) is associated with the concepts of classical physics, and the second (from 1913 to the present day) – with quantum concepts. According to the quantum concepts, description of atomic systems, as a rule, is reduced to solution of Schrödinger's differential equations [1 – 3]:

- *time-independent*, for describing internal energy and electron structures,

$$H\Psi = E\Psi \quad (1.1)$$

- *time-dependent*, for describing dynamic processes,

$$i\hbar \frac{\partial \Psi}{\partial t} = H\Psi, \quad (1.2)$$

where $H = T + U$ is the energy operator (or the Hamiltonian) of the atom containing operators of kinetic (T) and potential (U) energies; E – energy of atomic states (levels); Ψ – wave function serving as a solution to the equations. We are not going to discuss a relativistic variant of quantum mechanics where the Dirac's equations are used [4, 5].

Thus, modern atomic spectroscopy is based on the principles of quantum mechanics. It belongs to one of the most studied fields in physics (laser physics, astrophysics, spectroscopic methods in plasma diagnostics, etc.). However, it cannot be said that the theory of atom is close to be completed. Theoretical modelling of any atom and its energy spectrum is very useful even the accuracy of an approximation used is insufficient. At least, it allows us to qualitatively determine number and types of energy levels, evaluate spectral region of absorption and radiation, and interpret experimental data [6].

1.1 Approximation of centrally symmetric field

The Schrödinger's *time-independent* equation is precisely solved only for a hydrogen-like atom H. For atoms with more than one electron, the Schrödinger's equation can be solved only in the context of an approximate model.

Nevertheless, according to the reasonable physical assumption that each electron in atom moves in some effective centrally symmetric field $U(r)$ caused by nucleus and other electrons (here r – distance of the electron from nucleus), a quite effective zero approximation was proposed (it is also called the self-consistent field approximation). It is taken as a starting point in the theory of atomic spectra and permits successful description of the main features of atoms. Deviations from the field centrality are determined by weak electron-electron interactions $\sim (v/c)^2$, such as, for example, spin-orbit interaction, non-central part of the electrostatic interaction, spin-spin interaction; but since these interactions are weak, they can be taken into account in the context of the perturbation theory as small corrections to zero approximation.

In the approximation of a centrally symmetric field solutions for any atom are rather general. In fact, in this approximation the Schrödinger's equation for one electron in the potential field $U(r)$ is

$$\left[\frac{p^2}{2m} + U(r) \right] \Psi = E\Psi \quad (1.3)$$

or, if consider the fact that in quantum mechanics the translational momentum is expressed as $p = -i\hbar\nabla$,

$$\left[-\frac{\hbar^2\nabla^2}{2m} + U(r) \right] \Psi = E\Psi . \quad (1.4)$$

Then, writing the Laplace operator $\Delta = \nabla^2$ in the spherical coordinate system transforms the equation (1.4) into:

$$\left[\frac{1}{r^2} \frac{\partial}{\partial r} \left(r^2 \frac{\partial}{\partial r} \right) - \frac{l^2}{\hbar^2 r^2} + \frac{2m}{\hbar^2} (E - U(r)) \right] \Psi = 0, \quad (1.5)$$

where $\vec{l} = \vec{r} \times \vec{p}$ – angular momentum operator of the electron. Taking into account the spin of electron, solution to the equation (1.5) should be found in the expression

$$\Psi_{nlm_l m_s} = R_{nl}(r) Y_{lm_l}(\theta, \varphi) \chi_{m_s}(\sigma), \quad (1.6)$$

where $R_{nl}(r)$ – radial function, $\chi_{m_s}(\sigma)$ – spin function, $Y_{lm_l}(\theta, \varphi)$ – spherical function serving as a solution to the equation based on its own functions and values of the angular momentum operator:

$$l^2 Y_{lm_l}(\theta, \varphi) = \hbar^2 l(l+1) Y_{lm_l}(\theta, \varphi),$$

$$l_z Y_{lm_l}(\theta, \varphi) = \hbar m_l Y_{lm_l}(\theta, \varphi). \quad (1.7)$$

Function $R_{nl}(r)$ is a solution to the radial equation which is the equation (1.4) with a substitution of the operator l^2 with $\hbar^2 l(l+1)$. Indeed, placing (1.5) in (1.4) and considering (1.7) results in a searched radial equation:

$$\left[\frac{1}{r^2} \frac{\partial}{\partial r} \left(r^2 \frac{\partial}{\partial r} \right) - \frac{l(l+1)}{r^2} + \frac{2m}{\hbar^2} (E_{nl} - U(r)) \right] R_{nl}(r) = 0. \quad (1.8)$$

Thus, the state of the electron is characterised by the following quantum numbers: $n = 1, 2, 3, \dots$ – principal quantum number, $l = 0, 1, \dots, n-1$ – orbital quantum number, $m_l = 0, \pm 1, \pm 2, \dots, \pm l$ – eigenvalue (it is often called the magnetic quantum number describing a spatial orientation of the angular orbital momentum of electron) of the operator l_z , $m_s = \pm 1/2$ – eigenvalue of the operator of spin projection s_z . According to (1.8), energy levels of atom E_{nl} do not depend on m_l and m_s in the approximation of the centrally symmetric field. Therefore, in the approximation, at given n and l , the energy level is $2(2l+1)$ -fold degenerate. A particular type of solutions $R_{nl}(r)$ and E_{nl} depends on the type of potential $U(r)$ that is different for each atom. As a rule, radial equation (1.8) is solved by numerical methods.

One-electron wave function of spatial r and spin σ variables of $\Psi_{nlm_l m_s}$ is also called the atomic spin-orbital (AO).

Usually, atom states described by wave function (1.6) are defined depending on the values l expressed by the Latin alphabet (Table 1.1):

Table 1.1

Values l	0	1	2	3	4	5	6	...
Letter symbol	<i>s</i>	<i>p</i>	<i>d</i>	<i>f</i>	<i>h</i>	<i>i</i>	<i>k</i>	continue in alphabet

The distribution of electrons in atom by states with various n and l is referred to as the electronic configuration of atom $(n_1 l_1)^{k_1} (n_2 l_2)^{k_2} (n_3 l_3)^{k_3} \dots (n_r l_r)^{k_r}$.

For neutral atoms in the ground state the sequence of occupancy for atomic states is as follows: $1s < 2s < 2p < 3s < 3p < 4s \sim 3d < 4p < 5s \sim 4d < 5p < 6s \sim 5d \sim 4f < 6p < 7s \dots$

For example: Li: $1s^2 2s$; Na: $1s^2 2s^2 2p^6 3s$.

Electrons with the same n and l are called equivalent and they form the electron shell (Table. 1.2):

Table 1.2.

l	Shell	Maximum number of electrons in the shell, $2(2l+1)$
0	s	2
1	p	6
2	d	10
3	f	14
...

Sometimes atom shells are formed by another way (it is usually used for X-ray spectra). In this case, the electronic shells differ by the principal quantum number n (Table. 1.3):

Table 1.3.

n	Shell	Configuration of electrons
1	K	$1s$
2	L	$2s2p$
3	M	$3s3p3d$
4	N	$4s4p4d4f$
...	continue in alphabet	...

1.2 Hydrogen-like atoms

Hydrogen-like atoms consist of a nucleus with Ze charge and one electron (Z – atomic numbers in Periodic Table). In this case, the problem is reduced to solving the Schrödinger's equation of a particle $\mu = \frac{mM}{m+M}$ (m – mass of electron, M – mass of nucleus) in the Coulomb field

$$U(r) = -\frac{Ze^2}{r} :$$

$$\left[\frac{1}{r^2} \frac{\partial}{\partial r} \left(r^2 \frac{\partial}{\partial r} \right) - \frac{l(l+1)}{r^2} + \frac{2\mu}{\hbar^2} \left(E_n + \frac{Ze^2}{r} \right) \right] R_{nl}(r) = 0. \quad (1.9)$$

Equation (1.9) is solved precisely. Moreover, energy levels are defined only by the principal quantum number n and are degenerate by l :

$$E_n = -\frac{1}{2} \frac{Z^2 \mu e^4}{\hbar^2 n^2} = -\frac{1}{2} \frac{Z^2 e^2}{a_0 n^2} \quad (1.10)$$

or in cm^{-1} (this unit of measure is often used in quantum physics)

$$E_n = -\frac{Z^2 R}{n^2}, \quad (1.11)$$

where $a_0 = \frac{\hbar^2}{\mu e^2} \cong 0.529 \cdot 10^{-8} \text{ cm}$ – Bohr's radius, $R = \frac{\mu e^4}{4\pi c \hbar^3} \cong 109678.76 \text{ cm}^{-1}$ – the Rydberg constant.

The typical behaviour for radial function $R_{nl}(r)$ is:

$$R_{nl}(r) \rightarrow \begin{cases} \exp\left(-\frac{Zr}{na_0}\right), & r \rightarrow \infty \\ \text{const} \times r^l, & r \rightarrow 0. \end{cases} \quad (1.12)$$

According to (1.11), $R_{nl}(r)$ has significant values in the region $r \approx \frac{na_0}{Z}$. In particular, for the H atom in atomic units ($a_0 = 1$) $r \approx 1$.

Equation (1.11) immediately generates empirically found serial formulas for frequencies (wavenumbers) of optical transitions:

$$\nu_{nm} = E_n - E_m = -Z^2 R \left(\frac{1}{n^2} - \frac{1}{m^2} \right). \quad (1.13)$$

Fine structure of hydrogen-like atoms

Taking into account some relativistic corrections a fine structure or splitting of atomic levels of hydrogen-like atoms into two levels is easy to explain: the spin-orbit interaction and dependence of mass of electron on its speed. In this case, in the first order of the perturbation theory the energy level with a given value of the orbital quantum number l splits into two sublevels which are identified by the values of the total angular momentum $\vec{j} = \vec{l} + \vec{s}$: $j = l + 1/2$ and $j = l - 1/2$. Furthermore, the correction to the unperturbed value of the energy level $E_n \equiv E_{nl}$ will be

$$\Delta E_{nlj} = \alpha^2 \left(\frac{3}{4n} - \frac{1}{j + 1/2} \right) \frac{Z^4}{n^3} R, \quad (1.14)$$

where $\alpha = \frac{e^2}{\hbar c} \cong \frac{1}{137}$. Thus, the relativistic contribution $\sim Z^4$, i.e. their role increases as the charge of atom (ion) grows. Such a qualitative dependence is also common for many-electron atoms.

1.3 Classification of spectra of multi-electron atoms

As we have seen, in the approximation of a centrally symmetric potential field the energy of atom is completely determined by the task of its electronic configuration, i.e. by the task of quantum numbers n_i and l_i of all electrons of the atom. However, due to the influence of electrons the spherical symmetry of atom will go down, which in reality leads to the splitting of nl -levels. The structure of splitting of these energy levels is determined by the hierarchy of powers of electronic interactions. Let us consider the main limit types of electron coupling in atoms.

LS or Russell Saunders coupling

The experiment demonstrates that for light atoms as well as for electrons of outer shells of atoms in the middle part of Periodic Table the spin-orbit interaction is small in comparison with the electrostatic interaction of electrons. Therefore, the electrostatic interaction can be interpreted as an interaction of orbital and spin momenta, respectively. Such an interaction, neglecting the spin-orbit

interaction, leads to the atomic energy levels expressed (or identified) by total orbital momentum $\vec{L} = \sum_i \vec{l}_i$ and total spin momentum $\vec{S} = \sum_i \vec{s}_i$, more precisely by quantum numbers L and S associated with these momenta. Calculating possible values of L and S is quite complicated (see, for example, [2]), and we will not go into details. Taking into account a weak spin-orbit interaction of momenta \vec{L} and \vec{S} , levels with given values L and S split again. Moreover, the splitting determined by the spin-orbit interaction is much smaller than the splitting determined only by the electrostatic interaction of electrons. The interaction of momenta \vec{L} and \vec{S} leads to the fact that split atomic energy levels will be expressed by the quantum numbers of total angular momentum $\vec{J} = \vec{L} + \vec{S}$: $J = |L - S|, |L - S + 1|, \dots, L + S$. The considered type of electronic interactions and electronic coupling is called *normal coupling* or *LS-coupling*, or *Russell Saunders coupling scheme*. Within the frame of the coupling the energy levels of atom are expressed as $^{2S+1}L_J$, and wave functions of the state - $|LSJM\rangle$ or often just $|JM\rangle$, where $M = 0, \pm 1, \pm 2, \dots, \pm J$. Normally, energy levels disregarding spin-orbit splitting, i.e. only with given L and S , are called *terms* and respectively denoted as ^{2S+1}L , where $2S+1$ defines the multiplicity of the state. The function relevant to the term is $|LSM_L M_S\rangle$, where $M_L = 0, \pm 1, \pm 2, \dots, \pm L$ and $M_S = 0, \pm 1, \pm 2, \dots, \pm S$. In practice, instead of a numerical value L corresponding letters are used similar to the orbital momentum l of the individual electron. The only difference is that letters are capitalised:

Values L	0	1	2	3	4	5	6	...
Letter symbol	S	P	D	F	H	I	K	continue in alphabet

It must be said that the classification of atomic states is based not only on quantum numbers but also on the parity of states. The parity of the atom state is determined depending on the change in sign of the electronic wave function $\Psi_{nlm_l m_s}$ at inversion with respect to the centre of a coordinate system placed into the centre of the nucleus. At inversion coordinate signs of all electrons turn into opposite. In this case, change in the sign of the function $\Psi_{nlm_l m_s}$ is entirely determined by the spherical function $Y_{lm_l}(\theta, \varphi)$ which under the influence of inversion changes in the following way:

$$\hat{i}Y_{lm_l}(\theta, \varphi) = Y_{lm_l}(\pi - \theta, \varphi + \pi) = (-1)^l Y_{lm_l}(\theta, \varphi). \quad (1.15)$$

As a result, for multi-electron atom of the given configuration of electrons the wave function of each electron will have the multiplier $(-1)^l$, and the parity of the atom state will be defined by the multiplier $P = (-1)^{\sum_j l_j}$ where the summation is carried out over all electrons of the electronic shell. Therefore, the state of the atom is even if $\sum_j l_j$ is even; otherwise, it is odd.

Taking into account parity and splitting of terms by J sublevels, in *LS-coupling* energy levels are expressed as:

$$^{2S+1}L_J^\alpha,$$

where $\alpha = o$ for odd states, for even states α is usually omitted. Left low index ν is called the seniority quantum number and is used to distinguish terms with similar L and S in the electron shell. It is possible to assign some physical sense to the seniority quantum number: index ν is numerically

equal to the smallest number of electrons in the shell where a term with given L and S firstly appears.

Empirical rules

1. *Hund's rules for atomic energy levels.*

F. Hund has found some very useful recipe for LS -coupling to identify the energy levels for any electronic configuration depending on the values of L , S and J . The Hund's rules imply a specific order of actions to determine a relative position of energy levels:

- Firstly, groups of levels with the same multiplicity $2S+1$ (or spin S) are selected. A relative position of these groups of levels is determined by the values of their spin (or multiplicity). The bigger the value of spin, the smaller the energy of groups of levels, i.e. a group of levels with maximum multiplicity will have the smallest value of energy.
- After that, a relative position of levels is determined by the value of quantum number L in each group of levels with equal multiplicity: the bigger L , the smaller energy level.
- Finally, each LS -term splits into J -sublevels by the rule:
 - if the atom shell is occupied more than a half, position of J -levels in the multiplet is normal, i.e. with growing J the energy of levels increases.
 - if the atom shell is occupied less than a half, position of J -levels in the multiplet is inverted, i.e. with growing J the energy of levels decreases.
 - if the atom shell is half-occupied, there is no splitting by J .

2. *Landé interval rule.*

Landé rule defines the value of the energy gap between levels J and $J-1$ for the term ^{2S+1}L :

$$E_J - E_{J-1} = A(LS) \cdot J, \tag{1.16}$$

where for normal multiplet the constant of the spin-orbit interaction is $A(LS) > 0$ and for inverted multiplets – $A(LS) < 0$.

Example: Let us consider sp -configuration of electrons ($l_1 = 0, l_2 = 1$) for LS -coupling. Since for non-equivalent electrons $L = |l_1 - l_2|, |l_1 - l_2 + 1|, \dots, l_1 + l_2$, consequently, $L = 1$. Similarly, $S = 0, 1$ since spin of each electron is $1/2$. As the result, position of energy levels is $^1P_1^o > ^3P_2 > ^3P_1 > ^3P_0$.

3. *Laporte rule.*

This selection rule was discovered by O. Laporte in 1924. The main principle of the rule is that electronic transitions between terms of different parity ($g \leftrightarrow u$) or $\Delta l = \pm 1$ are allowed in atoms. It should be noted that in the configuration the rule is based on the analysis of electric dipole absorption and emission spectra. In general case of multipole absorption (emission) there are weak transitions between terms of the same parity ($g \leftrightarrow g, u \leftrightarrow u$).

jj-coupling

The coupling corresponds to the case when the energy of the spin-orbit interaction is much higher than the energy of the electrostatic interaction of electrons. Such a situation is typical, for example, of heavy atoms (big Z), since the energy of the spin-orbit interaction $\sim Z^4$, and the energy of the electrostatic interaction $\sim Z$. The idea of orbital and spin momenta is senseless at strong spin-orbit interaction. We can speak only of total angular momentum of the electron $\vec{j} = \vec{l} + \vec{s}$. Total angular moment, thus, will consist of total momenta of individual electrons: $\vec{J} = \sum_i \vec{j}_i$. This is *jj*-coupling. The terms (energy levels) for this type of coupling are expressed as $(j_1 j_2)_J$, where, as usual, for equivalent electrons $J = |j_1 - j_2|, |j_1 - j_2 + 1|, \dots, j_1 + j_2$ and $j_i = |l_i - s_i|, |l_i - s_i + 1|, \dots, l_i + s_i$. As for equivalent electrons: when $n_1 = n_2$, $l_1 = l_2$ and $j_1 = j_2$, a number of possible values J decreases in accordance with the requirement of anti-symmetry of wave atomic functions with

respect to permutation of any pair of electrons. Unlike *LS-coupling*, there is no recipe of relative distribution of levels like the Hund's rule for *jj-coupling* scheme. However, it must be said that there is a rule of correspondence between levels J for *LS-coupling* and *jj-coupling* which allows us to find relative position of levels for *jj-coupling* as well.

In its pure form *jj-coupling* cannot be found in atoms, but for heavy atoms the structure of spectra is very close to the structure of the coupling. As a result, for heavier elements, the *jj-coupling* scheme often gives better agreement with the experiment.

Example: Let us consider *pd*-configuration of electrons ($l_1 = 1, l_2 = 2$) for *jj-coupling*. Since the electron shell in question is formed by non-equivalent electrons, $j_1 = \frac{1}{2}, \frac{3}{2}$ and $j_2 = \frac{3}{2}, \frac{5}{2}$.

Therefore, the terms are $\left(\frac{1}{2}, \frac{3}{2}\right)_{J=1,2}$, $\left(\frac{1}{2}, \frac{3}{2}\right)_{J=2,3}$, $\left(\frac{3}{2}, \frac{3}{2}\right)_{J=0,1,2,3}$, $\left(\frac{3}{2}, \frac{5}{2}\right)_{J=1,2,3,4}$. Note that the number of levels of J does not depend on the coupling type.

Along with considered types of coupling there are intermediate types which reflect a different order of coupling of angular momenta of electrons, which is determined by various interrelations of the energy of spin-orbit and electrostatic interactions for different groups of electrons in atom.

1.4 Atomic wave functions

According to the principle of identity of particles in a general case the wave function Ψ of a many-electron system consisting of n electrons must satisfy anti-symmetry in relation to the permutation of any pair of electrons. It occurs if we make a determinant from one of the one-electron functions $\Psi_{nlm_l m_s}(\xi_i)$ called the Slater determinant. Particularly, for the system consisting of two electrons situated in the field of positively charged nucleus the determinant is

$$\frac{1}{\sqrt{2}} \begin{vmatrix} \Psi_{n_1 l_1 m_{l_1} m_{s_1}}(\xi_1) & \Psi_{n_1 l_1 m_{l_1} m_{s_1}}(\xi_2) \\ \Psi_{n_2 l_2 m_{l_2} m_{s_2}}(\xi_1) & \Psi_{n_2 l_2 m_{l_2} m_{s_2}}(\xi_2) \end{vmatrix}.$$

The total function of atom, taking into account the electronic correlation of electrons, is written as a linear combination of Slater determinants that meet different electronic configurations Ψ_k :

$$\Psi = \sum_{k=0}^M A_k \Psi_k = \sum_{k=0}^M A_k \det \left\| \Psi_{n_i l_i m_{l_i} m_{s_i}}(\xi_j) \right\|_k, \quad (1.17)$$

where M – number of accounted electronic configurations of atom (Slater determinants). Electronic configurations Ψ_k are defined as various means of distribution of electrons in atomic spin-orbitals. Coefficients A_k can be calculated by the variational method. The electronic configuration Ψ_0 corresponds to the ground atomic state, other – to excited states of atom.

Energetic spectra of atoms or their energy levels are calculated by means of atomic functions Ψ defined by expression (1.17) as mean Hamiltonians H from (1.1):

$$E = \langle \Psi | H | \Psi \rangle / \langle \Psi | \Psi \rangle. \quad (1.18)$$

1.5 Multiplet structure of atomic terms

A multiplet structure of terms $^{2S+1}L^\alpha$ (splitting of terms into sublevels $J: ^{2S+1}L_J^\alpha$) is a result of relativistic interactions. In most cases it is expressed by the spin-orbital interaction

$$W = \sum_i \xi(r_i) \vec{l}_i \vec{s}_i, \quad (1.19)$$

where $\xi(r_i) = \frac{\hbar^2}{2m^2 c^2 r_i} \frac{\partial U}{\partial r_i}$.

Perturbation (1.19) leads to the following corrections ΔE_{LSJ} to the energy of term $^{2S+1}L^\alpha$:

$$\Delta E_{LSJ} = A(LS) \frac{1}{2} \{J(J+1) - L(L+1) - S(S+1)\}. \quad (1.20)$$

As we see, the energy levels are determined not only by quantum numbers L and S of a term, but also by the quantum number of total angular momentum J that identifies sublevels of the term. Constants of the spin-orbital interaction $A(LS)$ are calculated by numerical methods of quantum mechanics. It is obvious that (1.20) automatically leads to the empirical Landé interval rule.

1.6 Electronic transitions. Selection rules

It is known from the radiation theory that intensity $I_{JM \rightarrow JM'}$ of radiation (absorption) of atom on the transition $JM \rightarrow JM'$ is proportional to probability W of this transition which, in its turn, is proportional to the square of a matrix element of multipole electric $\langle JM | Q_{k\sigma}^e | JM' \rangle$ or magnetic $\langle JM | Q_{k\sigma}^m | JM' \rangle$ momenta for electric and magnetic multipole radiation (absorption), respectively:

$$I_{JM \rightarrow JM'}^{e,m} \sim W_{JM \rightarrow JM'}^{e,m} \sim \left| \langle JM | Q_{k\sigma}^{e,m} | JM' \rangle \right|^2. \quad (1.21)$$

k – order of tensor of multipole momentum, and $\sigma = 0, \pm 1, \pm 2, \dots, \pm k$ – index of tensor component. Most intensive are spectral lines of the radiation (absorption) determined by the electrical dipole momentum ($k=1, \sigma=0, \pm 1$). This is electric dipole radiation.

Selection rules. Selection rules answer the question: is there a transition (or relevant spectral line) or not? (1.21) demonstrates that selection rules are directly defined by matrix elements of relevant multipolar momenta. There are exact and approximate selection rules.

Exact selection rules permit (or prohibit) atom transitions between states which are expressed by quantum numbers such as parity and quantum number of total angular momentum J . It must be noted that the degree of accuracy of these quantum numbers is a relative concept since the presence of small interactions (for example, relativistic) distorts parity. When taking into account hyperfine interactions (spin of nucleus) and placing atom in an external electric (Stark effect) or magnetic (Zeeman effect) field, the number of J also becomes approximate. Nevertheless, listed distortions are extremely small; therefore, the quantum numbers are more precise.

According to (1.21), selection rules by parity are determined by provided matrix elements (or integrals) different from zero, since multipolar momenta contain spherical functions $Y_{km_k}(\theta, \varphi)$:

$$\langle Y_l(\theta, \varphi) || Y_k(\theta, \varphi) || Y_{l'}(\theta, \varphi) \rangle \text{ and } \langle Y_l(\theta, \varphi) || Y_{k-1}(\theta, \varphi) || Y_{l'}(\theta, \varphi) \rangle \quad (1.22)$$

for electric (E_k) and magnetic (M_k) multipole radiation, respectively. As the result, we have selection rules by parity and associated with them selection rules by quantum orbital number l

participating in the electron transition. Thus, for electric multipole transitions $\Delta l = l' - l = 0, \pm 1, \pm 2, \dots \pm k$ with additional condition $l + l' + k$ – even number; for magnetic multipole transitions $-\Delta l = l' - l = 0, \pm 1, \pm 2, \dots \pm (k - 1)$ and $l + l' + k$ – odd number. For even Δl transitions are allowed between states of the same parity ($g \leftrightarrow g, u \leftrightarrow u$), and for odd Δl transitions between states of different parity ($g \leftrightarrow u$).

The selection rule by J has the following form for both types of radiation:

$$\begin{aligned}\Delta J = J' - J = 0, \pm 1, \pm 2, \dots \pm k; \quad J' + J \geq k; \\ \Delta M = M' - M = 0, \pm 1, \pm 2, \dots \pm k.\end{aligned}\tag{1.23}$$

Note, that the presence of selection rules by additional quantum numbers can restrict the selection rules in (1.23). For example, in case of LS -coupling, for magnetic dipole radiation ($k = 1$) $\Delta L = \Delta S = 0$, therefore, transitions only between components of the fine structure of the multiplet are allowed. Then, $\Delta J = 0$ corresponds to the absence of transition, i.e. only transitions with $\Delta J = \pm 1$ are allowed.

For more intensive spectral lines of the electric dipole radiation from the selection rules by parity and (1.23) we formulate the following selection rules agreed with the empirical *Laporte rule*: $\Delta J = 0, \pm 1, J' + J \geq 1$ and $\Delta l = \pm 1$.

Approximate selection rules. Let us consider the approximate selection rules on the example of LS -coupling where L and S are approximate quantum numbers. In this case, selection rules are determined by the reduced matrix element $\langle LSJ || Q_k || L'S'J' \rangle$. As a result, approximate selection rules are

$$\begin{aligned}J &= |L - S|, |L - S + 1|, \dots, L + S; \\ J' &= |L' - S'|, |L' - S' + 1|, \dots, L' + S'; \\ \Delta S &= 0; \\ \Delta L &= L' - L = 0, \pm 1, \pm 2, \dots \pm \tilde{k}; \quad L' + L \geq \tilde{k},\end{aligned}\tag{1.24}$$

where $\tilde{k} = k$ or $(k - 1)$ for E_k and M_k radiation, respectively.

LECTURE 2. BASIC ELEMENTS OF SPECTROSCOPIC TECHNIQUE: LIGHT SOURCES AND DETECTORS, OPTICAL ELEMENTS, BASIC PRINCIPLES OF SPECTROSCOPIC DEVICES

Optical radiation occupies the range of spectrum within the wavelengths from 1 nm to 1 mm. The main task of spectroscopy is studying the spectral content of radiation and its changes caused by different processes. The task is solved with the help of spectral devices. This part is devoted to classical slit spectral devices, where spatial splitting of light beam into monochromatic components occurs by means of spectral lens or diffraction grating. In general, geometrical optics will be used, the main concepts of which are light ray and beam.

2.1 Optical scheme of a spectral device

Typical optical scheme of a spectral device is illustrated in Figure 2.1.

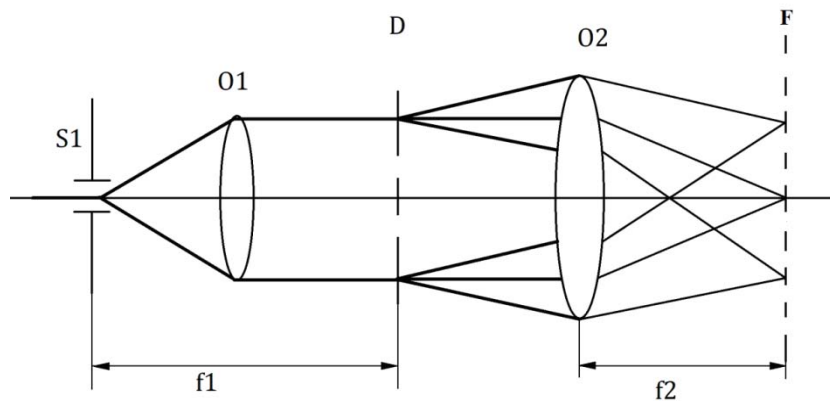


Figure. 2.1. Optical scheme of a spectral device:

- S_1 – input slit;
- O_1 – collimator lens;
- f_1, f_2 – focal length;
- D – dispersing element;
- O_2 – focusing object (camera lens);
- F – focal plane.

According to the scheme in Figure 2.1 at the exit of collimator lens O_1 there is a parallel beam of rays, since the point source S_1 is located at the focal length from O_1 . Dispersing element D deviates rays by various angles that depend on the wavelength of light λ , i.e. it turns the beam into divergent parallel beams of monochromatic rays which focus on the focal plane and form monochromatic images of the input slit, i.e. spectrum. In general, optical scheme of a spectral device also includes a radiation source with lighting system and detector system.

Spectral devices are divided into multichannel (for example, spectrographs) and single channel (monochromators). Spectrograph has a cassette with a photographic film (photographic plate) or photo-cassette with photodiode or linear CCD array in the focal plane. Monochromator contains an output slit in the focal plane, behind it there is a photodetector (photoelement, photomultiplier, photodiode). The last case requires scanning the spectrum in order to measure the entire spectrum, i.e. sequentially display different parts of the spectrum on the output slit using a stepping motor, and record them sequentially by means of computer, at monitor. If several output slits are installed in the focal plane, the device is called polychromator. Such devices are often used for emission spectral analysis in industry.

For a visible region of the spectrum (380-700 nm) spectroscopes and steelometers are also used for analysis of steels and other alloys by means of visual comparison of luminosities of

spectral lines. To date, such devices are equipped with additional photovoltaic consoles for more objective results of analysis. Monochromators serve as a basis for manufacturing spectrometers and spectrophotometers. These devices have built-in light sources (incandescent lamps, deuterium lamps), continuous spectrum, lighting system of slit and detector system. The devices are mainly designed for measuring wavelengths or frequencies of spectral lines or molecular bands in absorption spectra at absorption analysis.

2.2 Basic spectral characteristics

1. Dispersion

Normal dispersion D_l is expressed by:

$$D_l = \frac{dl}{d\lambda} [\text{mm}/\text{\AA}].$$

In practice, the concept of inverse dispersion of a device is frequently used:

$$D'_l = \frac{d\lambda}{dl} [\text{\AA}/\text{mm}].$$

D'_l – the range of wavelengths (in \AA or nm) per 1 mm of the focal plane.

Spectral devices are divided into devices with low inverse dispersion (hundreds $\text{\AA}/\text{mm}$); medium inverse dispersion (tens $\text{\AA}/\text{mm}$), and high inverse dispersion (some $\text{\AA}/\text{mm}$).

2. Resolution

Resolution is determined by:

$$R = \frac{\lambda}{d\lambda},$$

where $d\lambda$ – minimal distance between two monochromatic lines of equal intensity (Rayleigh criterion).

Spectral devices are divided into those with low resolution ($R = 1 - 10$), medium resolution ($R = 10 - 100$) and high resolution ($R = 100 - 1000$).

3. Aperture ratio of spectral devices

Aperture ratio (L) is a coefficient connecting illuminance or light flow at the exit of a device in the focal plane with the luminance of an input slit of the device.

Aperture ratio (L) is proportional to relative gap D/f (D – diameter of collimator; f – focal length of collimator) and transparency of optics T .

Devices can be of high, medium and low aperture. Devices with high lens speed are used to register weak light sources (luminescence, Raman spectroscopy, etc.).

2.3 Receivers of optical radiation

Radiation power of the majority of sources (except for lasers) in the narrow spectral range is not high. Therefore, one of the main requirements for radiation receivers is high sensitivity. Linearity of a receiver is also important, i.e. output signal must be proportional to the amount of the energy supplied to it. Methods for recording a signal and, consequently, receivers of radiation, can be divided into three groups:

1. Visual registrations

In a visible region of the spectrum (380-700 nm) eye is a very sensitive receiver. The maximum sensitivity of the eye – $\lambda = 555 \text{ nm}$.

2. Photographic registration

Photographic emulsion has high sensitivity and resolution. The main disadvantages of the photographic emulsion are non-linear dependence of the photographic effect on illuminance E and

influence of some factors on blackening of line S (wavelength of light, development time, temperature of the developer, chemical composition of the developer, etc.).

3. **Photoelectric registration**

Photoelectronic receivers are divided into thermal and photoelectric by the mechanism of converting the light signal into the electrical one.

Thermal receivers respond to the amount of energy spent on heating of the receiving element. Moreover, thermal energy is converted into electrical by means of thermoelectric effect, changes in electric resistance and so on. This group includes bolometers, thermal elements, Golay detectors (opto-acoustic).

Photoelectronic receivers converting light into photons are divided into several groups:

- 1) Receivers with external photoeffect – photoelements, photoelectronic multiplier tubes (PMT), electronic and optical converters.
- 2) Receivers with internal photoeffect (semi-conducting) – photoresistors, photodiodes.
- 3) Charge Coupled Devices – linear CCDs, CCD image sensors.

Photoelectronic receivers respond to the amount of photons incident on the detector. Quantum yield of these receivers is the relation of the number of emerged electrons to the number of absorbed photons. Quantum yield of the receivers is quite high. The disadvantage of the receivers is their selectivity at registration of signal and presence of noises. It also has advantages such as large dynamic range, linearity at registration of signal, high sensitivity and fast operation.

2.4 Light sources for spectral analysis

There are three types of sources in spectral analysis:

1. Sources of thermal radiation.
2. Gas-discharge sources.
3. Lasers (an abbreviation of *Light Amplification of Stimulated Emission of Radiation*).

Let us consider each type in more detail.

Sources of thermal radiation (heated bodies) have a solid spectrum. They are characterised by temperature T , luminosity R_l , luminance B , volume density of radiation $\bar{u}(\omega)$ (the energy of radiation per unit volume associated with modes whose frequencies lie in the range ω to $\omega + d\omega$).

Sources are divided into those close to the black body (etalons) and those which are grey bodies (incandescent lamps, globars, Nernst pin, halogen lamps). They are characterised by the distribution of energy in the spectrum close to the Plank distribution and two temperatures: brightness T_i and colour T_c .

Gas-discharge sources. In gas-discharge sources of radiation, plasma in volume limited by walls or just in atmosphere serves as a radiator. As a rule, plasma is in the state of local thermodynamic equilibrium and is described by a single temperature T .

Spectroscopy employs the following gas-discharge sources of radiation:

- 1) Hollow-cathode lamps.
- 2) Spectral lamps of low pressure with arc discharge with vapours of different metals (mercury, cadmium, zinc, thallium, rubidium, sodium, etc.). Such lamps are used to generate line spectra as etalons.
- 3) Hydrogen lamps of low pressure with continuous spectrum of radiation are used in spectrophotometers as sources in the UV region of spectrum.
- 4) Mercury lamps of high pressure and ultra-high pressure serve as bright sources of the line spectrum.

5) Gas lamps of ultra-high pressure – argon, krypton, xenon. These lamps have a large spectrum with individual spectral lines. Xenon lamps of ultra-high pressure have a spectrum close to the solar one.

6) Pulse lamps with duration of flashes 10^{-2} - 10^{-6} seconds with very high brightness. Powerful lamps have a spectrum close to the spectrum of the black body. Lamps are used for laser pumping.

7) Sources of excitation of the spectrum for emission analysis:

a) The arc of DC and AC. Plasma in the state of local thermodynamic equilibrium. Temperature of the arc $T = 5000$ - 6000 K. The arc burns between conductive electrodes (metal or carbon) where a sample is placed in. Electrodes in arc are heated, material of electrodes melts, boils, evaporates. Vapours come to the gap between electrodes and shine brightly. The energy of the arc charge is enough to excite most of the elements except for gases and elements that are difficult to excite (selenium, phosphorus, carbon, iodine). Ion lines are not excited in the arc.

b) Alternating-current (AC) spark. AC spark differs from the arc because discharge exists a shorter time, therefore, power of the spark is higher and temperature reaches 7000 - 9000 K. Over the half-cycle of the current there are 1 or 2 breakdowns and release of the electrode material into the interelectrode gap. Electrodes are almost cold. Ion lines, spectra of gases and elements that are difficult to excite become excited in the spark. The spectrum of the spark is much more complicated but sensitivity in detecting elements is lower than in the arc.

c) Source with inductively coupled plasma (plasma torch). There are three working argon streams in plasma torch: central stream carries a sprayed analyte, intermediate stream lifts plasma above the burner, and external stream cools walls of the burner and centres the torch. Temperature of plasma is ~ 10000 K.

Lasers.

The principle of operation of laser sources consists in three basic conditions:

1. Inverse of population in a medium (active medium), which is a condition for strengthening the photon flux density as it propagates through the active medium.

2. Positive feedback which permits switching the amplifier into the generation mode. Positive feedback is reached by placing the active medium into resonator consisting of two mirrors. One of the mirrors is partially transparent to emit radiation.

3. Threshold generation, i.e. it is necessary that amplification of radiation exceeds losses for a single pass between the mirrors of resonator.

Characteristic features of the laser radiation are:

- high intensity;
- directivity of a laser beam;
- high monochromaticity of radiation;
- coherent radiation determined by equal characteristics of stimulated and incident photons.

Thus, a typical laser consists of three basic elements enabling operating conditions: active medium, pumping source providing the inverse of populations, resonator providing a positive feedback (Fig. 2.2). The type of active medium: gas, plasma, fluid, solid body (crystals, semi-conductors, etc.) – is determined by the type of laser sources.

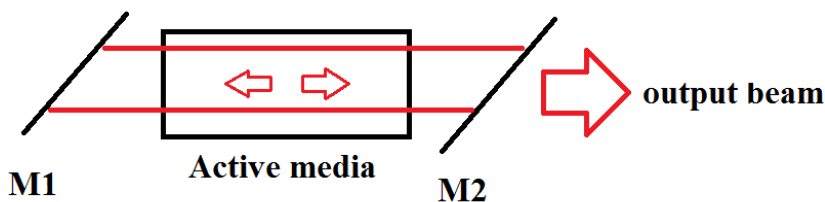


Figure 2.2 Typical scheme of a laser

When biological objects are exposed to the optical radiation there are two possible mechanisms or combinations:

- photochemical reactions;
- absorbed energy converts into the thermal one or mechanical processes.

In the visible and closest IR region of spectrum (Fig. 2.3) absorption of radiation is relatively small (absorption coefficient is $\sim 10\text{-}50\text{ cm}^{-1}$). Light scattering (scattering coefficient is \sim some cm^{-1}) plays the main role. Therefore, in this spectral region a deep penetration of radiation into biological tissues may occur. On the contrary, radiation of CO₂ laser ($\lambda = 10.6\mu\text{m}$) is mainly absorbed in the surface layer, that is the reason why this type of laser is an effective surgery tool.

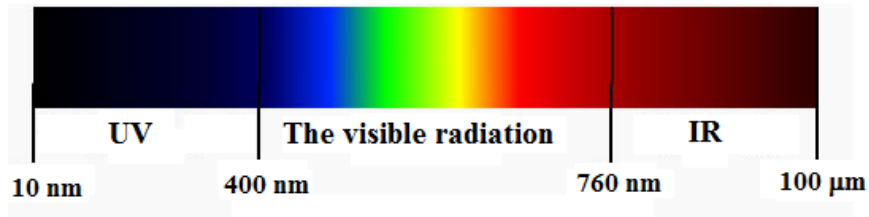


Figure 2.3 Spectrum of optical radiation

Lasers are widely used

- in photodynamic effect of radiation on biological objects, especially, on cancer cells;
- destruction of biological tissues without burning (ablation) which permits precise layer-by-layer removal of a biotissue with almost no heat release in the rest of volume.
- in biophysics of cell motility;
- in laser fragmentation of kidney stones.

PART 2. APPLICATION OF VIBRATIONAL-ROTATIONAL MOLECULAR SPECTROSCOPY IN MEDICINE

LECTURE 3. GENERAL CONCEPTS OF MOLECULAR ABSORPTION SPECTROSCOPY

Experimental spectra of molecules contain tens and hundreds of thousands of spectral lines united into ro-vibrational bands located from the far IR to UV region. Characteristics of molecular spectral lines along with the requirements for spectral apparatus used for studying them are described in this lecture [see also, [7 –10)].

3.1 Structure of molecular spectra

The vibration-rotation spectra of molecules are described by the Schrödinger equation. It is impossible to get a precise analytical solution to the Schrödinger equation $H \Psi = E_N \Psi$ and to determine stationary states of molecules with a large number of neutrons, that is why approximate methods of solution are employed. Thus, total molecular wave function Ψ can be written in frame of the Born–Oppenheimer approximation:

$$\Psi = \Psi_e \Psi_{\text{nuc}}, \quad (3.1)$$

where Ψ_e – electronic and Ψ_{nuc} – nuclear wave functions. In such a case, the “speed” of electrons moving in the molecule is many times higher than the “speed” of the shift of nuclei; electrons adiabatically, without changes in energy, follow the position of nuclei. In the next approximation, wave function Ψ_{nuc} can be also represented as a sum of two wave functions:

$$\Psi_{\text{nuc}} = \Psi_{\text{vib}} \Psi_{\text{rot}}, \quad (3.2)$$

where Ψ_{vib} – vibrational, Ψ_{rot} – rotational wave functions .

Therefore, total wave function of the molecule can be described as

$$\Psi = \Psi_e \Psi_{\text{vib}} \Psi_{\text{rot}}. \quad (3.3)$$

Such a division of the wave function allows us to solve the Schrödinger equation individually for the electronic, vibrational and rotational movement. In the approximation (3.3), the total energy of the molecule E is made up of the electron excitation energy E_e , vibrational energy E_{vib} and the energy of rotation of the molecule as a whole E_{rot} :

$$E = E_e + E_{\text{vib}} + E_{\text{rot}}. \quad (3.4)$$

The energies, included into (3.4), are considerably different in value. Theoretical and experimental evaluation demonstrates that

$$E_e > E_{\text{vib}} > E_{\text{rot}}. \quad (3.5)$$

Furthermore, at the approximation the movements with E_e , E_{vib} , E_{rot} can be considered as independent from each other. Under closer consideration of the energy states of molecules it is necessary to take into account possible development of electronic-vibrational, electronic-rotational and vibrational-rotational interactions.

Taking into account electronic-vibrational, electronic-rotational and vibrational-rotational interactions the Schrödinger equation is as follows:

$$(N_e + N_{\text{vib}} + N_{\text{rot}} + N_{e-\text{vib}} + N_{e-\text{rot}} + N_{\text{vib}-\text{rot}}) \Psi_n = E \Psi_n, \quad (3.6)$$

and energy in this case is

$$E = E_e + E_{\text{vib}} + E_{\text{rot}} + E_{e-\text{vib}} + E_{e-\text{rot}} + E_{\text{vib}-\text{rot}} \quad (3.7)$$

Figure 3.1 demonstrates a simplified scheme of the energy levels of the CH₂ molecule. A system of vibrational levels V corresponds to each electronic state; a sum of closely located rotational states J – to each vibrational level. Rotational levels of all molecules are located so closely that vibrational levels in Figure 3.1 might be represented as solid bands.

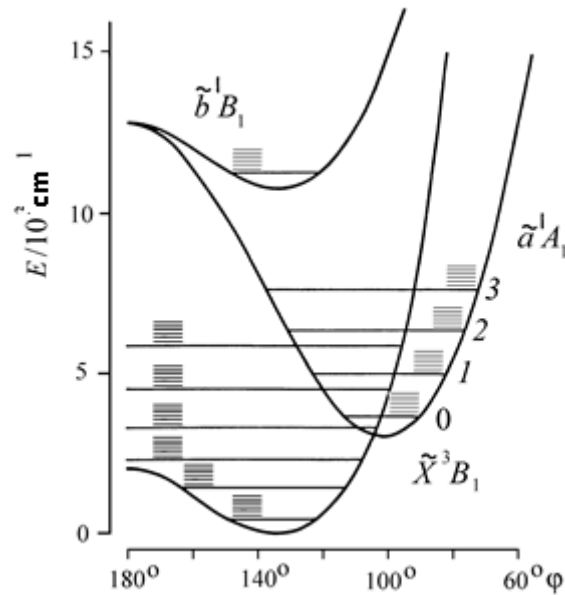


Figure 3.1. Vibrational and rotational structures of the electronic states of CH₂

Quantum mechanics allows us to study the following expressions for the levels of vibrational E_{vib} and rotational E_{rot} energies of a diatomic molecule:

$$E_{\text{vib}} = hc \left[\omega_e \left(V + \frac{1}{2} \right) - \omega_e x_e \left(V + \frac{1}{2} \right)^2 + \omega_e y_e \left(V + \frac{1}{2} \right)^3 - \dots \right], \quad (3.8)$$

$$E_{\text{rot}} = hc [B_e J(J + 1)], \quad (3.9)$$

where ω_e – frequency of vibration; B_e – rotational constant (cm^{-1}); $\omega_e x_e$, $\omega_e y_e$, –anharmonicity parameters (cm^{-1}); V and J – vibrational and rotational quantum numbers taking values of 0, 1, 2, 3.

The equation for the electronic energy of diatomic molecules is quite complicated and cannot be expressed only through quantum numbers. Therefore, the position of electronic levels is not regular.

All the preceded considerations concern an individual molecule. In practice, it is impossible to isolate a molecule and get its spectrum, since it is always engaged into the flows of relatively neighbouring molecules. As a result, there is the exchange of energy between molecules, which determines their distribution over all possible energy states.

At equilibrium conditions, the energy *distribution of molecules* is subordinate to the *Boltzmann law*

$$N_i = \frac{N}{\sum_i q_i \exp(-E_i / kT)} q_i \exp(-E_i / kT). \quad (3.10)$$

Thus, a number of molecules situated in the given energy state (population of the state) N_i depends on its energy E_i , temperature T and degree of degeneracy of the state q_i .

3.2 Thermal distribution of the population of quantum states

Quantum theory implies that only discrete values are possible for the vibrational energy. According to the *Boltzmann law for thermal equilibrium*, the population of the vibrational state N_V with the energy E_V is determined by the expression

$$N_V = (1/Q_V) N_0 q_V \exp(-E_V/kT). \quad (3.11)$$

Here, q_V – statistical weight (a share of molecules in the vibrational state V); Q_V – vibrational partial function; k – Boltzmann's constant.

Figure 3.2 illustrates thermal distribution of the populations of vibrational states of the molecule J_2 . The ordinates, corresponding to values of the vibrational energy with $V = 1, 2, 3 \dots$, are represented in Figure 3.2 by dashed lines. A number of molecules located in high vibrational states rapidly decreases. The decrease is extremely pronounced in such molecules as H_2 , N_2 , O_2 , and others that have large vibrational quanta. For further understanding of quantitative interrelations, Table 3.1 demonstrates the ratio of the number of molecules in the first vibrational state with $V = 1$ to the number of molecules in the vibrational states with $V = 0$ for some gases at the temperature of 300 and 1000 K. It is obvious that this ratio is extremely small for such gases as HCl , CO and N_2 even at 1000 K. Almost all transitions observed during the absorption in the IR region have $V'' = 0$ in their initial state. Only significant part of heavy molecules, such as J_2 , is in their first vibrational state at room temperature.

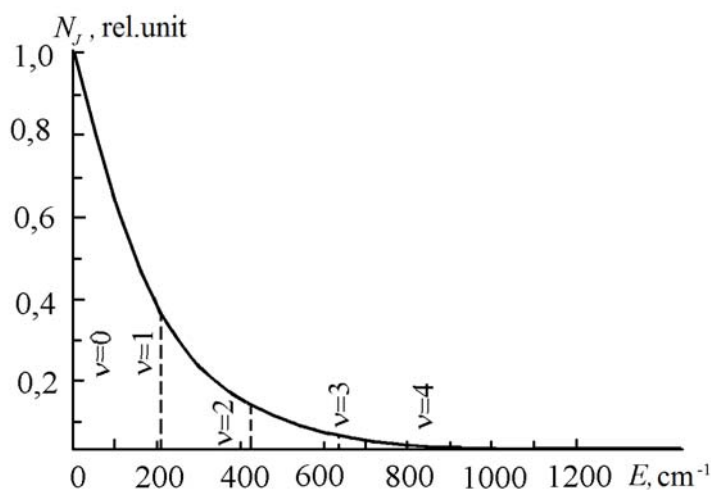


Figure 3.2. Boltzmann function and distribution of the vibrational states of J_2 at $T = 300$ K

Table 3.1

Ratio of the number of molecules in the first vibrational state to the number of molecules in the ground vibrational state at 300 and 1000 K

Gas	$E_V(\text{cm}^{-1})$	$N(V=1)/N(V=0)$	
		300 K	1000 K
H_2	4160.2	$2.16 \cdot 10^{-9}$	$2.51 \cdot 10^{-3}$
HCl	2885.9	$9.77 \cdot 10^{-7}$	$1.57 \cdot 10^{-2}$
N_2	2330.7	$1.40 \cdot 10^{-5}$	$3.50 \cdot 10^{-2}$
CO	2144.0	$3.43 \cdot 10^{-5}$	$4.58 \cdot 10^{-2}$
O_2	1556.4	$5.74 \cdot 10^{-4}$	$1.07 \cdot 10^{-1}$
S_2	721.6	$3.14 \cdot 10^{-2}$	$3.54 \cdot 10^{-1}$
Cl_2	556.9	$6.92 \cdot 10^{-2}$	$4.49 \cdot 10^{-1}$
J_2	213.1	$3.60 \cdot 10^{-1}$	$7.36 \cdot 10^{-1}$

The values of $e^{-(E(V)/kT)}$ give relative numbers of molecules in different vibrational states related to the number of molecules in the lowest vibrational state. If we want to relate these numbers to the total number of molecules, we must think that the latter is proportional to $1 + e^{-(E(1)/kT)} + e^{-(E(2)/kT)} + \dots$ (the so-called partial function).

Thermal distribution for rotational states cannot be expressed simply by means of the Boltzmann's factor $e^{-(E/kT)}$; we must take into account the fact that according to the quantum theory each state of the molecular system with the total angular momentum J consists of $2J + 1$ levels which coincide with each other in the absence of an external field, i.e. state is degenerate. Moreover, degree of degeneracy (q_J) for the linear molecules is $(2J + 1)$. Therefore, the frequency of occurrence of the J state (its statistical weight) will be $(2J + 1)$ higher than in case of the state with $J = 0$.

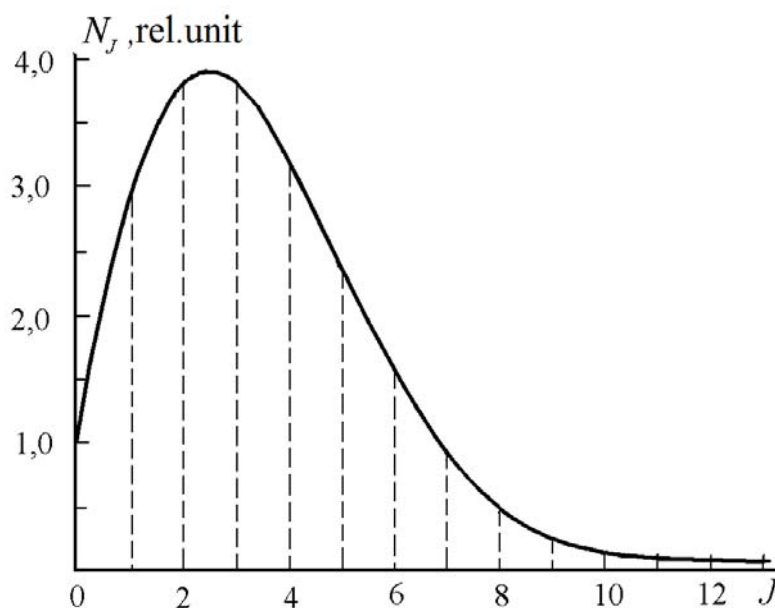


Figure 3.3. Thermal distribution of rotational states for HCl in the vibrational state at $T=300$ K

Thus, the population of the J -rotational level of the molecule with the energy E_J is expressed as the dependence

$$N_{VJ} = q_{VJ} N_V = (1/Q_R) N_V q_J \exp(-E_J/kT), \quad (3.12)$$

where q_{VJ} – parts of molecules of the vibrational state V located at the level J ; N_V – population of the vibrational state; q_J – statistical weight of the rotational level;

$$Q_R = \sum_J q_J \exp(-E_J/kT)$$

rotational partial function; k – Boltzmann's constant.

Figure 3.3 illustrates the function N_{VJ} for HCl at $T = 300$ K. Since the value of $2J + 1$ increases linearly with increasing J , the number of molecules in different rotational states does not initially decrease with the increasing rotational quantum number, but grows and passes through a maximum. The maximum lies at

$$J_{\max} = 0.5895 \sqrt{\frac{T}{B}} - \frac{1}{2}, \quad (3.13)$$

i.e. at the value of J which increases with the decreasing rotational constant B and with the increasing T .

Molecules can change their energy states not only due to collisions with each other, but also with absorption and emission of light quanta. The transition from one state with higher energy E' into a state with lower energy E'' is accompanied by energy release in form of a light quantum with the wavenumber ν , and the inverse transition $E'' \rightarrow E'$ is accompanied by its absorption:

$$\nu = \frac{E' - E''}{hc}. \quad (3.14)$$

In case of a large number of molecules distributed over all possible states, according to the Boltzmann's law, we observe emission (or absorption) of quanta of different energies which consequently form emission spectra and absorption spectra. Except for these spectra there are also Raman scattering spectra which are observed, if energy of the light quantum interacting with the molecule is less than the energy of the excitation of the state, i.e. when the electronic shell of the molecule is just "excited" but not completely transformed as in transition of the molecule from non-excited into excited state.

Thus, according to the principle of formation, molecular spectra can be divided into spectra of emission, absorption and Raman scattering. Vibrational-rotational absorption spectra consist of lines of absorption united into separate bands. They occupy the spectral range from the IR region to the UV one. Moreover, the intensity of bands dramatically decreases when moving into higher frequencies.

3.3 Bouger's Law and absorption coefficient

Quantitative measurements in absorption spectroscopy are based on the Bouger's law. *Absorption coefficient* $K(\nu)$ is a coefficient of proportionality in the Bouger's law in its differential form:

$$dI(\nu) = -K(\nu) \cdot I(\nu)dL, \quad (3.15)$$

where $dI(\nu)$ – attenuation of the intensity radiation $I(\nu)$ coming through the layer of a medium with the thickness dL .

In case of homogeneous medium, the Beer–Lambert–Bouger law is (integral form):

$$I(\nu) = I_0(\nu) \exp[-K(\nu)L], \quad (3.16)$$

where $I_0(\nu)$ and $I(\nu)$ – radiation intensity before and after passing the layer with the thickness L .

Optical thickness of a medium τ is the value of the exponent (3.16)

$$\tau = K(\nu)L. \quad (3.17)$$

Spectral transmittance $T(\nu)$ is the relation $I(\nu)/I_0(\nu)$:

$$T(\nu) = \frac{I(\nu)}{I_0(\nu)} = e^{-K(\nu)L}, \quad (3.18)$$

Spectral absorption $A(\nu)$:

$$A(\nu) = \frac{I_0 - I(\nu)}{I_0(\nu)} = 1 - e^{-K(\nu)L} \quad (3.19)$$

Integrated absorption coefficient K is the integral of $K(\nu)$ at the frequency range $\nu_1 \dots \nu_2$:

$$K = \int_{\nu_1}^{\nu_2} K(\nu) d\nu. \quad (3.20)$$

Integrated transmittance T is the integral of $T(\nu)$ at the frequency range $\nu_1 \dots \nu_2$:

$$T = \int_{\nu_1}^{\nu_2} T(\nu) d\nu. \quad (3.21)$$

Integrated absorption A is the integral of $A(\nu)$ at the frequency range $\nu_1 \dots \nu_2$:

$$A = \int_{\nu_1}^{\nu_2} A(\nu) d\nu. \quad (3.22)$$

For vibrational-rotational lines, absorption coefficient is expressed as a sum of the intensity of lines (strength of lines) S_{ij} multiplied by $F(\nu - \nu_0)$, normalised to the value 1.

In this case, the Bouguer law is:

$$I(\nu) = I_0(\nu) \exp[-S_{ij} F(\nu - \nu_0) NL], \quad (3.23)$$

where N – density of molecules; S_{ij} – intensity of the vibrational-rotational line for transition $i \rightarrow j$; $F(\nu - \nu_0)$ – spectral line shape with the centre ν_0 . There are three types of profiles used as spectral line profiles: Doppler profile is normally used at lower pressures $P < 1$ torr; Lorentzian profile describing the spectral line profile at high pressures $P \sim 1$ atm, or Voigt profile which is a convolution of Doppler and Lorentzian profiles.

Line intensity is determined by the expression

$$S_{ij} = \frac{8\pi^3}{3hc} q \frac{N}{Q} n_{ij} e^{-E''/kT} (1 - e^{-hc\nu_{ij}/kT}) | \langle i | m | j \rangle |^2, \quad (3.24)$$

where N – number of molecules per unit volume; q – degree of degeneracy of the low level; Q – partition function which is a sum of vibrational Q_V and rotational Q_R partial functions of the molecule; n_{ij} – centre of the vibrational-rotational line; $e^{-E''/kT}$ – Boltzmann's factor describing the population of the low level with the energy E'' ; the term in brackets determines the difference in the populations of upper and lower states of transition; $| \langle i | m | j \rangle |^2$ – square of the matrix element of the transition dipole moment.

3.4 Spectral line profile

Spectral lines of the experimental spectrum are not infinitely narrow and they have a certain width and shape. There are several reasons for the broadening of spectral lines.

Natural line width.

Excited molecule can lose its excitation energy in form of spontaneous radiation. Loss of the radiation energy results in optical radiation damping which is expressed by the damping constant γ . Because of gradually decreasing amplitude, the emitted radiation is not monochromatic. It has a form of some distribution by the frequency which is connected with the frequency range by the Fourier transformation. Normalised profile of the line of a damping oscillator is:

$$F_{\text{nat}}(\nu - \nu_0) = \frac{\gamma}{(\nu - \nu_0)^2 + \gamma^2} \quad (3.25)$$

The average lifetime τ_i of the molecular level E_i which experiences the exponential decay due to spontaneous emission is associated with the Einstein coefficient A_i by $\tau_i = 1/A_i$. When replacing classical damping constant γ with the probability of spontaneous transition A_i , formula 3.25 results in a proper expression of the frequency distribution of spontaneous emission and line width:

$$\delta\nu_{\text{nat}} = A_i = \frac{1}{\tau_i} \quad (3.26)$$

Expression (3.26) can be also produced by the Heisenberg's uncertainty principle $\Delta E \Delta t \geq h/2\pi$. According to this, at the average lifetime τ_i of the excited level i its energy can be defined only with uncertainty

$$\Delta E \approx h/\tau_i \quad (3.27)$$

Natural line width is determined by the total uncertainty of both transition levels

$$\Delta E = \Delta E_1 + \Delta E_2, \quad (3.28)$$

$$\delta\nu_{\text{nat}} = \frac{1}{\tau_1} + \frac{1}{\tau_2} \quad (3.29)$$

Natural line width is usually extremely small. For instance, $\delta\nu_{\text{nat}}$ of molecular transition lines lying in the IR region is $\delta\nu_{\text{nat}} = 100$ Hz at the typical lifetime $\tau = 10^{-3}$ s. Natural width D_1 of the sodium line with the wavelength of 589.1 nm, having the lifetime $\tau = 10$ ns, equals $\delta\nu_{\text{nat}} = 10$ MHz.

There are two principal effects of the broadening of spectral lines which are registered in the experiment, - Doppler's effect and broadening caused by collisions.

Doppler profile is caused by the Doppler's effect reflecting the distribution of molecules by rates. It plays a primary role in the broadening of molecules at small pressure $P < 1$ torr and is expressed as

$$F_D(\nu - \nu_0) = \frac{1}{\gamma_D} \sqrt{\frac{\ln 2}{\pi}} \exp \left[-\ln 2 \left(\frac{\nu - \nu_0}{\gamma_D} \right)^2 \right]. \quad (3.30)$$

For the half-width of Doppler profile at the half-height it can be written as

$$\gamma_D = \left(2 \ln 2 \frac{kT}{mc^2} \right)^{1/2} \nu_0, \quad (3.31)$$

where ν_0 – frequency of the line centre; m – mass of molecule; c – speed of light; T – temperature; k – Boltzmann's constant;

$$\gamma_D = 3.58 \cdot 10^{-7} \nu_0 (T/m)^{1/2}. \quad (3.32)$$

For instance, the Doppler's half-width for the main isotopomer H_2^{16}O at room temperature is $1.46 \cdot 10^{-3} \text{ cm}^{-1}$; $7.31 \cdot 10^{-3} \text{ cm}^{-1}$; $1.46 \cdot 10^{-2} \text{ cm}^{-1}$ and $2.19 \cdot 10^{-2} \text{ cm}^{-1}$ at the frequencies 1000 cm^{-1} , 5000 cm^{-1} , 10000 cm^{-1} and 15000 cm^{-1} , respectively.

Lorentzian profile is expressed by the formula

$$F_L(\nu - \nu_0) = \frac{1}{\pi} \frac{\gamma_L}{(\nu - \nu_0 - \delta_L)^2 + \gamma_L^2}, \quad (3.33)$$

where γ_L – half-width of the Lorentzian profile at the half-height; δ – shift of the centre of line. This profile describes the influence of collisions and determines the experimental profile at the pressure $P > 300\text{--}400$ torr.

For the mixture of gas, the expression is

$$\gamma_L = \sum_i \gamma_i^0 P_i \quad \text{and} \quad \delta_L = \sum_i \delta_i^0 P_i, \quad (3.34)$$

where P_i – the i -gas partial pressure; γ_i^0 – the broadening coefficient of the absorbing gas [$\text{cm}^{-1}/\text{atm}$], and δ_i^0 – the shift coefficient [$\text{cm}^{-1}/\text{atm}$].

Doppler and Lorentzian line profiles are illustrated in Figure 3.4. If Doppler profile decreases fast when moving from the centre of line, Lorentzian profile is characterised by large values even when moving away from the centre by several half-width ($0.2 K_0$ at 2γ ; $0,1 K_0$ at 3γ ; $0,02 K_0$ at 7γ from the centre).

Voigt profile is a convolution of Doppler and Lorentzian profiles and describes well the experimental profile at the intermediate area of pressures:

$$F_F(\nu - \nu_0) = \frac{1}{\gamma_D} \sqrt{\frac{\ln 2}{\pi}} \frac{y}{\pi} \int_{-\infty}^{\infty} \frac{e^{-t^2}}{y^2 + (x-t)^2} dt, \quad (3.35)$$

where $x = \sqrt{\ln 2} \frac{\nu - \nu_0}{\gamma_D}$; $y = \sqrt{\ln 2} \frac{\gamma_L}{\gamma_D}$.

Voigt profile is usually used for describing the experiment in the pressure area of 0.01–1 atm. New developed laser spectrometers register spectral line profile almost without any broadening by the instrumental function. This allowed us to question the adequacy of descriptions of the line profiles received by Voigt profile. As a result, systematic deviation of the experimental contour from Voigt profile was revealed. The deviation makes up several percent. These deviations can be eliminated, if modified spectral line profiles are used including the reduction of the Doppler broadening by means of collisions with a velocity change.

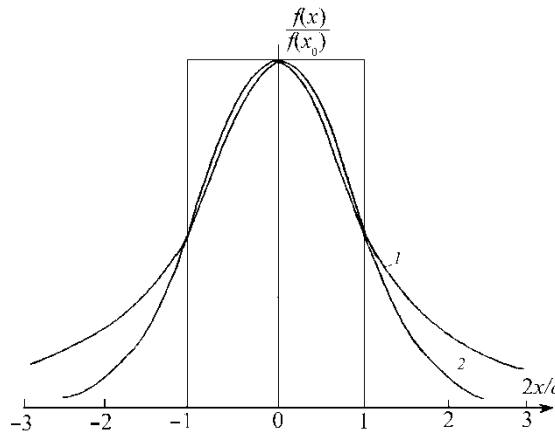


Figure 3.4. Doppler (2) and Lorentzian (1) spectral line profiles

3.5 Characteristics of spectrometers

General characteristics of spectrometers:

1. Spectral range $\Delta\nu$ – frequency region registered by spectrometer [cm^{-1}].
2. Spectral resolution $\delta\nu$ – capability of registering equipment to resolve the nearest spectral lines, [cm^{-1}].
3. Threshold sensitivity K_{th} – minimally detectable absorption coefficient [cm^{-1}].
4. Signal-to-noise ratio S/N.
5. Fast operation $\Delta\nu/\Delta t$ – recording rate of a spectrum, [cm^{-1}/s].
6. Instrumental function.

Threshold sensitivity

When registering the minimal absorption coefficient of a spectrometer, when the absorption coefficient is small, its sum multiplied by the length of absorbing layer $K_{th}L \ll 1$, we decompose the exponent in the Bouger's law (3.16) and limit ourselves by the first term of decomposition:

$$I = I_0 (1 - K_{th}L), \quad (3.36)$$

the result is

$$K_{th} = \frac{1}{L} \left(\frac{I_0 - I}{I_0} \right) = \frac{1}{L} \frac{\Delta I}{I_0}. \quad (3.37)$$

Thus, threshold sensitivity of spectrometer K_{th} at cell measurements is connected with the length of absorbing layer L and the capability of recording system to measure small changes in the emission intensity $\Delta I/I_0$.

If in the IR spectrum it is enough to use a path length about several centimeters, required path length increases up to tens of kilometers when moving into the visible range.

Instrumental function

If a spectral device is exposed by monochromatic radiation, it does not generate infinitely narrow lines. The spectral device registering monochromatic radiation records a profile of final width. Each element of the profile corresponds to the signal

$$dF = F f_{ins}(\nu) d\nu, \quad (3.38)$$

where F is the integrated signal corresponding to the registered radiation.

Profile $f_{ins}(\nu)$ is called the instrumental profile of device, and the function describing it is called the instrumental function of device which satisfies the requirements of normalisation

$$\int_0^{\infty} f_{ins}(\nu) d\nu = 1. \quad (3.39)$$

Sources of the broadening and distortion of the spectral line can be:

- 1) diffraction phenomena in device;
- 2) final width of the input slit image;
- 3) size of photodetector and source, etc.

When one of the reasons produces the profile described by the function $f_1(x)$ and other reason – profile $f_2(x)$, the resultant profile is received in the same way. One of the profiles, for example $f_1(x)$, needs decomposing into small elements with coordinates x' and width dx' (Fig. 3.5). Each of the elements being broadened by the second reason produces the profile described by the function f_2 , but moved by the value x' along the axis x . Furthermore, intensity at the maximum of the profile is proportional to $f_1(x')dx$ under the incoherent light. Thus, value of the element at the point x of the total profile is

$$dF(x) = f_1(x') f_2(x - x') dx'. \quad (3.40)$$

The total profile is produced by means of the integration of the equation by all the elements x' :

$$F(x) = \int_{-\infty}^{\infty} f_1(x') f_2(x - x') dx' = f_1(x) * f_2(x). \quad (3.41)$$

The integral in the right part of the equation (3.41) is called the convolution of two functions f_1 and f_2 . An important feature of the convolution of two functions is

$$F(x) = \int_{x_1}^{x_2} f_1(x')f_2(x-x')dx' = \int_{x_1}^{x_2} f_2(x')f_2(x-x')dx'. \quad (3.42)$$

Thus, if the observed broadening of the spectral line is caused by two reasons, the resultant profile is a convolution of two functions, each of which describes the profile determined by one of the reasons of the broadening.

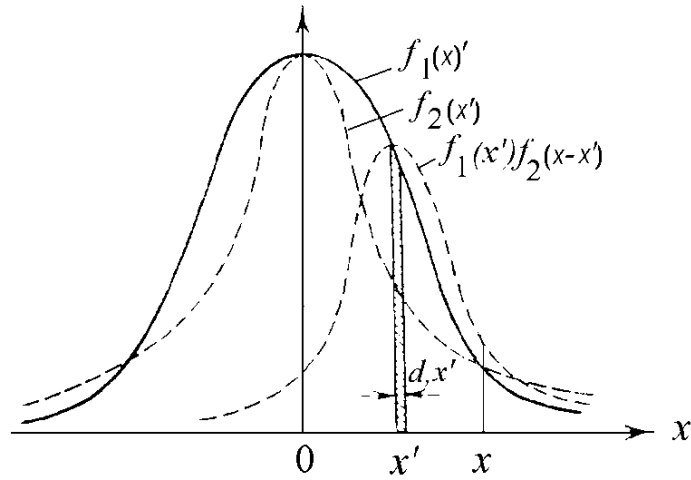


Figure 3.5. The convolution of two functions

If the instrumental profile is a convolution of individual profiles forming it, in case of a non-monochromatic line, its actually observed profile is also the convolution of the profile of the spectral line itself and total instrumental profile disregarding the effects of the instrumental broadening that produce the latter.

Expressing the instrumental profile, profile of the line and total profile respectively through $f_{\text{ins}}(x)$, $F(x)$, $U(x)$ results in

$$U(x) = \int_{-\infty}^{\infty} F(x')f_{\text{ins}}(x-x')dx. \quad (3.43)$$

In case when the half-width is small in comparison with the half-width of the instrumental profile, width and shape of the convolution of two profiles almost complies with the instrumental one.

Thus, we are entitled to consider the emission as monochromatic, if the half-width of the corresponding spectral distribution (spectral line) is small in comparison with the half-width of the instrumental profile of device. On the contrary, the instrumental profile width must be small in comparison with the recorded line width to directly produce the profile of the line.

When the widths of the line and instrumental profile are comparable in magnitude, the resultant profile and its width can be found by calculating the integral (3.43). The results of calculations for most common types of profiles are presented in Figure 3.6.

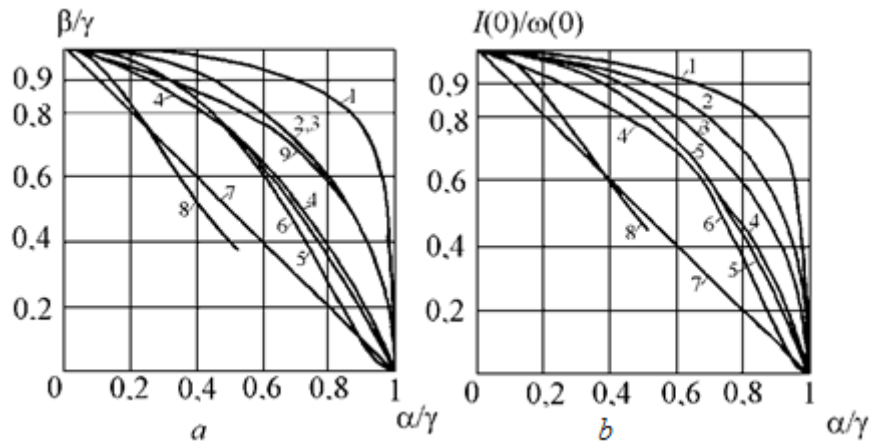


Figure 3.6. Dependence β/γ and $I(0)/\omega(0)$ on α/γ :

1 – rectangular instrumental function α and diffractive original spectral line profile β ; 2 – slit-like and dispersion functions; 3 – Gaussian and Gaussian; 4 – diffraction and dispersion; 5 – Gaussian and dispersion; 6 – triangle and dispersion; 7 – dispersion and dispersion; 8 – exponential and dispersion; 9 – Gaussian and triangle

Using the figure we can find a width of the resultant profile (γ) by the given line width (β) and instrumental profile (α). By means of the same curves we can also solve the reverse problem, i.e. to find original line width by measured width and width of the instrumental profile (the form of original distribution must be known). Figure 3.6b illustrates the dependence of ratio of the registered absorption at the centre of line $I(0)$ to the original absorption of the line $\omega(0)$ on the value α/γ .

LECTURE 4. HIGH-RESOLUTION MOLECULAR SPECTROSCOPY

4.1 Grating spectrometers

4.1.1 Principle of operation of a grating spectrometer

Grating spectrometers are characterised by a large spectral range and due to their simple construction they are widely used in spectroscopy of intermediate and low resolution [7, 8].

The principle of diffraction grating can be easily understood by considering the interference of individual plane waves experienced diffraction on the grooves of the grating (Fig. 4.1 and 4.2). As the result of the interferences of beams the maximums will be observed when the path difference of beams coming from adjacent slits $\Delta_2 - \Delta_1$ is equal to a whole number of waves.

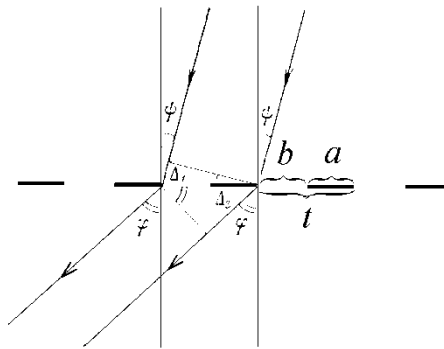


Figure 4.1. Diffraction by a transparent grating

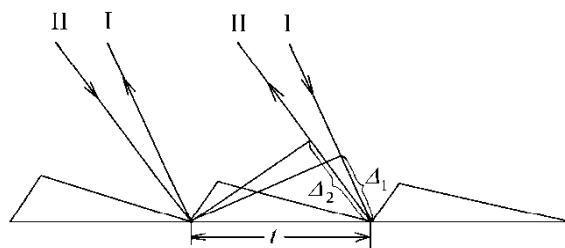


Figure 4.2. Diffraction by a reflecting diffraction grating

When producing a diffraction image from the diffraction grating we must take into account:

a) diffraction on one element of the grating which is expressed by the equations:

$$F_1(U) = \left(\frac{\sin U}{U} \right)^2, \quad (4.1)$$

$$U = \frac{\pi b (\sin \varphi + \sin \psi)}{\lambda}, \quad (4.2)$$

where ψ – angle of the light incidence on the grating; φ – diffracted angle; b – size of reflecting element of the grating; λ – radiation wavelength;

b) diffraction on N grooves of the grating which is expressed by the equations:

$$F_2(V) = \left(\frac{\sin NV}{\sin V} \right)^2; \quad (4.3)$$

$$V = \frac{\pi t(\sin \varphi + \sin \psi)}{\lambda}, \quad (4.4)$$

t – period of a groove of the grating.

Expression (4.1) demonstrates that the angular distribution of diffraction over one element has its maximum at $U = 0$ and a series of zero values at $\sin U = 0$, $U \neq 0$ (Fig. 4.3, *a*). Taking into account (4.2), the maximum occurs at the equal absolute values of the angles of incidence ψ and diffraction φ , i.e. when there is a mirror reflection of the beam, and zero values of function $F_1(U)$ are located at

$$\sin \psi + \sin \varphi = \frac{\lambda}{b}, \quad 2 \frac{\lambda}{b}, \quad 3 \frac{\lambda}{b} \dots \quad (4.5)$$

For diffraction on N grooves of the grating, the function $F_2(V)$ turns into zero if

$$Nt(\sin \varphi + \sin \psi) = n\lambda. \quad (4.6)$$

When $V = q\pi$, where $q = 0, 1, 2, \dots$, denominator in (4.3) also turns into zero. Revealing the uncertainty proves that in this case function $F_2(V)$ has its maximum values. Condition for the principal maxima:

$$NV = k\pi. \quad (4.7)$$

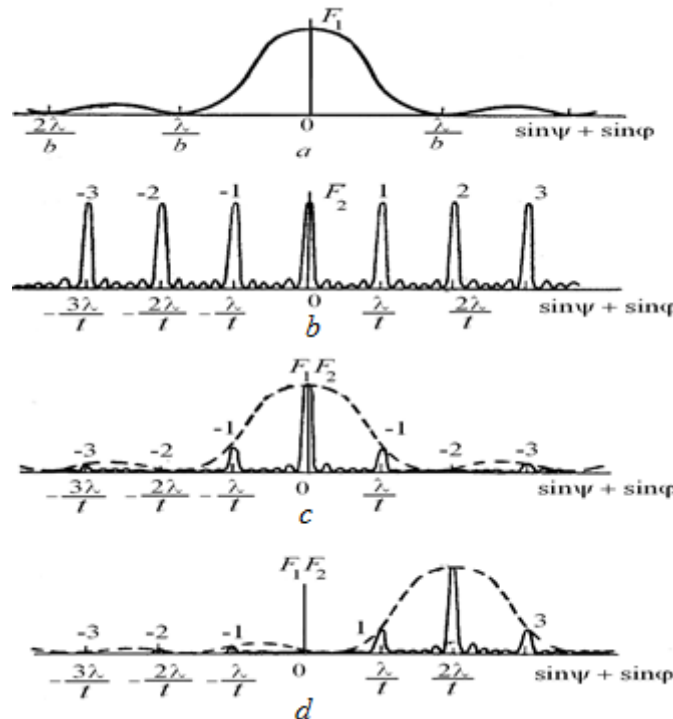


Figure 4.3. Angular distribution of energy in the diffraction image at diffraction: *a* – on the groove of the width b (function F_1); *b* – on the structure consisting of N equidistant grooves with a period t (function F_2); *c* – on the grating (sum of functions F_1 and F_2); *d* – on the grating with a profile groove (the blaze angle of the grating corresponds to the second order of diffraction for the considered wavelength)

Condition for the principal maxima provides *the main equation for the diffraction grating*

$$t(\sin \varphi + \sin \psi) = k\lambda, \quad (4.8)$$

k – order of diffraction.

For autocollimating case, when $\varphi = \psi$,

$$2t\sin\varphi = k\lambda. \quad (4.9)$$

The total image for the wavelength λ taking into account both diffraction on one element of the grating and N grooves is demonstrated in Figure 4.3c. The diffraction grating produces a series of spectra the order of which is defined by the value q . At the centre of the image there is a zero maximum corresponding to the radiation that is not decomposed in spectrum. If the grating is profiled, the maximum of the diffraction image moves into the region of higher orders by the angle called the “blaze angle”.

Spectra of different orders.

The grating produces numerous spectra corresponding to different values of k . If $k = 0$, the spectrum is of zero order with $\sin\varphi = \sin\psi$ regardless of the wavelength. The upper value of the diffraction order k is limited by the condition $|\sin\varphi + \sin\psi| \leq 2$. From 4.4 we have $k\lambda \leq 2t$, therefore, maximum value of k is

$$k_{\max} \leq 2t/\lambda. \quad (4.10)$$

Condition $t > \lambda/2$ must be satisfied in order to the grating produces at least the spectrum of the first order. Thus, for $\lambda = 5000 \text{ \AA}$ the grating constant must be more than 2500 \AA , i.e. the grating must have less than 4000 grooves/mm. Modern gratings have from 24 to 2400 grooves /mm, i.e. are close to the stated limit. For the region of 10000 \AA , the grating with 2400 lines /mm is not suitable, since it is impossible to observe even the spectrum of the first order. Therefore, for the longer wavelength region it is necessary to use the gratings with 300 grooves/mm or less.

Re-overlapping of orders.

The principal equation of the grating (4.8) demonstrates that the same angles of diffraction will be observed for a total sum of wavelengths λ_i meeting the relation

$$t(\sin \varphi + \sin \psi) = \lambda_i k_i. \quad (4.11)$$

Here k_i – all numbers of a natural row of k possible for the grating.

Thus, if for the most observed wavelength λ the spectrum of the first order is located at the angle φ , the radiation with the wavelength $\lambda/2$ in the spectrum of the second order and $\lambda/3$ in the spectrum of the third order will be observed at the same angle.

When using low orders of spectra it is quite easy to separate the overlapped radiations. Suppose that we observe the region near 7000 \AA in the spectrum of the first order. The radiation with the wavelength of 3500 \AA from the second order will overlap it. This radiation is easily cut off by a glass filter. The same filter does not transmit the radiation with $\lambda = 2300 \text{ \AA}$ from the third order and higher short-wave radiation observed at the same angle in the spectra of higher orders.

The region that is free of overlapping becomes smaller, if the grating for observing the spectra of higher orders is used (it has some advantages: first of all, it alleviates the requirement for mechanical components since transformation of the spectrum occurs within a narrow operational interval of the diffraction angles).

Moreover, it is mandatory to take a number of measures to separate the spectra of adjacent orders. Let us to find the region free of overlapping, i.e. distance in wavelengths between the two spectra of adjacent orders diffracted at one and the same angle φ . Since the incidence angles and diffraction angles for adjacent overlapping orders are similar, the equation (4.11) results in

$$k \lambda = (k + 1) (\lambda - \Delta\lambda), \quad (4.12)$$

therefore,

$$\Delta\lambda = \frac{\lambda}{k + 1}. \quad (4.13)$$

Angular dispersion of the diffraction grating is expressed by

$$D_{\varphi} = \frac{d\varphi}{d\lambda} = \frac{k}{t \cos \varphi}, \quad (4.14)$$

it dramatically increases when φ approaches 90° .

Linear dispersion

$$D_{\ell} = \frac{dl}{d\lambda} = D_{\varphi} \frac{f_2}{\sin \varepsilon}, \quad (4.15)$$

where f_2 – focal length of the lens; ε – angle between linear photodiode array and incident light.

Resolving power of the diffraction grating

$$R = \frac{\lambda}{\delta\lambda} = kN, \quad (4.16)$$

where N – total number of grooves.

Normal width of a slit. The magnification factor of the grating spectrometer is normally equal to 1, since the focal lengths of the eyepiece and lens are the same, consequently, at a large width of the input slit of spectrometer S_1 its image in the focal plane S_2 is equal to S_1 . When the width of the input slit becomes smaller, its image also follows S_1 until diffraction starts emerging on the aperture D of the beam then remaining unchangeable, while the width of the input slit is getting smaller.

Normal width of a slit – the input slit of device, when its image on the photographic plate is equal to the distance between the first minima at diffraction on the aperture D of the beam that is incident on the grating, is:

$$S_{\text{norm}} = \frac{f_1 \lambda}{D}, \quad (4.17)$$

where f_1 – focal length of the eyepiece of spectrograph; λ – wavelength; D – aperture.

Usually, the width of the input slit of a grating spectrometer is set as equal to the normal width of the slit, since further decrease in the width will not lead to the decrease of its image at the focal plane of spectrograph and only will cause a decreasing luminance.

Defects of grating.

Errors in operation of the ruling engine, when the grating is produced, lead to emerging false spectral lines (“spirits”), satellites of lines.

If an error period is several grooves, “spirits” are significantly far from natural lines and can be easily recognised as false lines, especially when working with the laser radiation.

The position of “spirits”:

$$\lambda_g = \lambda(1 \pm k' / km), \quad (4.18)$$

where λ – wavelength of the spectral line; k – spectral order; k' – order of spirit; m – number of grooves corresponding to the period of defect.

4.2 Configurations of grating spectrometers

Configurations of spectrometers with gratings.

Spectral devices with plane diffraction gratings usually have mirror lenses. For devices with the greater linear dispersion the Ebert configuration is used (Fig. 4.4, *b*). Different parts of the same concave mirror serve as collimator and chamber lenses in the configuration. In such devices, the entire spectrum does not fit on a single photodiode array; therefore, turning the grating provides the registration of the spectrum. Short-focal-length high-transmission devices employ the Czerny-Turner configuration (Fig. 4.4, *a*) with a separate collimator and chamber mirrors. Dispersion and resolving power of a grating device may be doubled by using double reflection of the beam from the diffraction grating.

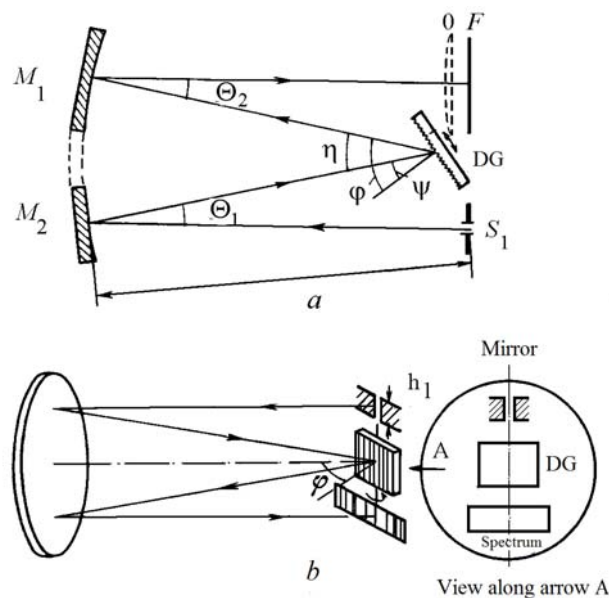


Figure 4.4. Horizontal Czerny-Turner configuration (*a*) and vertical Ebert configuration (*b*):
DG – diffraction grating; S_1 – input slit; F – focal plane

Recently, registering apparatus have rapidly developed – multichannel photodetectors (CCD-chamber) provide new possibilities of creating diffraction polychromators permitting simultaneous registration of over 2000 spectral elements.

4.3 Fourier transform spectroscopy

The idea of a spectroscopic method based on a double-beam interferometer with further Fourier transform has long been known. In 1891, Michelson demonstrated that light intensity measured at the exit of a double-beam interferometer with a variable path difference represents a cosine Fourier transform of the incident radiation. Since the Fourier transform is a reversible operation, in order to recover the studied spectrum it is enough to perform the cosine Fourier transform of interferogram of the radiation which describes a change in the intensity of the radiation passing through the interferometer as a function of the path difference between the interfering beams. Nevertheless, a real progress in the development of a Fourier spectroscopy became possible only thanks to modern computers permitting the Fourier transform of interferograms with a million or more points [1, 2].

4.3.1 Principle of operation of a Fourier transform spectrometer

If the Michelson interferometer (Fig. 4.5 a) is illuminated by the monochromatic radiation at the frequency ν_0 , the electric field on the plane of a beam-splitter will be:

$$E_1 = E_0 \cos \omega t, \quad (4.19)$$

where $\omega = 2\pi c\nu$.

A beam-splitter splits the incident light into two beams of equal intensity. Then, two waves reflect from the mirror (fixed and movable), and when the waves interfere, on the compensating plane there is a time delay t_0 of one wave in relation to another.

The resultant electric field is

$$E_2 = \frac{E_0}{2} [\cos \omega t + \cos \omega(t + t_0)], \quad (4.20)$$

where

$$\omega t_0 = 2\pi \nu_0 \delta \quad (4.21)$$

– phase shift of the second beam; δ – path difference.

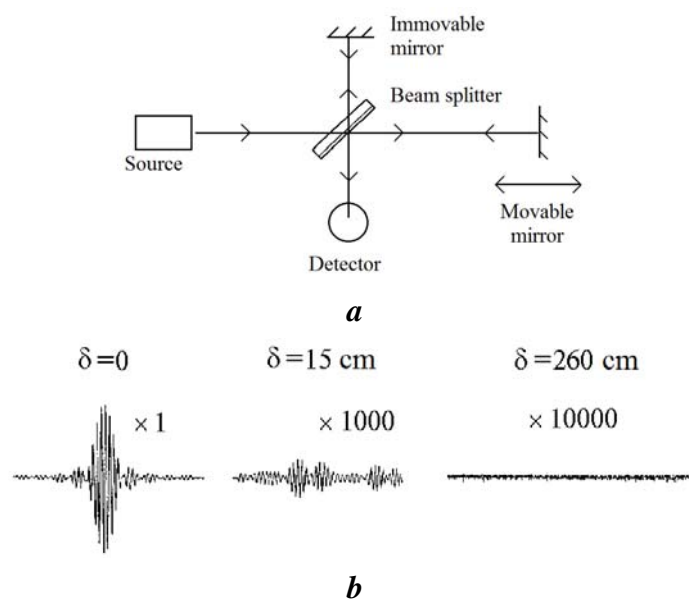


Figure 4.5. Michelson interferometer: a – configuration; b – part of the interferogram at various path differences

A detector placed at the exit of the interferometer will register signal $I(\nu_0, \delta)$ that is proportional to the square of the amplitude of the electric wave:

$$I(\nu_0, \delta) = \frac{1}{2} I_0 [1 + \cos(2\pi\nu_0\delta)]. \quad (4.22)$$

It consists of constant and variable parts; the final part represents the very interferogram. Therefore, if the interferometer is illuminated by the monochromatic radiation, at the exit of the detector there is a sine electric signal with constant amplitude proportional to the brightness of the incident radiation. If the interferometer is irradiated by several monochromatic waves, each of them will similarly propagate in the interferometer and the resultant signal will represent the superposition of the individual signal of each wave. Analysis of the signal permits detecting the frequency of each incident signal ν_0 .

In case of the spectrum $B(\nu)$ lying in the range between ν_1 and ν_2 and limited by either radiation spectrum or filter, sensitivity of detector, the interferogram is

$$I(\delta) = \int_{\nu_1}^{\nu_2} B(\nu) \cos(2\pi\nu\delta) d\nu, \quad (4.23)$$

which is a sum of intensities $dI(\nu_1\delta) = B(\nu) \times \cos(2\pi\nu\delta)$ for each spectral element in the spectrum.

As Figure 4.5, *b* illustrates, the amplitude of the signal of the interferogram rapidly decreases with path difference, consequently, a registering system must provide linearity of a signal varying from 1 to 10^7 and more times.

If $B(\nu)$ – radiation spectrum of a point source, the interferogram is expressed by

$$I(\delta) = \int_0^{\infty} B(\nu) \cos(2\pi\nu\delta) d\nu = \int_{-\infty}^{\infty} B_e(\nu) \cos(2\pi\nu\delta) d\nu$$

where $B_e(\nu)$ – even part of the function $B(\nu)$ defined by the expression

$$B_e(\nu) = \frac{1}{2} [B(\nu) + B(-\nu)].$$

Restoring spectrum by interferogram requires the Fourier inverse transform

$$B(\nu) = \int_{-\infty}^{\infty} I(\delta) \cos 2\pi\nu\delta d\delta. \quad (4.24)$$

4.3.2 Instrumental function of a Fourier transform spectrometer

If it was possible to measure the interferogram within the interval of changes δ from 0 to ∞ , the spectrum would be completely restored. However, the value δ changes within the limits from 0 to some infinite value L ; therefore, the value $B'(\nu_i)$ will be only an approximate image of the original spectrum $B(\nu_i)$ which can be expressed as

$$B'(\nu_i) = \int_{-\infty}^{\infty} I(\delta) D(\delta) \cos 2\pi\nu_i\delta d\delta, \quad (4.25)$$

where $D(\delta)$ – rectangular function;

$$D(\delta) = \begin{cases} +1 & \text{at } -L < \delta < +L; \\ 0 & \delta > |L|. \end{cases} \quad (4.26)$$

A cosine Fourier transform (FT) of a sum of two even functions represents a convolution of cosine Fourier transforms of each function.

$$B'_q(\nu_i) = \text{FT}\{I(\delta)\} * \text{FT}\{D(\delta)\} \quad (4.27)$$

A cosine transform of the Fourier-interferogram $I(\delta)$ represents the studied spectrum $B_f(\delta)$.

If a cosine transform of the Fourier-function $D(\nu)$ is defined through $f(\nu)$, expression (4.27) is

$$B'_f(\nu_i) = \frac{1}{2} \int_{-\infty}^{\infty} B_f(\nu) [f(\nu_1 - \nu) + f(\nu_1 + \nu)] d\nu = \int_{-\infty}^{\infty} B_f(\nu) f(\nu_{i1} - \nu) d\nu \quad (4.28)$$

Produced spectrum is a convolution of the even part of the original spectrum with the function $f(\nu)$, i.e. function which is usually represented as the instrumental function of device.

If the original spectrum has only one line (with wavenumber ν_0 and unit brightness), the restored spectrum is

$$B'_f(\nu_i) = \frac{1}{2} [f(\nu - \nu_0) + f(\nu + \nu_0)].$$

Therefore, the produced spectrum is a convolution of the original spectrum and the instrumental function of the Fourier spectrometer:

$$B'(\nu_i) = \int_{-\infty}^{\infty} B(\nu_i) f_{\text{an}}(\nu_i - \nu) d\nu. \quad (4.29)$$

The FT of the rectangular function $D(\nu)$ is expressed by:

$$f_{\text{ins}}(\nu) = 2L \frac{\sin(2\pi\nu L)}{2\pi\nu L} = 2L \text{sinc } 2\pi L \quad (4.30)$$

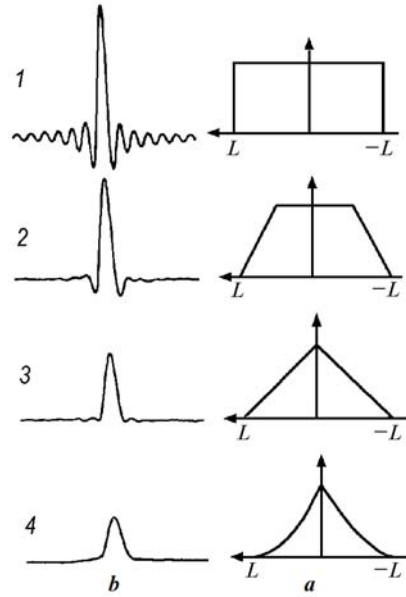
The instrumental function has zeros at $\nu - \nu_0 = \frac{1}{2L}$ and significant secondary maxima (Fig. 4.6, 1).

The apodisation of the interferogram is used to decrease secondary maxima: the rectangular function is replaced by the function $A(\delta)$ called the apodization function. Figure 4.6 illustrates the instrumental functions produced at some apodization functions. Applying the apodization functions makes the width of the instrumental function slightly wider, consequently, it deteriorates the spectral resolution of the device from $\delta\nu = 1/2L$ when using the rectangular function $D(\delta)$ to $\sim 1/L$ when using the triangle apodization function:

$$A_1(\delta) = \begin{cases} 1 - \frac{|\delta|}{L}, & -L < \delta < +L; \\ 0, & \delta > |L|, \end{cases} \quad (4.31)$$

or function

$$A_2(\delta) = \left(1 - \frac{\delta^2}{L^2}\right)^2. \quad (4.32)$$



No	$A(d)$	f_{ins}	$D_{n1/2}$	Parasitic peak
1	$D(x) = \begin{cases} 1 & x \leq L; \\ 0 & x > L \end{cases}$	$2L \text{sinc}(2\pi nL)$	$\frac{1.207}{2L}$	-21 %
2	$2D(x) \cdot [1 - x /L] - D(2x) \cdot [1 - 2 x /L]$	$2L \text{sinc}^2(\pi nL) - \frac{1}{2} \cdot \text{sinc}^2(\pi nL/2)$	$\frac{1.546}{2L}$	-15 %
3	$D(x) \cdot [1 - x /L]$	$2L (\text{sinc}(2\pi nL))^2$	$\frac{1.772}{2L}$	+45 %
4	$D(x) \cdot [1 - x /L]^2$	$\frac{4L}{(2\pi nL)^2} [1 - L \text{sinc}(2\pi nL)]$	$\frac{2.359}{2L}$	+0.7 %

Figure 4.6. Examples of apodization functions (a) and relevant instrumental functions (b)

According to [9], the information about any function with a limited spectrum is contained in a countable set of discrete equidistant values of this function.

A number of equidistant values of the interferogram $I(\delta)$ is enough to calculate the spectrum. Then, the integral

$$B'_2(\nu_1) = 2 \int_0^L I(\delta) A(\delta) \cos(2\pi \nu_1 \delta) d\nu$$

is replaced by the sum

$$B_f(\nu_1) = h [I_0 A_0 + 2I_h A_h \cos(2\pi \nu_1 h) + \dots + 2I_{nh} A_{nh} \cos(2\pi \nu_1 nh)], \quad (4.33)$$

where $I_0, I_h \dots I_{nh}$ – values of the interferogram at path differences $0, h, \dots, nh$; $A_0, A_n \dots A_{nh}$ – relevant values of the apodization function.

Sum (4.33) is equivalent to the integral

$$B'_f(\nu_1) = h \int_{-\infty}^{\infty} I(\delta) A(\delta) R(\delta) \cos(2\pi \nu_1 \delta) d\nu, \quad (4.34)$$

where $R(\delta)$ – Dirac periodic function with period h . Therefore,

$$B'_f(\nu_1) = \frac{1}{2} \int_{-\infty}^{\infty} B(\nu) F(\nu_1 - \nu) + F(-\nu_1 - \nu) d\nu \quad (4.35)$$

where $F(\nu)$ – Fourier transform of functions $A(\delta)$ and $hR(\delta)$. Fourier transform of the periodic Dirac function with step h is another Dirac function with step $1/h$.

New instrumental function

$F(\nu) = 2hF'(\nu)$, where

$$F'(\nu) = \sum_{m=-\infty}^{\infty} \frac{\sin\left(2\pi L\left(\frac{m}{n} - \nu\right)\right)}{2\pi L\left(\frac{m}{n} - \nu\right)}, \quad (4.36)$$

and m and n – integer numbers.

New instrumental function is a set of identic maxima repeated in the interval $1/h$. A proper choice of the step h is very important, since calculated spectra are repeated in the interval $1/h$. To prevent overlapping of calculated spectra, the interferogram of the spectrum keeping the portion of wavenumbers from 0 to ν_m must be digitised with the step $h \leq \frac{1}{2\Delta\nu}$ ($\Delta\nu = \nu_m - 0$).

4.3.3 Multipass gas cell

The threshold sensitivity of a spectrometer is determined by the path length of the radiation in an absorbing cell. Multipass gas cells are widely used for detecting weak absorbing lines.

Multipass mirror optical systems, where the light beam passes multiple times in a limited volume between mirrors, give an opportunity to get greater length of the optical path and register weak absorption of a substance located between the mirrors of the optical system.

If each reflection from the mirror implies a decrease in the beam intensity by ε -part, after N reflections the optical path of the beam will be $S = NL$. Moreover, time delay is $\tau = NL/c$, where c – speed of light. Furthermore, the transmittance T , determined by the ratio of the beam intensity passing the optical path S in the cell to the intensity of the entering beam, is equal to

$$T = (1 - \varepsilon)^N. \quad (4.37)$$

The Table 4.1 demonstrates the intensities of the beam exiting optical system after N reflections

Table 4.1

Transmittance of multipass cell after N reflections

r	ε	$N = 4$	$N = 16$	$N = 64$	$N = 128$
0.8	0.2	0.11	0.17	0.07	0.056
0.9	0.1	0.66	0.43	0.28	0.25
0.99	0.11	0.96	0.92	0.88	0.87

As the table demonstrates, even relatively good mirrors with the reflection coefficient 0.9 make the intensity of the beam transmitted through the optical system very small; only dielectric mirrors with the reflection coefficient $R \geq 0.99$ permit creating the multipass cell where about 100 beam passes are realised.

Three-mirror system of White was firstly proposed for studying weak absorption spectra of gases. The optical system is presented in Figure 4.7. All three spherical mirrors $3a$, $3b$, $3c$ have the same radius of curvature. Centres of curvature a and b of mirrors $3a$ and $3b$ respectively are located on the surface of $3c$; centre of curvature of mirror $3c$ is situated midway between mirrors $3a$ and $3b$.

Thus, pairs of mirrors {3a, 3b} and {3a, 3c} form confocal mirror systems with axes ab and bc respectively, which when reflected do not change the diameter of the beam.

The slit image in the cell is illustrated as beams passing from the input slit I , they are focused by the mirror $3a$ at the point 2 symmetrical to the point 1 with respect to the axis ab . The mirror $3b$ transfers beams coming from the mirror $3a$ on the mirror $3c$ which, in its turn, creates the image of the point 2 at the point 3 symmetrical to the point 2 with respect to the axis bc . After that, the beam goes back to the mirror $3a$, and so on. Final image of the slit is formed in exit N .

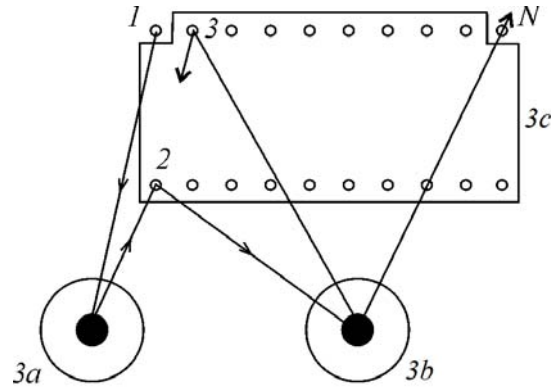


Figure 4.7. Three-mirror optical system of White

Such an optical system has a significant benefit which is a possibility of smooth change in number of steps. It is easily carried out by turning mirrors $3a$ or $3b$. Position of the points on the collective $3b$ can be single or double depending on the position of mirrors $3a$, $3b$, $3c$. Optical system of White at $R = 1$ m and sizes of the collective 10×18 cm provides for required path length in a cell of 100 m.

4.3.4 New features of an FT spectrometer using LED sources

The signal to noise ratio in a detector noise-limited model for a spectrometer is given by

$$\text{SNR}(\nu) = L(\nu) (\Theta \xi \Delta\sigma \sqrt{t D^*}) / (A_D)^{1/2}. \quad (4.38)$$

Here, $L(\nu)$ is the measured signal brightness of the source, $\Delta\sigma$ is the equivalent width of the instrument line shape, ξ is the overall efficiency of the system also called overall transmittance, which includes reflection losses, transmittance of optical elements such as the beam splitter, modulation efficiency, and other losses due to aberrations and misalignment), Θ is the etendue, t is the measurement time, A_D is the detector area, and D^* is the specific detectivity of the detector.

The equivalent width, the etendue, the measurement time, the detector area, and the detectivity of the detector remain unchanged with replacement with a thermal source by LEDs. The main parameters affecting the SNR in these conditions are the brightness of the source and overall transmittance of the system.

a. Brightness

The brightness of the sources was measured in the same conditions which were used for gas absorption recording: the same aperture, multipass cell, and the spectral resolution. Measurements show that the emitting power of the modern commercial LEDs reaches 0.2 to 1 W in a narrow spectral range ($\sim 1000 \text{ cm}^{-1}$). A halogen 20 W lamp, the LEDs series CREE XPE LED and 3GR-R were alternately installed in the experimental setup. The output radiation of the cell was directed to

the emission input of the FT-spectrometer. Figure 1a shows intensities of nine diodes and 20W halogen lamps in the region between 10000 cm⁻¹ and 23000 cm⁻¹. Figure 1b shows the ratio of the LED sources brightness as compared with halogen lamp brightness. It can be seen that the brightness of modern LED light sources is relatively constant when moving to the high-frequency region, but the brightness of the thermal sources in the same direction is characterised by an exponential decrease. As a result, this ratio exponentially increases with frequency up to 300 in the UV region.

The width of the emission spectrum of commercial LEDs $\Delta\nu$ varies from 1000 to 2000 cm⁻¹. It covers the whole spectral range between 10000 and 23000 cm⁻¹, but since only the intervals of the spectrum in which the LED emission exceeds emission of the halogen lamp is of interest, then removing the radiation wings, one can decrease the spectral range of the individual LEDs ($\Delta\nu=500\dots1000$ cm⁻¹), which, however, allows one to study the resonant polyads of vibrational states using only one diode. The entire range of 10000-23000 cm⁻¹ is currently not fully covered, and there are some gaps where the diodes offer advantages due to the low radiation intensity.

b. Overall transmittance of the system

Using a multipass cell decreases the value of SNR. The threshold sensitivity of a Fourier transform spectrometer (the minimal detectable absorption coefficient), K_{th} , depends on two quantities: the absorption layer path length L , and the ability of the measuring system to detect small changes of the signal ($\Delta I/I$). For example, for the absorption layer length of 1 m and the detection ability ($\Delta I/I$) = 0.001 the threshold sensitivity K_{th} equals 10⁻⁵ cm⁻¹. The absorption layer length L is usually treated as the primary enhancement factor that affects the sensitivity, disregarding the fact that a sharp fall of the radiation intensity upon reflection from the cell mirrors makes the second factor predominant in limiting the spectrometer threshold sensitivity. The quantity ($\Delta I/I$) is a reciprocal of the signal-to-noise ratio S/N and is, in its turn, defined by two factors: the source luminance I and the amount of spectral noise. In this case the value of ΔI is the limiting signal still reliably detectable by the measuring device (usually to be taken as a double of the instrument noise $\Delta I = 2N$.)

As the number of reflections n increases, so will the absorption layer length $L=nL_0$ (L_0 is the cell length), whereas the radiation intensity will decrease resulting in the change of the ratio ($\Delta I/I$). The intensity of the light beam passed through the cell (in the absence of the absorbing gas) is defined by reflections losses on the mirrors and is given by the formula $I = I_0 \cdot R^n$, where I_0 is the intensity of the incident light, R is the reflection coefficient of the cell mirrors and n is the number of reflections. The expression for K_{th} then becomes

$$K_{th} = (1/nL_0) \times (\Delta I/(I_0 \cdot R^n)). \quad (4.39)$$

The dependence of K_{th} on the number of reflections n for different values of R (0.9, 0.95, 0.98 and 1) is plotted in Figure 4.8. For the sake of example, we have chosen the following values for the parameters: the cell base length $L=100$ cm, signal to noise ratio of input signal $S/N=2000$ and 200000.

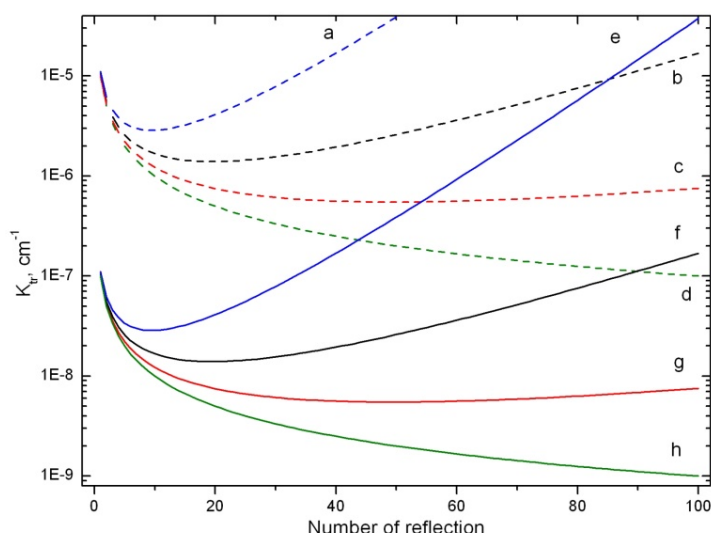


Figure 4.8. The dependence of K_{th} on the number of reflections n for different R (0.9(a), 0.95(b), 0.98(c) и 1(d)) at $S/N=2000$ and (0.9(e), 0.95(f), 0.98(g) и 1(h)) at $S/N=200000$

It can be seen from the plot that, as the number of reflections increases, the value of K_{th} will significantly differ from the threshold sensitivity of the spectrometer with a perfect mirror cell ($R=1$). This sensitivity deterioration is the more prominent, the smaller is the mirror reflection coefficient. At a certain number of reflections, there appears a minimum in the curve depicting the spectrometer sensitivity vs. the number of reflections. This minimum becomes sharper and is observed at smaller values of n , the smaller is the mirror reflection coefficient. It means that, for a given reflection coefficient, increasing the path length by way of increasing the number of reflections, in order to reduce the minimal detectable absorption coefficient, is only expedient up to a certain limit.

It has been shown earlier [10] that without accounting for the photodetector sensitivity, an optimal number of reflections n_{op} , after reaching the threshold value ($\Delta I/I$), is defined by the equality between the relative optical path increase and the relative intensity decrease

$$n_{op} = 1/(1 - R) \quad (4.40).$$

Thus, the radiation intensity, which is registered by the instrument photodetector, on par with the absorption layer length, has a significant effect on the threshold sensitivity. Small values of ($\Delta I/I$) can be achieved either by increasing the mirror reflection coefficient, by increasing the number of scans; or by increasing the source luminance. Whereas the first two approaches have already reached their optimal limit, there is still a certain room for improvement in the use of high luminance sources.

4.4 Analytical capabilities of spectral apparatus

4.4.1 Gas markers of diseases

Spectroscopic methods are widely used in gas analysis. They serve as a basis for different techniques for identifying parameters of blood and urine. Moreover, spectroscopic methods provide new opportunities for specialists to control diseases by analysing exhaled air and body fluids of patient. Table 4.2 encompasses gas markers. Diagnosis of some diseases can be carried out by measuring the concentration of a gas in exhaled air.

Gas markers of diseases

Gas	Norm	Pathology
Acetone	0.3-1.4 ppm	Cardiopulmonary disease – 1.4-20 ppm Cardiovascular disease – 14 ppm Asthma – 8 ppm
Acetaldehyde	0.012 ppm	Europeans – 0.1 - 1 ppm Japanese – 5-10 ppm
Butane	0.05 ppm	Alcohol-induced liver disease – 0.06 ppm Primary biliary cirrhosis – 0.1 ppm
Pentane	0.06-0.1ppm	Mild schizophrenia – 0.2 ppm Acute schizophrenia – 0.3 ppm Heart failure – 0.15 ppm Myocardial infarction – 0.2 ppm Multiple sclerosis – 0.3 ppm Asthma – 0.3 ppm Chronic active hepatitis – 0.1 ppm Alcohol-induced liver disease – 0.2 ppm
Ethanol	0.08-0.2 ppm	Heart failure, atherosclerosis, diabetes – 3 ppm Cardiopulmonary patients – 0.6-4 ppm
Limonene	0.001ppm	Liver diseases – 0.02 ppm-0.15 ppm

Spectrometers with high spectral resolution permit registering the spectrum without distortion. Spectrometers with low resolution are simple and cheap, that is why they are widely used in analytical measurements. However, they have some peculiarities which must be taken into account.

The convolution of the atmospheric transmission function with the instrumental function of a spectral device with a greater half-width of $1-10\text{ cm}^{-1}$ significantly reduces holes in the transmission function caused by analytical lines, since the width of holes increases by 10-100 times due to individual lines, while the square of the hole remains unchanged. This is particularly important for separate lines. Figure 4.9 represents a part of the CH_4 spectrum within the line ν_3 in the region of 3 mcm with high ($\sim 0.01\text{ cm}^{-1}$) and low (10 cm^{-1}) spectral resolution where R -, P - and Q -branches are seen. Lines of R - and P -branches consist of groups of separate lines and have a greater length of $\sim 200\text{ cm}^{-1}$. Q -branch is a dense group of unresolved lines occupying the range of about 10 cm^{-1} . The convolution of the methane transmission function with the triangle instrumental function of a spectrometer with the half-width of 10 cm^{-1} makes depth of the hole within Q -branch smaller by 3 times, while holes within R - and P -branches become smaller by 10-20 times. Therefore, registering CH_4 with low resolution at the same concentrations requires the path length by 3 times longer when using analytical lines of Q -branches and by 10-20 times longer when using lines of R - and P -branches.

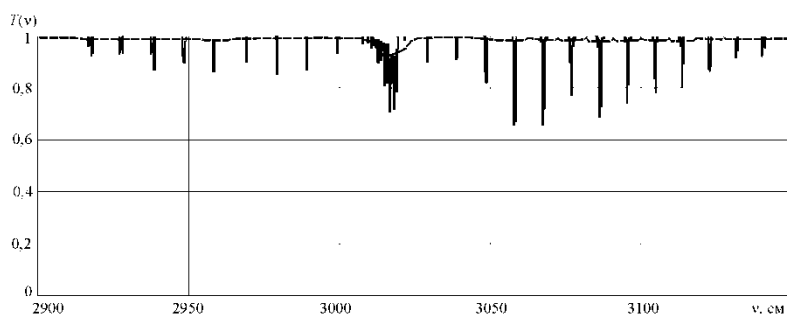


Figure 4.9. Part of the atmospheric spectrum with lines of CH_4 produced by high (—) and low (---) spectral resolution

Other peculiarity of analytical measurements with low resolution is the interference of lines of different gases. Measurements with high spectral resolution ($\sim 0.01 \text{ cm}^{-1}$) make it easy to find micro-windows of transparency in the atmosphere where only analytical lines of a measured gas are located. However, increase in the width of the instrumental function of the device by 10-100 times makes the task in detecting a micro-window of transparency free of lines of other gas components almost unsolvable. Consequently, it is necessary to change the algorithm for solving the inverse task in measuring gas concentration and include fitting of the calculating spectrum to the experimental one taking into account all interfering gases.

Let us consider in next Section the possibilities of spectroscopic methods for controlling methane in atmosphere.

4.4.2 Registration of methane in exhaled air

A background content of methane (1 ppm) was measured by means of the grating rapid-scan spectrophotometer.

Device is a grating rapid-scan spectrophotometer. The registered absorption spectrum is compared with the absorption spectra of etalon samples which are recorded into computer database and then it is analysed by special software. General functional configuration of the spectrometer is presented in Figure 4.10. The Ebert's configuration is used as the main optical configuration: O – light source, M – spherical mirrors, DG – diffraction grating, F – photodetector, S – optical slits.

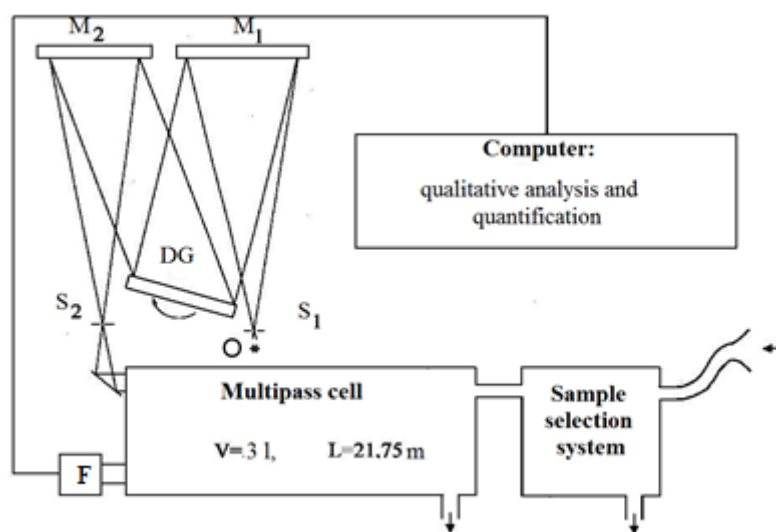


Figure 4.10. Functional configuration of a spectrophotometric gas-analyser

The spectrophotometer differs from ordinary grating spectrometers by the fast controlled rotation of diffraction grating and the use of computer to correct produced spectra. Rotating in the dispersion plane, the grating gradually reflects the entire spectral range. However, computer will only perceive a part of the spectrum which is detected by the sensors located in synchronisation module. Unwanted overlapping of orders is cut off by filter. Synchronisation module is designed to generate a synchronising signal of the scanning of spectrum and synchronising pulse of the reference signal. Elements of synchronisation of signals are magnetically sensitive sensors and magnet located on the rotation disk of the grating. When a digitised signal is received, computer processes the spectrum by specially developed software and analyses 50-1000 realisations of the spectrum, on average.

The spectral range of operating device is $1800-10000 \text{ cm}^{-1}$. Scanning and processing of one registration of the spectrum takes 0.5 – 1 sec, spectral resolution is 10 cm^{-1} . Spectrometer consists

of computer which is responsible for correction of unsteady speed of scanning. Statistic processing of spectra, corrected by the computer, provides significant improvement in SNR. For example, if SNR is 100 – 200 at a single realisation, when accumulating 100 spectra, SNR increases by 10 times, when accumulating 1000 spectra – by 33 times, and so on. At the statistical accumulation of 1000 realisations of the spectrum, the photometric sensitivity of spectrometer by transmittance makes up $5 \cdot 10^{-4}$. A multipass cell with the path length of the beam provides for the registration of absorption $2.3 \cdot 10^{-7} \text{ cm}^{-1}$.

Figure 4.11, *a* illustrates the part of the atmospheric absorption spectrum in the region of $2 \mu\text{m}$ produced by a low resolution spectrophotometer with the beam path length in the cell being 22 m.

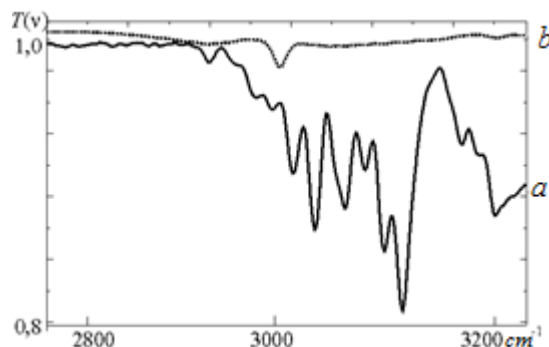


Figure 4.11. Absorption spectrum of wet (*a*) and dry (*b*) atmospheric air in the region of $3 \mu\text{m}$

Water vapour in the air disguises the analytical line of CH_4 , therefore, measuring methane requires either preliminary air drying (Fig. 4.11, *b*) or spectrum splitting with the help of computer by separating the signal responsible for absorption by water vapour from the signal produced by methane. Both of these approaches enable the reliable detection of methane in the atmosphere at its natural concentration – 1.7 ppm.

Questions

1. How is it possible to experimentally determine the instrumental function of spectrometer?
2. What are the processes that detect the broadening of spectral lines?
3. Calculate the Doppler's half-width of spectral lines of H_2O at the temperature $T = 77 \text{ K}$, 300 K , 1200 K in the region of 10000 cm^{-1} .
4. Calculate the Lorentzian half-width of the line of H_2O (partial pressure of 17 torr) in the atmospheric air ($P = 1 \text{ atm}$), if $\gamma_{\text{H}_2\text{O}-\text{N}_2}^0 = 8 \cdot 10^{-2} \text{ cm}^{-1}/\text{atm}$, $\gamma_{\text{H}_2\text{O}-\text{O}_2}^0 = 9 \cdot 10^{-2}$, $\gamma_{\text{H}_2\text{O}-\text{H}_2\text{O}}^0 = 1,5 \cdot 10^{-2} \text{ cm}^{-1}/\text{atm}$.
5. What is transmission and absorption of the cell with the length 1 m and 1 cm, if the absorption coefficient is 10^{-3} cm^{-1} ?
6. What is the spectral resolution of a Fourier transform spectrometer if a movable mirror is moved by 1 mm, 1 cm and 1m, and with the triangular instrumental function?
7. What is resolution of a Fourier transform spectrometer if the mirror is moved by 1 mm, 1 m without apodization?
8. What must be the movement of the movable mirror of a Fourier transform spectrometer to produce the resolved spectrum characterised by the Doppler's broadening at room temperature in the region of 1000 cm^{-1} for gases: a) H_2 , b) H_2O , SF_6 ?
9. What must be the movement of the movable mirror of a Fourier transform spectrometer to produce the resolved spectrum of CO_2 characterised by the Doppler's broadening at room temperature in the region of a) 1000 cm^{-1} , b) 5000 cm^{-1} , c) 10000 cm^{-1} ?

LECTURE 5. STRUCTURES AND SPECTRA OF WATER ABSORPTION

5.1 General concepts

5.1.1 Structure and spectra in absorption of water vapours

Molecular water absorption spectra – spectra of absorption, emission or dispersion emerging at the quantum transitions of molecules from one energetic state into another. The spectrum of low pressure vapours of H₂O is the most characteristic when there is no broadening of spectral lines due to collisions of gas molecules: such a spectrum consists of narrow lines which broaden only due to the Doppler's effect.

In accordance with three systems of energy levels in molecule – electronic, vibrational and rotational, molecular spectra consist of a sum of electronic, vibrational and rotational spectra and lie in a large range of electromagnetic waves – from radiofrequency to the X-ray spectral region.

Frequencies of transitions between rotational levels of energy usually fit into a microwave region (according to the scale of wavenumbers 0.03-30 cm⁻¹), frequencies of transitions between vibrational levels – into the IR region 400-10000 cm⁻¹, frequencies of transitions between electronic levels – into visible and UV regions of spectrum. Electronic transitions are accompanied by changes in the vibrational energy of the molecule, while the rotational energy changes at vibrational transitions. Therefore, more often the electronic spectrum represents a system of electronic and vibrational bands at high resolution of spectral apparatus.

In the IR region a free molecule of H₂O has three main normal modes of vibrations which are related to: $\nu_1(\text{OH})=3657\text{ cm}^{-1}$, $\nu_2(\text{OH})=1595\text{ cm}^{-1}$, and $\nu_3(\text{OH})=3756\text{ cm}^{-1}$.

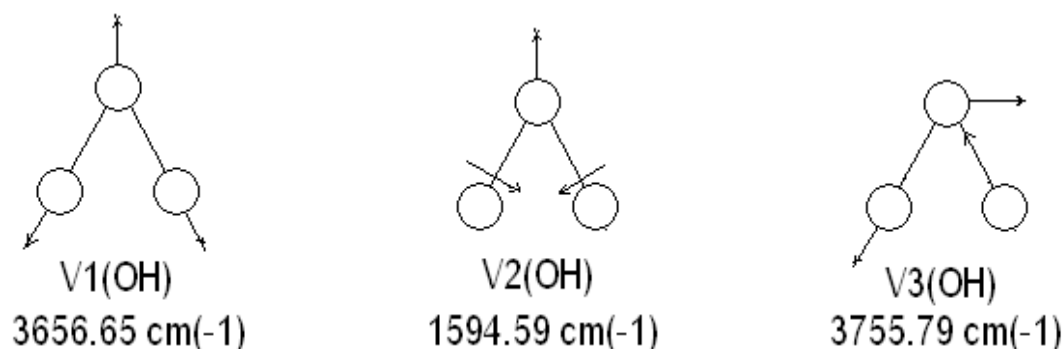


Figure 5.1. Normal modes in water molecule. ν_1 , ν_3 – symmetric and asymmetric stretching vibrations, ν_2 – bending vibration

Movements of H₂O nuclei at vibrations ν_1 (OH) and ν_3 (OH) occur almost along the direction of O-H bonds (Fig. 5.1). These modes are usually called stretching vibrations of O-H. At vibrations ν_2 (OH) nuclei of H move in direction almost perpendicular to O-H bonds. The mode ν_2 is called bending vibration H-O-H or flexural vibration of the hydrogen bond (δ). This vibration plays an important role in the H₂O molecule, since it leads to various spectroscopic effects.

The total vibrational-rotational wave function of water molecule and relevant energetic states are expressed by three vibrational quantum numbers ν_1 , ν_2 , ν_3 and three rotational quantum numbers J , K_a , K_c . Since the function belongs to a pointgroup of symmetry C_{2v} , it refers to one of four types of symmetry A_1 , A_2 , B_1 or B_2 . The energies of vibrations ν_1 , $2\nu_2$ and ν_3 are very close, which causes the resonance affecting formation of vibrational bands of the spectrum.

Most frequently, water vapours imply vapours of low density – 10⁻³g/cm³ and lower. At such conditions distance between water molecules is, on average, 300 nm, which is much higher than the radius of their specific interaction. Due to a large spatial separation, water vapour molecules can make free translational and rotational motions. The latter, interacting with the vibrational level of

the molecule, lead to their splitting. As a result, the spectrum of water vapours (Fig. 5.2) consists of a large set of lines with the half-width of $0.05\text{-}0.5\text{ cm}^{-1}$ corresponding to rotational transitions instead of wide (several tens of inverse centimeters) vibrational bands typical of substances in condensed states. Frequency ranges of fundamental vibrational bands by decreasing intensity are presented in Table 5.1.

Table 5.1

Vibrational bands of monomer H_2O by frequencies. Transition into the ground state 000 are mentioned

Vibrational identification of the upper level	Frequency range, cm^{-1}		Intensity, $\text{cm}/\text{molecule}$
	ν_{\min}	ν_{\max}	
000	0.741691	1743.977290	2.676E-18
010	701.964330	2819.848150	3.246E-19
001	2894.657700	4640.360890	2.445E-19
011	4608.207110	6567.823150	2.820E-20
100	2823.074330	4589.854880	2.251E-20
101	6441.955200	8050.535000	1.856E-20
110	4568.067070	6071.399150	3.623E-21

Studying manifestations of intra- and intermolecular interactions in spectra, laws of formation of vibrational water bands and structural features of water implies conducting the research into the behavior of Raman bands and absorption under the influence of various factors, in particular, changing temperature and dissolution of substances in water.

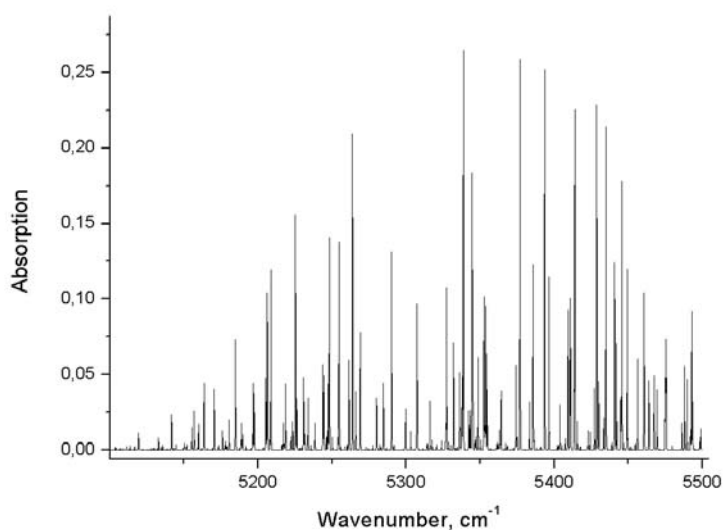


Figure 5.2. Spectrum of monomer H_2O calculated linearly at the temperature $T = 296\text{ K}$ within the range of 5100 cm^{-1} - 5800 cm^{-1} (spectral resolution 0.1 cm^{-1})

5.1.2 Hydrogen bonds

Hydrogen bonds between water molecules are caused by specific distribution of the electronic density which results in the shift of an only electron of hydrogen towards very electronegative oxygen atom.

The electronic structure of the H_2O molecule defines the conditions for association of individual molecules into a complex three-dimensional structure. The electronic structure of the water molecule allows it to be both donor and acceptor and makes it an ideal material for building

an extensive network of hydrogen bonds. The most perfect form of such a network exists in ice. Each proton-hydrogen of every water molecule can be tightly bound to lone elongated electron of other molecule (moreover, the first molecule is a donor, the second is an acceptor) and form a new hydrogen bond. Two protons plus two lone electrons – consequently, each molecule of H₂O can simultaneously participate in four hydrogen bonds formed by the same molecule.

A proton involved into the hydrogen bond and situated between atoms A and B of oxygen has two equilibrium positions: it can be close to the atom A of oxygen, at distance about 1 Å, or next to the atom B, at distance of 1.7 Å from A, i.e. along with ordinary dimer HO-H...OH₂, ion pair HO...H-OH₂ is also stable.

5.1.3 Water models. Cluster water structure

To date, there is no unanimous opinion on the structure of liquid water. Some scientists are sure that there is a three-dimensional network formed by molecules connected by hydrogen bonds. Structure of the network is variable; it does not have dominant configurations similar to structures of any crystals and other *a priori* given structures. However, other part of the scientific community believes that the structure of fluid, in particular, water must be approached from the perspective of the crystal structure. Of course, it does not mean that the structure of liquid water is similar to the crystal structure. Molecular configurations constantly transform, the average lifetime of hydrogen bonds is several picoseconds, although, some of them may exist for a longer period of time.

There is also a fluctuating conception of the hydrogen bond. According to the conception, very wide bands in the IR absorption spectrum of OH-water oscillators reflect the inherent to fluids (unlike crystals) statistical distribution of geometrical configurations of the hydrogen bridge O-H...O generated by fluctuations of the local environment of various molecules of H₂O. The statistic profile described for OH-oscillator is a probability of having a determined frequency in continuous ensemble of hydrogen bonds, which is calculated from the experimental Raman spectra of the HDO molecule. This approach allows us to restore profiles of original spectra of the HDO molecule in liquid water and extrapolate them on a wide temperature range.

5.1.4 IR spectroscopy of liquid water

The rotational structure of the water monomer bands within the ranges of 3600-4300 cm⁻¹, 5100-5600 cm⁻¹, and 6700-7400 cm⁻¹ is formed by transitions to the first (ν), the second triad ($\nu + \delta$) and the first hexad (2ν) of resonance vibration states, respectively

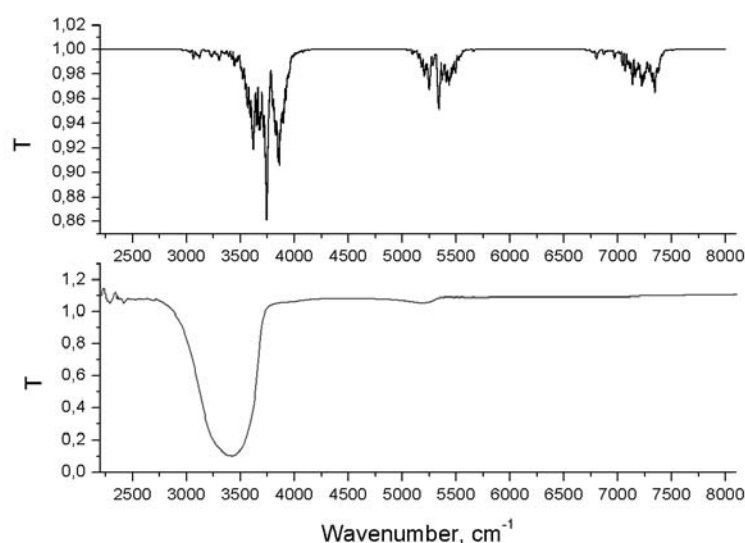


Figure 5.3. The transmission spectra of H₂O monomer (up), and bulk water (low)

The absorption bands of bulk water do not have a rotational structure and are shifted from the spectrum of the water monomer (Fig. 5.3) towards the lower frequencies. At room temperature, their centres are located respectively at frequencies of 3430 cm^{-1} , 5180 cm^{-1} and 6800 cm^{-1} . Table 5.2 represents the data on the reference of absorption bands of liquid water within the fundamental frequency range (4000-1600 cm^{-1}), and close (14300-5000 cm^{-1}) IR region of the spectrum.

Table 5.2

Reference of vibrational bands in the spectrum of liquid water

Types of vibration	Frequency of the band centre, cm^{-1}
Torsional ν_L	780
Deformational ν_2	1645
Combination $\nu_L + \nu_2$	2150
Symmetrical stretching ν_1	3450
Symmetrical stretching ν_3	3428
Overtone $2\nu_2$	3290
Combination $\nu_1 + \nu_2, \nu_3 + \nu_2 (v + \delta)$	5183
Overtone $2\nu_1, 2\nu_3, \nu_1 + \nu_3$	6920
Combination $2\nu_1 + \nu_2, 2\nu_3 + \nu_2 (v + \delta), \nu_1 + \nu_2 + \nu_3$	8370
Overtone $3\nu_1, 3\nu_3, 2\nu_1 + \nu_3, 2\nu_3 + \nu_1$	10262
Combination $3\nu_1 + \nu_2, 3\nu_3 + \nu_2, 2\nu_1 + \nu_2 + \nu_3 \dots$	11700
Overtone $4\nu_1, 4\nu_3, \dots$	13300

Absorption bands of liquid water are characterised by the pronounced mode structure which is determined by the network of hydrogen bonds between water molecules of various degree of OH-binding. Each molecule interacts with several adjacent ones; moreover, it serves as a donor or acceptor in each bond. Numerical modelling of instant configurations in water demonstrates that there are three most probable configurations “donor-acceptor”. These are the terms used to describe the degree of molecules bonding.

The temperature dependence of the absorption spectrum.

The maximum of the absorption band of liquid water is at the frequency of 5180 cm^{-1} slightly increasing with temperature. When the temperature decreases from +20.3 to 0°C, the line profile undergoes small changes: there is a gradual redistribution of the intensity with the trend towards lower frequencies (Fig 5.4).

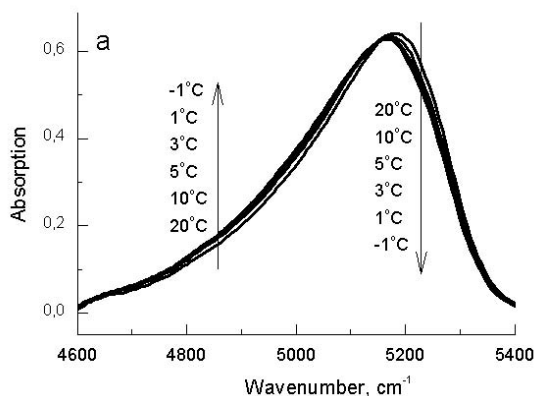


Figure 5.4. Change of the absorption band of water upon cooling (liquid water)

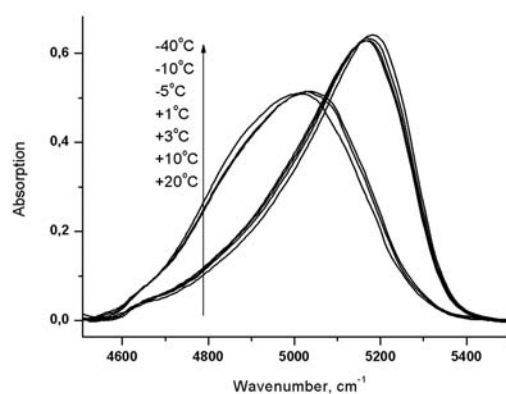


Figure 5.5. Change of the absorption band of water upon cooling (phase transition)

When the temperature varies, there is a deformation of profile (Fig. 5.4) and redistribution of the intensity of constituents, which indicates the retransformation of the structure of water. It is

extremely pronounced in case of the observation of changes in the water absorption spectrum during the phase transition (Fig. 5.5).

Vibrational modes.

The profile of absorption bands of water is represented as a sum of three Gaussian profiles in accordance with the number of most probable configurations of absorbing molecules. Figure 5.6 demonstrates the decomposition for the spectrum at the temperature +20°C. The quality of fitting (~2%) is expressed by the difference in sum of fitting and experimental profiles.

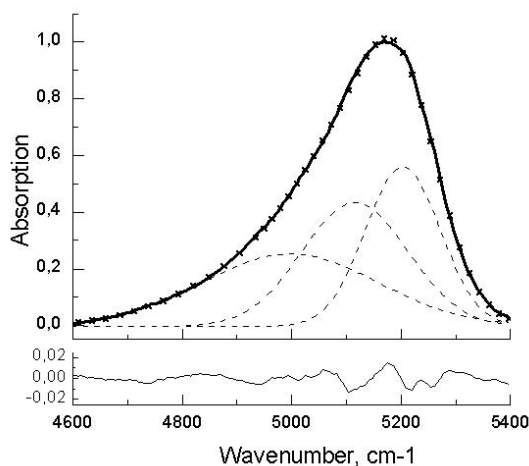


Figure 5.6. Fitting of the experimental (solid curve) absorption band of liquid water. Fitted profiles (Gaussians) are indicated by dotted curves, and their sum is denoted by crosses. The difference between the Gaussian sum and the experimental profile is shown below

Each Gaussian profile corresponds to the absorption by molecules of different bonding. The low frequency component corresponds to strongly bound molecules; each of them has 4 hydrogen bonds. With increasing frequency, components correspond to medium- and weakly bound molecules. It must be noted that the intensity of modes is proportional to the number of absorbing molecules of the relevant bonding.

In the spectrum of liquid water, high-frequency ((II) 4890 cm^{-1} , (III) 5080 cm^{-1} , and (IV) 5200 cm^{-1}) components are present, and in the spectrum of ice, the low-frequency ((I) 4700 cm^{-1} , (II) 4890 cm^{-1} , and (III) 5090 cm^{-1}) ones are present. Intensities of modes obtained during cooling and heating of water are shown in Figure 5.7. A high-frequency mode (IV) disappears at negative temperature and a low-frequency mode appears.

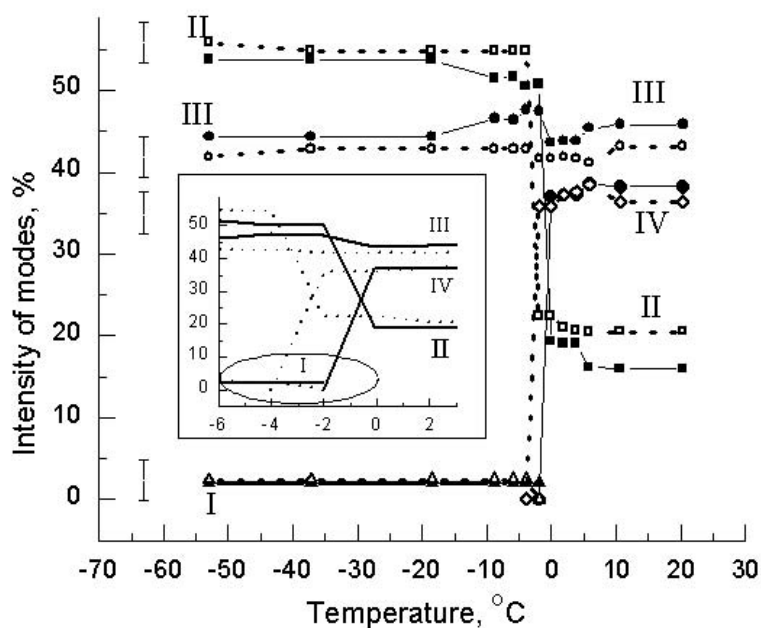


Figure 5.7 Change of mode intensity. Dashed curves connect points corresponding to the cooling, and solid curves – to heating. The temperature range from -6 to $+3^{\circ}\text{C}$ is shown in more detail in the inset. ErrorBar denotes the random error

The modes intensity is directly proportional to the number of absorbing molecules with some bonding depending on the temperature. The intensity of mode (IV) in liquid water decreases slowly with temperature from $+20.3$ to -2.0°C , during the phase transition water-ice, the mode (IV) disappears. The intensity of the mode (III) characterised by three hydrogen bonds in liquid water decreases slowly with temperature, during the phase transition it slightly increases, and upon further cooling of ice it decreases slowly forming complexes of more closely bound water molecules.

The intensity of mode (II) in liquid water characterised by four hydrogen bonds increases slowly with decreasing temperature, during the phase transition, it more than doubles sharply, and then continues to increase slowly with decreasing ice temperature due to reduction of mode (III). In addition, low-frequency mode (I) arises in ice, and its intensity decreases with temperature.

5.1.5 IR spectrum of water absorption in nanopores

Absorption spectra of the portions of water removed from the SiO_2 samples contain strong absorption band in the range of $3300\text{-}3800\text{ cm}^{-1}$, which causes almost 100% attenuation of radiation in the tablet of 4 mm length and weak band in the range of $4570\text{-}5400\text{ cm}^{-1}$, which causes 20-40% attenuation of the radiation. The first band corresponds to stretching vibrations of the monomer, and the second band is determined by combination vibration (stretching plus bending). Other weaker overtone bands of water in SiO_2 are located in the $5800\text{-}7200\text{ cm}^{-1}$ range with a maximum of 6500 cm^{-1} and in $7300\text{-}9000\text{ cm}^{-1}$ with maxima at 7600 cm^{-1} and 8500 cm^{-1} . These bands arise from transitions to the resonance polyads (2ν) and ($2\nu + \delta$) of water monomer, respectively.

Water monomer absorption in the range of $3100\text{-}3600\text{ cm}^{-1}$ is very large, and the absorption lines of atmospheric air do not allow us to study the spectra of water in nanopores quite correctly. For this reason, the OH-stretching vibration was investigated in the Raman spectra using the Fourier transform spectrometer NICOLET 5700 with NXR FT-Raman module. The Raman spectra of bulk water and water in the SiO_2 samples with pore diameter of 2.6 nm and 11.8 nm at temperature of 300K are presented in Figure 5.8, *a*.

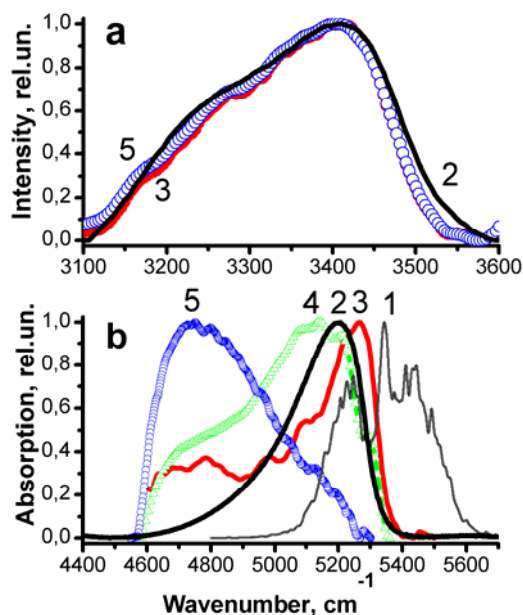


Figure 5.8. Raman spectra in the range of 3400-3800 cm^{-1} (a) and absorption spectra in the range of 4500-5800 cm^{-1} (b) of water monomer (1), bulk water (2), water clusters in the SiO_2 samples with pores of 2.6 nm (3), 6.4 nm (4) and 11.8 nm (5) [11]

The figure shows that the bands of water in all samples have a maximum at a frequency of 3430 cm^{-1} and its band contour is only slightly changed with the variation of pore size. The situation changes drastically in the 5000-5600 cm^{-1} region where the spectra of water in the SiO_2 samples with pores of different diameter (2.6 nm, 6.4 nm and 11.8 nm) consist of several sub-bands, which are well resolved (the interval between the sub-band peaks reaching 580 cm^{-1} for pores of the same size), and the band maxima for different size pores are located at different frequencies (Fig. 5.8, b).

With decreasing pore diameter the centers of the recorded bands are shifted to higher frequencies. For the pore size of 11.8 nm, the band maximum is centered at 4700 cm^{-1} , for the 6.4 nm pores band, the centre is located at a frequency of 5100 cm^{-1} , and for 2.6 nm - at a frequency of 5250 cm^{-1} . For comparison, Figure 5.8 b also shows the absorption spectrum of water monomer and bulk water. The band centre of the water monomer is 5340 cm^{-1} whereas the absorption band of bulk water, which characterizes the absorption of large water clusters, is centered at the frequency of 5180 cm^{-1} , therefore, there is a big negative shift of the $(\nu + \delta)$ bands of water clusters with increasing strength of hydrogen bonding.

The direction of the centre shift for the band describing water clusters is the same for the first and the second triads – the shift with increasing hydrogen bond occurs in the direction of low frequencies. Despite the fact that the second $(\nu + \delta)$ triad includes both the OH-stretching (ν) and bending (δ) vibrations, and the bending vibration is experiencing a positive shift with increasing confinement, the role of OH-stretching vibration in the formation of the second triad is paramount. Moreover, the shift of the combination band greatly increases as compared with the shift of the band in 3000 cm^{-1} . The maximum of the first triad (ν) when changing the pore size from 6 nm to 20 nm is shifted by less than 50 reciprocal cm, the absorption maxima of the second triad ($\nu + \delta$) are shifted by 530 cm^{-1} when changing the pore diameter from 2.6 nm to 11.8 nm.

5.1.6 Phase transition of water in nanopores

An interesting fact is that water in pores of small diameter does not have phase transition of the first order at $T = 0^\circ\text{C}$ in its classical understanding. The transformation of water structure in pores with diameter 2.6 nm and 11.8 nm passes gradually at cooling and heating as compared to jumping nature of crystallization/melting of liquid water. Furthermore, temperature ranges, where changes in water structure take place, are shifted to the region of negative temperatures for pores with smaller diameters and to the region of positive temperatures for pores with larger diameters.

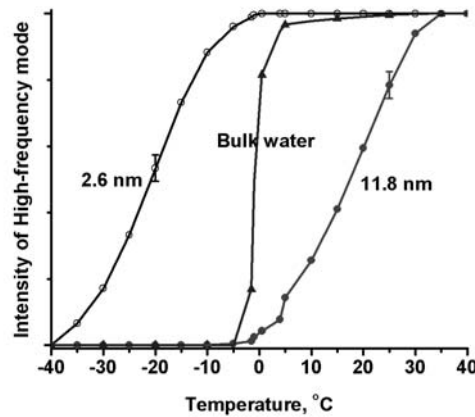


Figure 5.9. Changes in the mode intensity corresponding to the absorption by weakly bound molecules in the water absorption spectrum: in pores with $D = 2.6$ nm within the temperature interval from $+5^\circ\text{C}$ to -40°C ; in pores with $D = 11.8$ nm within the temperature interval from $+30^\circ\text{C}$ to -5°C ; in liquid water

Figure 5.9 illustrates changes in the intensity of high-frequency constituent (number of weakly bound molecules) at changing temperature, where the temperature dependence of the number of weakly bound water molecules in pores of SiO_2 is observed. The dependence is fundamentally different from the case with liquid water, when at cooling the intensity of high-frequency mode (IV) drops to zero at $T = 0^\circ\text{C}$.

LECTURE 6. DYNAMIC REGISTRATION OF WATER CLUSTERS IN NANOPORES AND BIO-OBJECTS

6.1 Dynamic Registration

Dynamic registration of the absorption spectrum of water was used to study the SiO₂ nanoporous sample. Firstly, we recorded the absorption spectrum of the tablet filled with water, then the water was removed by the vacuum pumping and the sample's spectrum was recorded at 10-20 min intervals at constant vacuum pumping (I₁ ... I₁₀). The signal (I_i) includes the absorption of dry tablets (with the absorption coefficient K(SiO₂)) and the absorption coefficient of water in the sample K (water), so that the total absorption coefficient is K_i = K_i(SiO₂) + K_i(water).

Registration of the absorption spectrum of water monomer, bulk water and water in the nanopores was performed in the 2000-9000 cm⁻¹ region using the Fourier spectrometer Bruker IFS-125 M. The spectral resolution of the spectrometer varied from 1 to 20 cm⁻¹.

The ratio of the light intensity passed through the tablet of water (I_i) to the light intensity passed through the dry tablet at the last moment of pumping (I₀) gives the absorption spectrum of the water contained in the sample at the moment of measurement. Changes of the water absorption spectrum in a SiO₂ sample with 11.8 nm pores during the vacuum pumping are shown in Figure 6.1. The sample's water contents slope down to zero while changes in the water absorption spectrum are not monotonous – they are small at the initial moment and become significant in the middle of pumping.

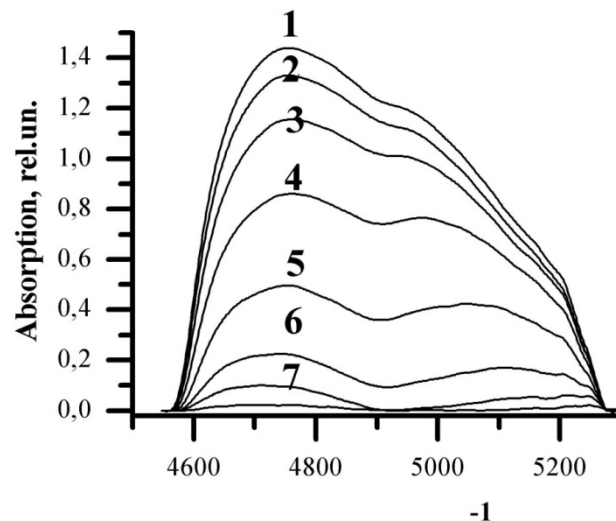


Figure 6.1. The absorption spectra of water in the SiO₂ sample with pores of 11.8 nm in the 4570 - 5300 cm⁻¹ range recorded at 10 (1), 20 (2), 30 (3), 40 (4), 50 (5), 60 (6), 70 (7) minutes after the start of vacuum pumping

The ratio of the light intensity passed through the tablet of water (I_i) to the light intensity passed through the tablet at the successive moment (I_{i+1}) gives the absorption spectrum of the portion of water removed from the sample between the measurements:

$$A_i^*(\nu) = 1 - I_i / I_{i+1} = 1 - \exp [- (\Delta K_i (\text{water}) L)],$$

where $\Delta K_i (\text{water})$ is the absorption coefficient of the portion of water evacuated from the sample of length L during the time interval Δt_i . The magnitude of the microportion absorption is very small ($1 - I_i / I_{i+1} < 10\%$), and goes down to zero within 60-90 minutes of the vacuum pumping. In this case, the spectrum becomes more variable and informative.

Inverse procedure is also possible. Firstly, we record the absorption spectrum of the dry tablet and then the spectrum of the sample continuously being filled with water where the readings

are taken at 40 min intervals. In this case, the process develops more slowly and the whole procedure takes about 3-4 hours.

Transformation of the spectrum of water in the pores becomes more significant when using the dynamic registration [11]. Absorption spectra $A_i^*(\nu)$ of water microportions registered in the vacuum pumping which depart from the SiO₂ samples with a pore diameter of 11.8 nm and 2.6 nm are shown in Figure 6.2. It is seen from the figure that the time behaviour of water clusters for pores of different sizes varies significantly.

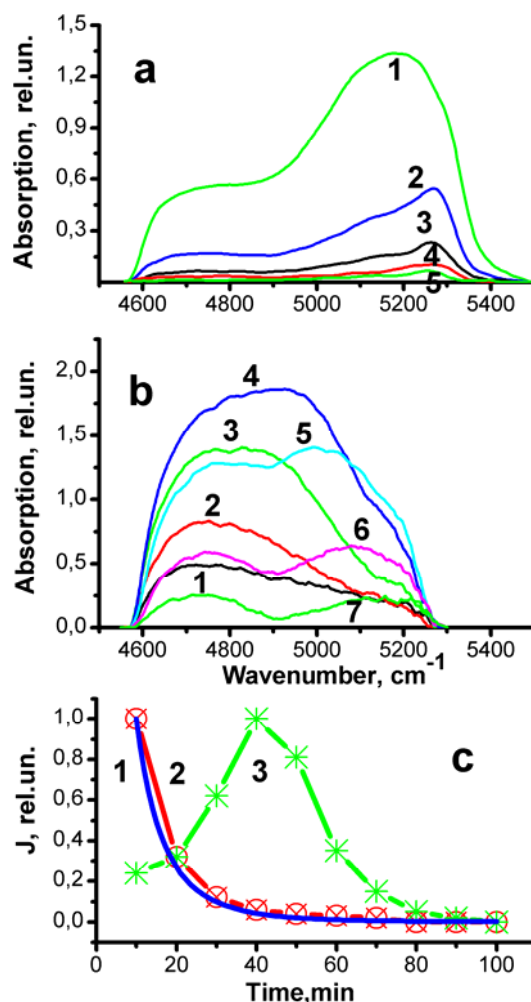


Figure 6.2. The absorption spectra of water microportions removed from the SiO₂ sample with pores of 2.6 nm (a) and 11.8 nm (b) in the 4570 - 5300 cm⁻¹ range, recorded at 10 (1), 20 (2), 30 (3), 40 (4), 50 (5), 60 (6), 70 (7) minutes after the start of vacuum pumping. The integral evacuation rate (c) from pores with a diameter of 2.6 nm (2), 11.8. nm (3) and calculated by gas kinetic theory(1)

The length of the water monomer is 0.3 nm, so that the pore diameter (2.6 nm) which only 8 times larger than the H₂O molecule. It follows from purely geometrical consideration that large clusters of water cannot be formed in these pores. This is manifested in the spectrum where the low-frequency component of the absorption band of water is absent, which is characteristic of high order clusters. The spectrum has a maximum absorption at a frequency of 5250 cm⁻¹ which is much closer to the absorption band of water monomer and determines the absorption of small-size water clusters.

The time behavior of the spectrum of water clusters during the evacuation of the pores with diameter of 2.6 nm seems quite monotonous (Fig. 6.2, a). The number of water clusters characterized by low-, medium-, and high- frequency sub-bands decreases equally during the vacuum pumping.

The spectral contour of the ($\nu + \delta$) band in this sample can be described by the sum of different components. Three Gaussian profiles provide a good contour fitting describing the large (4740 cm^{-1}), medium (5150 cm^{-1}), and small (5250 cm^{-1}) water clusters. The area under the curve ΔK_i (water) is proportional to the number of molecules departing from the sample during the interval between measurements, i.e. to the evacuation rate of the molecules.

According to gas dynamics, the diffusion rate J is proportional to the negative of gradient of the concentration dp/dx :

$$J = - D dp/dx,$$

where D is the diffusion coefficient.

In our case the gradient dp/dx is determined by the number of water molecules in the tablet and continuously decreases with pumping, and the solution of the diffusion equation is exponential which is shown in Fig. 6.2, *c*. As can be seen from this figure, the evacuation rate of the molecules from the pores of small diameter (2.6 nm) decays exponentially in accordance with the solution of the diffusion equation.

The pore size of 11.8 nm, exceeds significantly (40 times) the water monomer length. The spectrum of water microportions recorded during the pumping is extremely variable in time (Fig. 6.2, *b*). At the initial stage of vacuum pumping the combination band in the pores of SiO_2 has a maximum at a frequency of 4740 cm^{-1} , which shifted from the monomer band in the low-frequency region much more than the band of bulk water. In the pumping-out process, the band contour changed resulting in the appearance of new absorption maxima and redistribution of sub-band intensities. The absorption centre of gravity is shifted up to higher frequencies, i.e. in the direction of the corresponding monomer band of water. The molecules which are bound by strong hydrogen bonds are removed from the nanopores at the initial moment of the pumping (see curves 1-3 in Fig. 6.2, *b*). The removal of loosely bound water molecules with a peak at a frequency of 5150 cm^{-1} occurs at the end of pumping (see curves 4 – 6 in Fig. 6.2, *b*). The direction of the band shift is similar to that of pure stretching vibration which occurs in the nanopores with increasing temperature of the sample.

The integral (for all types of water clusters) evacuation rate of the molecules in pores with a diameter of 11.8 nm is different from that in small pores with a diameter of 2.6 nm (see Fig. 6.2, *c*), and differs from the diffusion rate of molecules. The absorption spectrum of water microportions evacuated from pores with a diameter 11.8 nm is more complicated; it includes more water clusters and three Gaussian profiles do not allow them to make fitting correctly. The growth of water cluster size with increasing water concentration is characterised initially by a peak related to small clusters in the size distribution function, with a second peak corresponding to larger clusters being formed later. In our case, with decreasing concentration of water, an inverse process takes place – initially the number of large clusters reduces and the water molecules are redistributed in small-sized clusters.

6.2 Studying water absorption spectra in bio-objects

6.2.1 Optical probe

Studies have shown that the combination of the dynamic registration method with the overtone vibrational transitions opens new possibilities for investigation of water clusters in nanoporous samples. The use of the overtone bands in the high frequency range can effectively resolve the structure of the water cluster absorption bands in the nanoscale pores. Dynamic registration of spectra of microportion water in nanopores allows us to detect changes in the strength of hydrogen bonding in the sample depending on the water concentration and the pore

diameter, and enables studying the dynamics of the water molecule clustering in low-dimensional objects.

The absorption band of water in the region of 4600-5500 cm^{-1} and its temporal behavior can be an effective criterion regarding the presence and size of nanopores in biological systems. Dynamic registration allows us to use different test molecules by changing the strength of hydrogen bonding and the strength of the molecule-surface interaction.

As the result of conducted studies, optical probe was created. It permits obtaining the information about water clusters in objects and physical and chemical features of the nanoporous structure in living and artificial samples about:

- a) water clusters in object,
- b) the presence of the nanoporous structure in object,
- c) the spectral distribution of the band as a function of pore size,
- d) the distribution of water clusters by size,
- e) water viscosity,
- f) variations in the water cluster structure and nanoporous structure of object in relation to the degree of damage of a bio-object.

6.2.2 Skin examination

A newly developed method and recent device helped to obtain essentially new results about bullous dermatoses. Studies conducted by means of the dynamic method show:

The absorption spectrum of healthy skin (at its evacuation) demonstrates strong variability. The amount of water in healthy skin decreases proportionally to the pumping of a sample, while in unhealthy skin damaged by pemphigus water does not decrease at evacuation.

6.2.3 Nanoporous structure of bone matrix at osteoporosis based on the IR spectroscopy

Experiments were conducted with Wistar rats having a body weight of 250 g; osteoporosis was modeled by bilateral testiclectomy during 3 month. It was found by dynamic IR spectroscopy that in an osteoporotic bone the fraction of nano-sized pores decreases, the mineral phase amorphises, hydrated shells around mineralised particles of the bone matrix thicken, and adhesion forces increase. This contributes to the formation of larger-size water clusters compared to the healthy bone tissue and leads to the accumulation of more viscous liquid with increased intermolecular interaction forces in pores of the bone matrix [12].

Healthy Bones.

The water was introduced in the sample keeping bones in water at temperature 35°C during 24 hours. The centers of the water absorption bands for the bones are situated near 5200 cm^{-1} . Spectra of water microportions registered in the vacuum pumping which depart from the bones samples are shown in Figure 6.3. It is seen from the figure that the time behavior of water clusters for pores of healthy and osteoporotic bones varies significantly.

As seen from Figure 6.3 a, maximum of the water absorption band in the healthy bone varies during vacuum pumping from 5000 cm^{-1} to 5200 cm^{-1} , thus the band centre is shifted from water monomer band in the region of large (ice-like) clusters. The area under the absorption curve is proportional to the number of molecules departing from the sample during the interval between measurements (10 min), i.e. to the evacuation rate of the molecules. The figure shows that the rate of water removal from the healthy bone does not obey the exponential law and behaves non-monotonically. All these three factors (the band centers, its variability during vacuum pumping and evacuation rate) clearly indicate that healthy bones have distinct nanoporous structures whose dimensions are close to 10 nm.

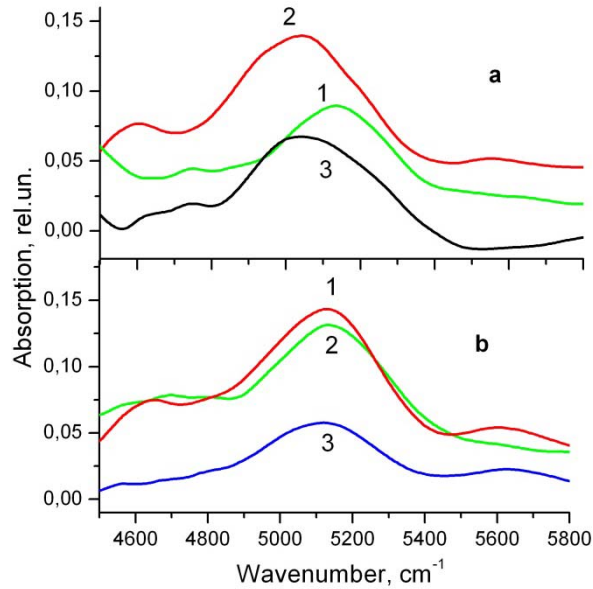


Figure 6.3. The absorption spectra of H₂O in bone of healthy (a) and osteoporotic (b) rats in the 4570-5800 cm⁻¹, recorded in 10 (1), 30 (2), 50 (3), minutes after the start of vacuum pumping

Osteoporotic bones

As seen from Figure 6.3, *b* maximum of the water absorption band (5250 cm⁻¹), in the osteoporotic bone is situated closer to absorption of bulk water, in the spectrum there are no bands characterising ice-like water clusters; and there is no variability during water evacuation from the bones. The area under the absorption curves, which is proportional to the number of molecules departing from the sample during the interval between measurements, decays exponentially. All these three factors (the band centers, its variability during vacuum pumping and evacuation rate) indicate that osteoporotic bones have lost nanoporous structures, and represent an object with larger pores.

Thus, the spectroscopic investigation of water absorption in the bones supports the increase of ultra-thin channels of collagen fibrils in osteoporotic bones in comparison with healthy ones. Therefore, it is possible to maintain that a main factor in the formation of osteoporosis is deformation of ultra-thin sections of the main channels of collagen fibril of bone matrix:

- a) the cross-section of the channels in the case of osteoporosis increases as compared with the size of the channels of healthy bones;
- b) mineral phase undergoes amorphisation and the thickness of the hydration shell nanocrystals of HAP increase;
- c) the viscosity of water in the bone matrix increases. This contributes to the loss of the ability of collagen fibrils of channels to catalysing the crystallisation of hydroxyapatite.

PART 3. METHODS OF ELECTRONIC SPECTROSCOPY FOR BIOMEDICINE

LECTURE 7. GENERAL SCHEME OF PHOTO PHYSICAL PROCESSES

Interactions between molecules can be both relatively weak and strong; they can exist directly between molecules or can be transmitted through the environment. Such interactions are of great importance to photophysics and photochemistry of molecules and various chemical and biological phenomena. It is difficult to run the properties of a single molecule; however, properties of a complex can be modified by means of a proper medium. It provides an opportunity to manage parameters of photophysical and photochemical processes of organic molecules in solutions. Therefore, it is necessary to study the influence of intermolecular interactions on photoprocesses in molecules.

When considering the conversion of energy of the absorbed photon in complex molecular systems, attention was always paid to the deactivation of electronically excited states, i.e. to the processes leading to decrease in the electronic energy of excitation. Deactivation processes can be determined by both intra- and intermolecular interactions. Mainly the former type will be further considered. Intermolecular interactions more often modify energy systems of states (thus, changing the ratio of deactivation channels), whereas the principle of this or that mechanism of deactivation, as a rule, is determined by the peculiarities of intramolecular interactions.

Naturally, deactivation processes are radiative and non-radiative. Spontaneous radiation of molecules accompanying the transition between two electronic states is called luminescence. Radiative transition $S_i \rightarrow S_0$ is fluorescence and $T_i \rightarrow S_0$ – phosphorescence. Non-radiative deactivation processes are non-optical (not directly accompanied by the photon radiation) transitions between electronic states where the difference in electronic energies is fully or partially transferred to nuclei and realised in vibrational motion.

To date, term “processes of non-radiative conversion” is widely used in scientific literature and will be further used in the lecture. Non-radiative transition between states of common multiplicity is called internal conversion, between states of different multiplicity – intercombination conversion. Non-radiative transition into the ground electronic state is often called degradation.

Figure 7.1 represents a typical scheme of photophysical processes occurring in polyatomic molecules after the absorption of light quantum

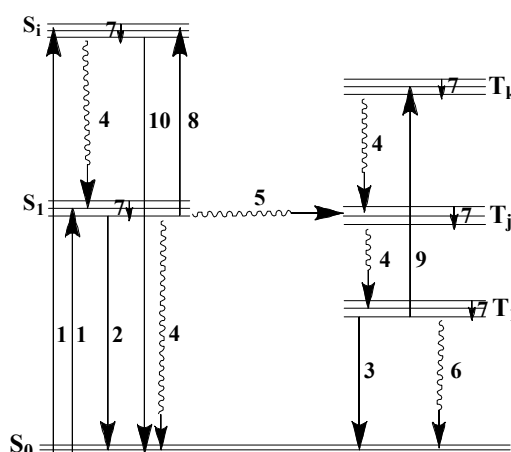


Figure 7.1. General scheme of photophysical processes occurring in polyatomic molecule

All the photophysical processes are numbered: 1 – absorption, 2 – fluorescence (radiative $S_i \rightarrow S_0$); 3 – phosphorescence; 4 – internal conversion; 5 – singlet-triplet conversion; 6 – $T_1 \rightarrow S_0$ conversion; 7 – vibrational relaxation; 8 – $S_1 \rightarrow S_i$ absorption; 9 – $T_1 \rightarrow T_k$ absorption; 10 –

luminescence from the highest electronic states. The main task for the researchers in photophysics of polyatomic molecules consists in finding the laws of interrelation of photophysical processes with the structure of molecule, conditions of excitation and intermolecular interactions.

Ratio of the number of emitted photons to the total number of the absorbed ones is a quantum yield of fluorescence γ . It can be said that in absence of any other processes but fluorescence and non-radiative conversion the quantum yield can be calculated according to the relation

$$\gamma = k_r (k_r + k_{nr})^{-1}, \quad (7.1)$$

where k_r and k_{nr} – rate constants (probability) of radioactive decay and non-radiative conversion.

The rate constant of radioactive decay k_r is calculated by the formula. The power of oscillator can be calculated on the basis of the experimental data by formula

$$f_{if} = 4.32 \cdot 10^{-9} \int \varepsilon_\nu d\nu, \quad (7.2)$$

where $\int \varepsilon_\nu d\nu$ – integral absorption, ε_ν – decimal molar absorption coefficient.

It is obvious that in absence of the conversion γ would be 1. Thus, experimental confirmation of the existence of non-radiative deactivation consists in measuring the quantum yield of fluorescence which is usually smaller (sometimes considerably) than one in both condensed and gaseous phase (including diluted molecular vapours, when the lifetime of the excited state is smaller than the time between molecular collisions, and molecules may be considered as isolated).

Phenomenon of decreasing γ under the influence of any internal or external factors is called “quenching”. Chemical and structural changes can occur in optically excited electronic states; these processes are called photochemical in comparison with the processes that do not lead to similar changes and are called photophysical. Fluorescence, phosphorescence, intercombination and internal conversion are photophysical processes. Their peculiarity consists in the presence of two electronic states – initial and final with respect to the process. There is also one more type of photophysical processes which occurs within the same electronic state. This is vibrational relaxation, which represents the process of establishing an equilibrium energy distribution over the vibrational levels of the electronically excited state due to the interaction with the environment. Moreover, excess of the equilibrium value over the vibrational energy in the electronically excited state is transferred to the environment.

Similar process may also occur in an isolated molecule which does not interact with the environment (for example, diluted vapours), virtually, redistribution of the vibrational energy over the vibrational degrees of freedom (over normal modes or oscillators) determined by the intramolecular interactions (anharmonicity of vibrations). The process is called the intramolecular vibrational redistribution; unlike the vibrational relaxation it does not always lead to the establishment of equilibrium distribution of the vibrational energy over vibrational degrees of freedom.

Tasks

1. Explain the dependencies for $\gamma_{fl.}$, $\gamma_{phos.}$, k_{ST} (Table 7.1) of the naphthalene substituted

Table 7.1

Quantum yield of fluorescence, phosphorescence, rate constant of the intercombination conversion for naphthalene and its substituted

Molecule	$\nu_{0,0}^{fl.}$ cm ⁻¹	$\nu_{0,0}^{phos.}$ cm ⁻¹	$\gamma_{fl.}$	$\gamma_{phos.}$	$\gamma_{fl.} / \gamma_{phos.}$	$\tau_{phos.}$	$k_{ST} \cdot s^{-1}$
Naphthalene (H)	31750	21250	0.55	0.051±0.003	0.093	2.3±0.1	~10 ⁵
1-Methyl -H	31450	21000	0.85±0.1900	0.044±0.013	0.053	2.1±0.1	~2·10 ⁵
1-Oxy -H	30775	20600	0.76±0.0400	0.036±0.004	0.047	1.9	~2·10 ⁵
1-Fluorine-H	31600	21150	0.84±0.0080	0.056±0.009	0.068	1.5	~2·10 ⁵
1-Chlorine-H	31360	20700	0.058±0.0050	0.30±0.006	5.2	0.29±0.01	~1.5·10 ⁷
1-Bromine-H	31280	20650	0.0016±0.0005	0.27±0.040	164	2.0·10 ⁻²	~5·10 ⁸
1-Iodine-H	–	20500	<0.0005	0.38±0.060	>1000	2.0·10 ⁻³	>3·10 ⁹

Data refer to glassy solutions at 77K

2. Calculate the lower limit of the rate constant of the internal conversion from state S₂ into state S₁ for the molecule with its own lifetime of fluorescence $\tau_f = 10^{-8}$ seconds and quantum yield $\gamma_f = 0.1$. Quantum yield and emission spectrum of the molecule do not depend on the wavelength of the exciting light, quantum yield of fluorescence from state S₂ is less than 10⁻⁴.

Basic laws of deactivation of electronically excited states

A common term of fluorescence was given by S.I. Vavilov: “Luminescence is an excess over the body thermal emission, if the excess has its final duration exceeding the period of light vibrations.”

1. Vavilov’s law states that quantum yield of fluorescence in condensed phase at excitation of Stoke region does not depend on the energy of absorbed quantum.

Observation of Vavilov’s law in condensed media is associated with the fact that intermolecular interactions cause fast transfer of the excess over the equilibrium value of the vibrational energy in electronically excited states into the medium. Despite its versatility, Vavilov’s law is often violated. Violations of the law are possible:

- if in heterocyclic compounds the value of the energy gap between S states of $\pi\pi^*$ ($n\pi^*$) type and underlying T states of $n\pi^*$ ($\pi\pi^*$) type is less than $\approx 2000 \text{ cm}^{-1}$, which results in competition between intercombination conversion $S_{\pi\pi^*} \rightarrow T_{n\pi^*}$ and vibrational relaxation;
- if there are conformers with various spectral-luminescent properties;
- in case of photochemically unstable systems, when there is an energy transfer from highly excited states; other relaxation processes depending on the excitation energy may also occur.

2. Kasha’s rule states that for the majority of molecules the internal conversion between electronically excited states lasts $< 10^{-11}$ seconds, and obvious luminescence yield ($\gamma \geq 10^{-3}$) may be observed only for transitions from the lower excited state of the multiplicity.

Kasha’s rule, as well as Vavilov’s law, is a result of the existence of fast relaxation processes occurring in the electronically excited states of molecules.

3. Ermolaev-Sveshnikova rule states that intercombination conversion serves as the main channel for non-radiative deactivation in many photostable molecules in condensed phase.

Experimentally confirmed rules of Kasha and Ermolaev-Sveshnikova are the results of a common law concerning the correlation of the effectiveness of the internal conversion with the energy gap between electronic states. Dependence of the constant rate of the internal conversion (k_{ic}) on the energy slit was calculated by V.G. Plotnikov and B.A. Dolgikh and is represented in Figure 1.8.1 (hatched is the region of most typical values of the rate constants of radioactive decay (k_r) and singlet-triplet conversion (k_{ST}) for well luminous molecules).

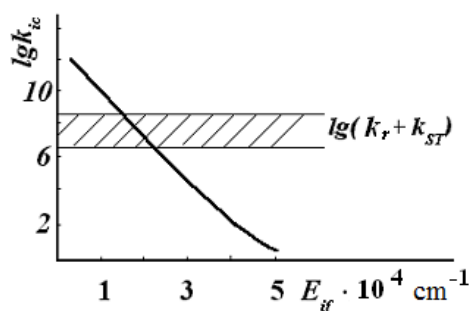


Figure 7.2. Dependence of the rate of internal conversion on energy gap

Analysis of Figure 7.2 demonstrates that it is possible to distinguish three characteristic regions of values of the energy gap between electronic states. In the first region ($< 10^4 \text{ cm}^{-1}$), i.e. internal conversion is the main channel for deactivation (region where Kasha's rule is satisfied). In the second region ($10^4 \leq 2 \cdot 10^4 \text{ cm}^{-1}$), i.e. radiation and internal conversion compete. The third region ($\leq 2 \cdot 10^4 \text{ cm}^{-1}$) corresponds to characteristic values of energy gaps between S_1 and S_0 states in aromatic and heteroaromatic molecules. In this case, since $k_{ic} < k_r + k_{ST}$, dominant channels for deactivation are radioactive decay and $S \rightarrow T$ conversion, which complies with Ermolaev-Sveshnikova rule.

4. Stokes' law was discovered in 1852. Essentially, Stokes' law states that there is a difference between positions in the spectrum of the maxima of bands (or the beginning of bands) of absorption and luminescence determined by the same electronic transition. As a rule, there is always observed the emission shift relative to absorption towards longer wavelengths, i.e. there is energy loss (except for atoms in gas phase). A typical value of Stokes' shift in organic molecules is $10^3 - 10^4 \text{ cm}^{-1}$. Usually, luminescence observed on the longer wavelength than absorption is stronger than luminescence observed on the shorter one than absorption. The latter can be called anti-Stokes' shift.

Figure 7.3 explains Stokes' shift. It illustrates two electronic states of the molecule which are involved into absorption and radiation. It is necessary to take into account the Franck-Condon principle and presence of the relative shift of minima of potential curves of excited S_1 and ground S_0 states in order to explain Stokes' shift.

According to the Franck-Condon principle, absorption and fluorescence (lines 1 and 2 in Fig. 7.3, respectively) will be without changes in internuclear distances. Moreover, since minima of potential curves are shifted, at absorption (fluorescence) a molecule will be in the excited vibrational state. Then, due to actually continuous collisions of molecules in liquid phase relaxation occurs (lines 3 in Fig. 7.3) during about 10^{-12} seconds on the lower vibrational levels of states S_1 or S_0 after absorption or fluorescence respectively. Vibrational relaxation processes, as it can be seen in Figure 7.3, leads to the absorbed energy loss, i.e. decrease in the radiation energy with respect to the absorption energy. Consequently, the radiation frequency declines in comparison with the absorption frequency; therefore, the wavelength increases, thus, explaining Stokes' shift. In gas phase of atoms and molecules Stokes' shift is not always observed due to insufficient gas concentration for excited molecules to collide with other molecules before emission.

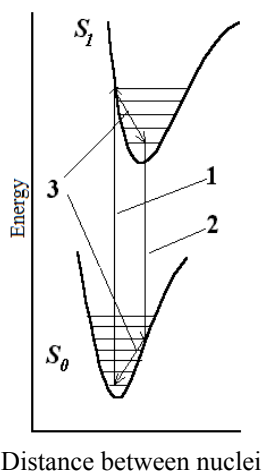


Figure 7.3. Stokes' shift. 1 – absorption; 2 – fluorescence; 3 – vibrational relaxation.

Questions

1. Why the mirror-symmetry rule of the spectra of absorption and fluorescence is often approximate?
2. According to the law, will be there a quenching of 1-naphthol in alcohol solution with added water (50% water and 50% alcohol)?

LECTURE 8. SPECTRAL-LUMINESCENT PROPHECIES OF MOLECULES AND INTERMOLECULAR INTERACTIONS

8.1 Classification of intermolecular interactions

There are various types of intermolecular interactions (IMI) which can be divided into two large groups: universal and specific. The universal implies the interactions which occur at all the situations without exceptions. Here belong common van der Waals forces of orientation, induction and dispersion nature and repulsive forces. Different authors call interactions of this group as massive, long-range or universal [13 – 24]. The energy of a universal IMI is determined by physical properties (dipole moment, polarizability, ionic potentials) of interacting molecules. On the contrary, specific interactions, which do not occur in every system and are naturally individual, i.e. peculiar to a pair of interacting particles, have high selectivity with respect to the properties of molecules and lead to formation of more or less strong donor-acceptor bond between them. Common examples of specific interactions are presented by complexes formed by means of hydrogen bonding and complexes of the donor-acceptor type, associates of molecules.

The classification considerably simplifies the analysis of experimental material, as well as allows us to see contributions of IMIs of different types based on summary effects observed in experiments. Actuality of the task is explained by the fact that specific IMIs (if they occur) always appear on the background of the universal influence of a medium.

Studies of spectral-luminescent properties of molecules can be conducted in various phases (gas phase, solution, liquid, solid body, etc.), however the research into properties of molecules in solutions is the most popular.

8.2 Main processes in solutions

Solutions are homogeneous liquid phases consisting of several substances in non-constant relations. For convenience, one of the substances called solvent, which may also be a mixture, is considered separately from other substances called solutes.

Solvent must be considered as a discrete phase consisting of numerous individual interacting molecules. Degree of interaction can widely vary: some solvents (for example, water) are characterised by deep internal structure, others – insignificant intermolecular interactions.

Mutual solubility of two substances is determined by interactions between the molecules of solute and solvent. Compound *A* dissolves in solvent *B* only when interaction forces K_{AB} in the solution can overcome intermolecular attraction forces K_{AA} and K_{BB} acting in relevant pure compounds.

The total effect of interactions between molecules of solvent and solute is usually associated with polarity of *A* and *B*. If strongly interacting compounds are called *A – A* and *B – B* polar, and weakly interacting – non-polar (a-polar), there are four situations that allow us to qualitatively predict mutual solubility of substances (Tab. 8.2.1).

Table 8.2.1

Correlation between solubility and polarity

Solute, <i>A</i>	Solvent, <i>B</i>	Interaction			Solubility of <i>A</i> in <i>B</i>
		<i>A – A</i>	<i>B – B</i>	<i>A – B</i>	
Non-polar	Non-polar	Weak	Weak	Weak	Can be high
Non-polar	Polar	Weak	Strong	Weak	Probably low
Polar	Non-polar	Strong	Weak	Weak	Probably low
Polar	Polar	Strong	Strong	Strong	Can be high

Studying the properties of molecules in solutions is extremely important for various scientific fields. Knowledge can be applied both in theory and practice. Of particular importance is the use of studies in medicine and ecology, as well as biology and chemical technologies. After thorough studies [25], researchers proved that solvents greatly affect the rate of chemical and photochemical reactions [26–27].

The rate of a chemical reaction is associated with a dielectric permeability of the solvent. Applying the Kirkwood equation to the transition state theory for biomolecular reactions



where $A + B$ – reagents, $(AB)^\ddagger$ – activated complex, $C + D$ – reaction products, we can formulate the following expression for the rate constant of reactions between two bipolar compounds A and B with dipole moments μ_A and μ_B forming the activated complex with dipole moment μ_\ddagger :

$$\ln k = \ln k_0 - \frac{1}{4\pi\epsilon_0} \frac{N_A}{RT} \frac{\epsilon_r - 1}{2\epsilon_r + 1} \left(\frac{\mu_A^2}{r_A^3} + \frac{\mu_B^2}{r_B^3} - \frac{\mu_\ddagger^2}{r_\ddagger^3} \right). \quad (8.2.2)$$

Here, k – reaction rate constant in any medium with dielectric permeability ϵ_r , μ_A and μ_B – dipole moments of two bimolecular reagents A and B in vacuum, k_0 – rate constant of the same reaction in the condensed phase with dielectric permeability of one. As it can be seen from the equation (8.2.1), reaction rate will increase at increasing dielectric permeability of the medium, if activated complex is more polar than reagents.

Influence of the dielectric permeability of the medium on the reaction rates is expressed by:

$$\ln k = \ln k_\infty - \frac{1}{4\pi\epsilon_0} \frac{2\mu_A\mu_B N_A}{RT\epsilon_r r^3}, \quad (8.2.3)$$

where k_∞ – reaction rate constant in the medium with infinitely high dielectric permeability.

It must be noted that linear dependencies $\ln(k/k_0)$ on $(\epsilon_r - 1) / (2\epsilon_r + 1)$ and $1/\epsilon_r$ expressed by equations (2) and (3), respectively, do not contradict each other. Dividing $(\epsilon_r - 1)$ by $(2\epsilon_r + 1)$ we find that $(\epsilon_r - 1) / (2\epsilon_r + 1)$ with a good approximation depends on $1/\epsilon_r$. At $\epsilon_r = 8$, error associated with neglecting the terms of the second and higher order does not exceed one percent [25].

Rates of photochemical reactions are also significantly affected by the solvent. It can be noticed on the example of the benzophenone molecule. In some solvents (for example, water or benzene) the quantum yield of photorecovery of benzophenone is close to zero (0.02 – 0.05); in other solvents (ethanol, hexane) the quantum yield linearly depends on the concentration of benzophenone and tends to limit value of one [26]. In isopropyl alcohol the quantum yield depends on the concentration of benzophenone and tends to limit value of 2 [26].

Numerous processes occur in solutions, the main of them fall into three groups: solvation, hydration and association. Solvation is a sum of all the processes accompanying the transfer of a studied particle from the state where it is maximally isolated from the interaction with other particles (ideal gas) into solution. If solvent is water, the process is called hydration. Solvation does not include processes which lead to destruction of compounds in the molecules of solvent or solute (dissociation, hydrolysis, etc.) [25].

Association is an association of individual particles into an aggregate: interaction of dissolved molecules between each other, interaction of the solvent molecules with each other, interaction of oppositely charged ions in ion pairs and clusters of ions.

It is difficult to study solvation and association due to the lack of sequential theory of solutions, impossibility of dividing different processes and studying them individually. Before describing these processes, we need to study the properties of solvents.

8.3 Classification of solvents

Differences in physical properties between multiple organic and non-organic solvents make classification of solvents rather complicated. Physical characteristics are used to describe the properties of solvents such as refractive index, density, viscosity, dipole moment, dielectric permeability (ϵ), and polarizability. Dipole moments and dielectric permeability are often used to quantitatively describe the polarity of solvents. Dielectric permeability is directly associated with the ability of solvent to split charges and orient its own dipoles. Solvents with high dielectric permeability and solvents whose molecules have a permanent dipole are called polar. Solvents with lower ϵ and dipole moment of zero are called non-polar (a-polar), unlike solvents with high (ϵ). The closer to zero is the value of dipole moment of the solvent molecules, the less polar it is.

Polarity of a solvent can be approximately estimated by means of separate physical characteristics (dielectric permeability, dipole moment, refractive index). Since the concept of polarity of solvent is ambiguous, solubility of solvent (its solvating properties) cannot be described with sufficient accuracy. Polarity is also treated as molecular properties of interacting molecules (dipole moment, polarizability, donor-acceptor properties of dissolved molecule and solvent, dielectric permeability and refractive index of solvent). A sum of these properties defines the solvent solubility.

Obviously, polarity of solvent cannot be described by one physical parameter. Ideally, it requires quantitative measuring (empirical parameter) of the solvent polarity which reflects a total effect of IMIs occurring in the solution and, consequently, describe the solvent polarity more precisely than any individual physical parameter.

Such attempts have been made. Moreover, influence of the solvent on a depending standard process (for example, speed or equilibrium of chemical reaction, absorption band position) was used. Let us consider empirical parameters of polarity of solvents which were found due to solvatochromic effect. Mostly, they reflect values of combined IMIs acting in the solution; therefore, they serve as a more common characteristic of the solvent solubility than individual physical constants.

It is convenient to use a molar energy of the electronic transition from MCT (molecular charge transfer) E_T (expressed by $\text{kcal}\cdot\text{mol}^{-1}$) in the solvent as a parameter of the solvent polarity Z :

$$E_T = hc\nu N_A = 2.859 \cdot 10^{-3} \nu \equiv Z, \quad (8.3.1)$$

where h – Planck constant, ν – wavenumber of the photon inducing electronic excitation (cm^{-1}), N_A – Avogadro constant. Parameter of Z varies within the range from 94.6 $\text{kcal}\cdot\text{mol}^{-1}$ (water) to approximately 60 $\text{kcal}\cdot\text{mol}^{-1}$ (isooctane). Primarily, there were determined Z parameters of 21 pure solvents and their 35 binary mixtures, as well as solutions of some electrolytes and surfactants. The list was further extended to 45 pure solvents.

Nevertheless, it turned out that determination of Z parameters is associated with some practical problems. Dimroth and Reichardt [25] proposed the parameter of the solvent polarity $E_T(30)$ based on the dependence on the solvent of the electronic transition energy, which the band of the long-wave absorption of solvatochromic N-phenoxypyridine-betaine (NPB) corresponds to. $E_T(30)$ parameter of the solvent is equal to the electronic transition energy (expressed by $\text{kcal}\cdot\text{mol}^{-1}$) of the NPB dye in the solvent. The advantage of the NPB dye consists in the fact that its absorption band depending on the solvent is located in the region of longer waves, which permits recording the solvatochromatic effect in the extremely wide range: from $\lambda = 810$ nm (diphenyl ether, $E_T(30) = 35,3$ $\text{kcal}\cdot\text{mol}^{-1}$) to $\lambda = 453$ nm (water, $E_T(30) = 63,1$ $\text{kcal}\cdot\text{mol}^{-1}$).

Although, $E_T(30)$ parameters, by definition, have a non-systemic unit $\text{kcal}/\text{mol}^{-1}$ and cannot be combined with units expressed in SI units. Therefore, the so-called normalised option is used E_T^N [25]:

$$E_T^N = \frac{E_T(\text{solvent}) - E_T(\text{TMS})}{E_T(\text{water}) - E_T(\text{TMS})} = \frac{E_T(\text{solvent}) - 30.7}{32.4} \quad (8.3.2)$$

In this case, standard solvents with extreme polarities are water and tetramethylsilane (TMS). In accordance with their value, parameter changes within the range from 0 (TMS) to 1 (water). In accordance with the value, solvents approximately can be divided into three groups. The first group includes proton solvents (donors of hydrogen bond) – $\approx 0.5 \div 1.0$, the second – polar solvents – $\approx 0.3 \div 0.5$, and the third – a-polar solvents – $\approx 0.0 \div 0.3$.

Kamlet, Taft et al. [28] proposed parameters of β – basicity, α – acidity of solvents and π^* – parameter of polarity and polarizability of solvents using the solvatochromic comparison method.

Basicity defines the ability of solvent to receive a proton, i.e. to be an acceptor of the hydrogen bond. On the contrary, acidity implies a donor ability of solvent, i.e. ability to donate a proton engaged in the hydrogen bond. Both parameters vary within the range from 0 to 1.

The name of π^* parameter reflects the influence of solvents on the electronic transition $\pi\pi^*$ in different nitroaromatic compounds (4-nitroanisole, N, N-diethyl-3-nitroaniline, 4-methoxy- β -nitrostyrene, 1-ethyl-4-nitrobenzene, N-methyl-2-nitro-n-toluidine, N, N-diethyl-4-nitroaniline and 4-dimethylaminobenzophenone). Thus, the averaged π^* – scale of polarity and polarizability was developed. It reflects their relative ability to stabilise a charge or a bipolar structure by means of their dielectric permeability. It is assumed that the normalised π^* parameter of solvents varies within the range from 0 (cyclohexane) to 1 (dimethylsulfoxide).

To evaluate donor and acceptor properties of solvent there are donor DN and acceptor AN numbers. Unlike acidity and basicity, donor and acceptor numbers are micro-characteristics of the medium. These parameters are obtained by measuring chemical shifts of the signal in the NMR spectrum.

A donor number, as Gutmann proposed, is taken equal to the negative value ΔH (enthalpy) of the reaction of formation of the equimolecular adduct (1:1) of the antimony pentachloride and EPD solvent (electron pair donor) in a dilute solution in the non-coordinating solvent 1,2-dichloroethane. Since donor numbers have been defined in the non-SI unit ($\text{kcal}\cdot\text{mol}^{-1}$), a scale of dimensionless (normalised) donor numbers DN^N was presented:

$$DN^N = \frac{DN}{38,8 \text{ kcal}\cdot\text{mol}^{-1}} \cdot \quad (8.3.3)$$

The non-donor solvent 1,2-dichloroethane ($DN = DN^N = 0.0$) and the strong donor solvent hexamethylphosphoric triamide ($DN = 38.8 \text{ kcal}\cdot\text{mol}^{-1}$, $DN^N = 1.0$) have been used to define the scale.

The donor number has proven very useful in coordination chemistry, since it can be correlated with other physical observables for such reactions, including thermodynamic, kinetic and others.

The empirical parameter proposed by Gutmann and employees was called the acceptor number AN . It is a dimensionless value describing accepting features of the solvent in comparison with the properties of SbCl_5 (antimony pentachloride).

Swain et al. proposed the equation which helps to describe all the effects of solvents and, which contains two complementary parameters of the properties of the solvent A_j and B_j expressing the ability of the solvent to solvate anions and cations and called acity and basity of the solvent, respectively:

$$A = A_0 + \alpha_i A_j + b_i B_j \cdot \quad (8.3.4)$$

In the equation, A_j and B_j define the j solvent, and A and A_0 , and coefficients of multiple regression of α_i and b_i are determined only by the studied solute i . Furthermore, α_i and b_i constants reflect the sensitivity of the A parameter of the i matter to changing nature of the solvent. Swain et al. proposed to use the sum of parameters A_j and B_j ($A_j + B_j$) to evaluate the solvation on anions and cations [29]. Parameter ($A_j + B_j$) should be considered as a measure of the polarity of solvent, if polarity is understood as its general solvating power.

However, the disadvantage is that the above parameters are only defined for a limited number of solvents. The parameters of polarity are quite often used in studying the spectral properties of molecules as characteristics of solvents [30]. It must be noted that using several parameters at once may result in obtaining a generalised criterion of polarity of solvents used in highly effective liquid chromatography.

Among the advantages of the empirical approach are very high coverage of experimental data and the possibility of a more effective choice of solvents in the formation of a solvation shell of molecule. Nevertheless, a number of significant disadvantages inherent to the approach should be also kept in mind: plurality of scales of solvents often related to each other by a linear dependence and problem of choosing the “best” scale (parameter).

Empirical parameters of polarity for some solvents used in the manual are presented in Table 8.3.1.

Table 8.3.1

Polarity of some solvents

Solvent		π^*	A_j+B_j	AN	DN ^N	α	β
Hexane	0.009	-0.08	–	0	–	0	0
Triethylamine	0.043	0.14	0.27	1.4	0.82	0	0.71
Carbon tetrachloride	0.052	0.28	0.43	8.6	–	0	0
Acetone	0.355	0.71	1.06	12.5	0.44	0.08	0.48
Acetonitrile	0.460	0.75	1.22	18.9	0.36	0.19	0.31
Nitromethane	0.481	–	1.31	20.5	0.07	–	–
Propanol	0.617	0.52	1.08	37.3	–	0.78	–
Isopropanol	0.546	0.48	1.03	33.6	–	0.76	0.95
Ethanol	0.654	0.54	1.11	37.9	–	0.83	0.77
Methanol	0.762	0.60	1.25	41.5	–	0.93	0.62
Water	1	1.09	2.00	54.8	–	1.17	0.47

The most frequently used parameter of polarity is dielectric permeability. Table 8.3.2 for the same solvents contains ϵ value and its function $f(\epsilon)$. Data presented in the table were obtained at 25°C.

Table 8.3.2

Parameters describing polarizability of solvents

Solvent	ϵ	n	$\eta \cdot 10^3$, mP	$f_1(\epsilon)$	$f_2(\epsilon)$	$f(n)$	Δf
Hexane	1.88	1.3749	2.92	0.18487	0.11340	0.18623	-0.00136
Triethylamine	2.42	1.4010	3.94	0.24315	0.16063	0.19546	0.04769
Carbon tetrachloride	2.23	1.4602	9.69	0.22527	0.14539	0.21506	0.01021
Acetone	20.56	1.3587	3.16	0.46438	0.45361	0.18030	0.28408
Acetonitrile	36.20	1.3441	3.45	0.47941	0.46046	0.17484	0.30457
Nitromethane	38.60	1.3819	6.08	0.47941	0.46046	0.18875	0.28616
Propanol	20.45	1.3856	20.0	0.46420	0.45337	0.19006	0.27414
Isopropanol	19.92	1.3772	17.7	0.46327	0.43156	0.18706	0.27621
Ethanol	24.55	1.3614	10.8	0.47005	0.44350	0.18131	0.28874
Methanol	32.66	1.3284	5.45	0.47738	0.47029	0.16882	0.30856
Water	78.30	1.3330	10.1	0.49048	0.44281	0.17060	0.31988

The dielectric constant defines polarity of the solvent. It includes the influence of re-orientation of the solvent molecules. Due to slower re-orientation of molecules, $f(\epsilon)$ the component is called a low-frequency polarizability of the solvent. There are two formulas to define it: Kirkwood-Onsager formula (8.3.5) and Lorentz formula (8.3.6):

$$f_1(\varepsilon) = \frac{\varepsilon - 1}{2\varepsilon + 1}, \quad (8.3.5)$$

$$f_2(\varepsilon) = \frac{\varepsilon - 1}{2(\varepsilon + 1)}. \quad (8.3.6)$$

High-frequency polarizability is a function of refractive index $f(n)$ and is defined from the following relation [31]:

$$f(n) = \frac{n^2 - 1}{2n^2 + 1}. \quad (8.3.7)$$

The difference between high-frequency and low-frequency polarizability is called the orientation polarizability of the solvent and is equal to Δf :

$$\Delta f = \frac{\varepsilon - 1}{2\varepsilon + 1} - \frac{n^2 - 1}{2n^2 + 1}. \quad (8.3.8)$$

Values n , $f(n)$ and Δf for the selected solvents are demonstrated in Table 8.3.2. η defines viscosity of a solvent. If the dipole moment of a solvent is equal to zero, $\varepsilon \approx n^2$ and $\Delta f = 0$. According to Δf values, we can judge the value of spectral shifts for various solvents. However, according to the results [32] concerning the research based on the molecules of coumarin-153 and coumarin-120, Δf parameter does not reflect all the effects of the solvent.

Tasks

Build the dependence of parameters of the solvents from Table 8.3.1 on dielectric permeability and answer the question: which parameter best describes polarity? In what region?

8.4 Binary solvents

The study of intermolecular interactions between molecules of solute and solvent has great theoretical and practical importance. Of particular interest to the practice are multicomponent systems. Application of these systems permits selecting solvents in the way that it is possible to study any type of intermolecular interaction, since each solvent has individual physical and chemical properties, i.e. binary solvents make predictions of spectral-luminescent properties possible; they also permit modelling various types of interactions for the molecule.

Sometimes, it is necessary to get a small change in dielectric permeability. Binary solvent is used to obtain this. Let us provide the example of the use of a binary solvent to obtain the needed change in dielectric permeability. Dielectric permeability of a binary mixture of solvents is calculated by the formula:

$$\varepsilon_{mix} = \varepsilon_1 \times C_1 + \varepsilon_2 \times C_2, \quad (8.4.1)$$

where ε_1 , C_1 , ε_2 , C_2 are dielectric permeability and concentration (share, %) of the first and the second components of the mixture, respectively. The formula does not take into account the interaction of components of the mixture. However, it can be used to approximately define ε of the mixture.

Let us consider water-ethanol mixtures as the example. Water has $\varepsilon \approx 78$, and ethanol has $\varepsilon \approx 24$. According to the formula, when fitting various concentrations of water and alcohol we may significantly change the value of dielectric permeability within the range from 24 to 78. For example, at concentration in the mixture of 30% water and 70% ethanol ε of the mixture is ≈ 40.2 , and in the mixture of 70% water and 30% ethanol – ≈ 61.8 .

The experimental results on dielectric permeability of mixtures of different solvents are listed in [33].

Studying binary mixtures (analysing the response of absorption bands, fluorescence bands, or changes in the intensity of fluorescence depending on the content of a solvent) can provide us with information about the content of the solvent shell of the molecule.

Task

Calculate function $f(\varepsilon)$ for the mixtures of hexane+ethanol when added ethanol is 5, 10, 20, 50 and 80%; volume of the mixture is 10 cm³. Compare the results with the experimental data in [33].

LECTURE 9. SOLVATION OF MOLECULES AND ITS SPECTRAL MANIFESTATION

9.1 Solvation

Solvation is one of the most important phenomena occurring in solution of chemical substances. Driving force of solvation is intermolecular interactions between solute and solvent. Research into ions and molecules in mixtures of solvents is getting more difficult; therefore, besides interactions between solvent and solute, of great importance is the interaction between molecules of different solvents. The fact that the content of the first coordination sphere of the solvation shell (i.e. the nearest neighbours) differs from the bulk composition was called selective solvation. If a molecule in the mixture of two solvents has two centres and they are solvated by the same solvent, the term applied is homoselective solvation; if one centre is solvated by one solvent, and another – by the other solvent, it is termed heteroselective solvation.

Measure of the solvation energy of molecule (ion) is the standard molar Gibbs energy of solvation, i.e. the transfer of a molecule (ion) from the gas phase into the solution [25]. The absolute value of free energy of solvation of protons in water is very high – 1089 kJ / mol.

To evaluate possible centres of solvation of molecules we can use the distribution of the electronic density as the authors in [34] did for the molecules of coumarin-153 and coumarin-151. The authors demonstrated that a positive charge is located on a nitrogen atom of aminogroups of coumarin-153 and coumarin-151; whereas negative is distributed over some atoms of carbon of aromatic skeleton, which, consequently, helps to explain how molecules of the solvent can be located in the first coordination sphere.

The molecular electrostatic potential method (MEP) can be used to consider the interaction of a molecule with proton-donor solvents (to find centres of solvation). MEP is defined as the energy of the electrostatic interaction of nuclei and electronic distribution of molecules with a positive point charge placed into the point of space surrounding the molecule. For example, for 1-naphthol molecule (Fig. 9.1.1) results of the MEP proved the presence of the centre of solvation close to the oxygen atom both in the ground and in the second excited states. Moreover, the minima over the aromatic skeleton of the molecule are observed at distance of 1.5 Å from the density of the molecule in S₁ state.

According to [25], there are primary (chemical) and secondary (physical) solvation. Primary, chemical solvation refers to the “hard” bonding of the solvent with the molecule in the first coordination sphere. Secondary, physical or dielectric solvation – partial ordering of more remote molecules of the solvent outside the primary solvation shell.

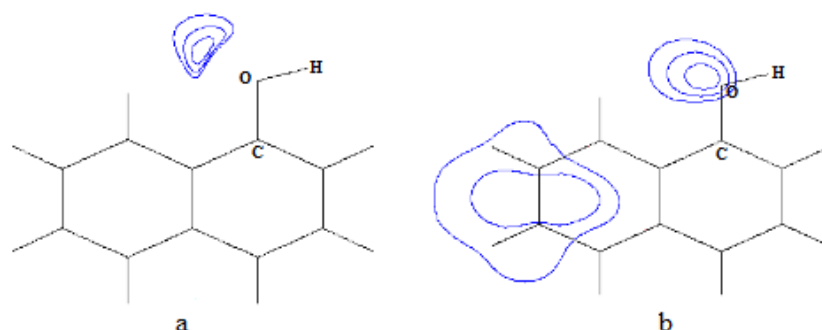


Figure 9.1.1. Maps of isolines IRENA for the 1-naphthol molecule, S₁ state: in the plane of the molecule (a), removed from the plane of the molecule by 1.5 Å (b)

The work [35] is devoted to the selective non-specific solvation (re-solvation); it defines the process as a change in the content and properties of the solvation shell caused by a tendency of the system to decrease free energy by means of non-specific IMIs. Of a particular interest are the results

referring to the solute molecules whose solvation shells contain (besides neutral) only one molecule of the active component of a binary solvent, since particularly the solvates of this content provide the most favourable conditions for a paired non-linear dipole-dipole interaction leading to the formation of highly ordered molecular structures (primary solvation complex) where energy of the orientation interaction reaches its maximum value. The authors of [36] consider solutions of two dyes in a set of binary solvents where n-heptane serves as a neutral component, and active components were organic, mainly, polar liquids (benzene, toluene, hexane, dimethylformamide, etc.). From spectral shifts of the fluorescence bands for binary mixtures the authors conclude that orientation IMIs significantly contribute to the value of the solvation shift (except for the cases when benzene and toluene were used as the active components). The conclusion is based on the comparison of the experimental value of the fluorescence band shift ($\Delta\nu_{0-1}^f$) with the calculated values of the shift ($\Delta\nu_{0-1}^{f(op)}$), i.e. defined by the influence of the orientation molecular forces. Moreover, values of spectral shifts ($\Delta\nu_{0-1}^f$) and ($\Delta\nu_{0-1}^{f(op)}$) were in satisfied agreement, nevertheless, with the range up to 400 cm^{-1} .

Thorough analysis of the results of the work demonstrated that the paper did not take into account the influence of the hydrogen bond on the fluorescence shift. The shift of the fluorescence bands at the transition from acetone to hexanol (and isobutanol) with respect to n-heptane dramatically increases by 1500 cm^{-1} . Since acetone and alcohols have slight difference in the value of dielectric permeability and are significantly different in their proton-donor ability, it may be assumed that the shift is associated with the transformation of the hydrogen bond.

The concept of solvation also includes specific interactions which are often presented by hydrogen bonds between solvent and reagents. They affect the rate, mechanism and direction of chemical reactions and define acid-base properties of organic compounds in solutions, their photochemical stability. Specific interactions in solutions emerge simultaneously with the universal ones. Therefore, evaluating a quantitative contribution of the latter requires determination and separation of spectroscopic effects associated with the complex-formation (non-specific solvation) from effects defined by the other types of IMIs. Normally, the influence of general effects of the solvent on spectra is described by the solvent function [25], but this approach actually ignores the specific (quasi-chemical, structural) interaction which considerably affects the spectral-luminescent properties of molecules. The overwhelming majority of works devoted to the influence of IMIs on absorption and fluorescence spectra of molecules deal with the research into the spectral band shift. However, this is valid only for the bands having a vibrational structure, such as molecules of 1- and 2-naphthol. Long-wave absorption bands of these molecules have a vibrational structure [37], which allows researchers to study the influence of IMIs for the complexes of the compounds. Nevertheless, if the value of the shift is significant, we cannot limit ourselves by the vibrational structure only.

Variety of the types of interactions complicates the determination of the content of the solvation shell of molecule. It must be noted that the primary solvation complex can transform in both excited and ground states. Furthermore, structure of the primary solvation shell is important for studying the complex. IRENA method can determine the centres of possible interaction of molecules with the solvent. It helps to suppose a type of the interaction, but it is impossible to calculate the molecule – solvent ratio in the solvation shell. If a researcher deals with binary mixtures, the task becomes much more complicated.

The content of the solvation shell can be determined from the absorption bands shift at changing content of the solvent. However, shifts are very small in most of the compounds (for example, 1- and 2-naphthol, etc.). Therefore, the evaluation is not always possible. Response to the content of the solvation shell is the intensity of fluorescence or shifts of the fluorescence bands depending on the content of the solvent. Let us consider the molecule of prodan in binary mixtures of isooctane+isopropanol which, as mentioned above, is extremely sensitive to the solvent by the fluorescence spectra. Maximum fluorescence of prodan in isooctane is 24820 cm^{-1} [32]. When

adding different concentrations of isopropanol to isooctane, we can observe a significant shift of the fluorescence band. Figure 9.1.2 illustrates the dependence of the fluorescence band shift on adding different concentrations of isopropanol to the solution of prodan in isooctane. By connecting the points relevant to zero and 100% concentration of isopropanol, it is possible to obtain theoretically possible dependence, i.e. the case when the content of the solvation shell corresponds to the content of the solvent. As Figure 9.1.2 illustrates, it is not observed since the points obtained from the experimental research do not lie on the line but are located higher. Therefore, the content of the solvation shell exceeds the solvent content. By projecting the point directly on the line, as shown in Figure 9.1.2, it is possible to determine the content of the solvation shell in each concrete case. For example, at 30% concentration of the isopropanol solution the solvation shell contains $\approx 69\%$ of alcohol, at 70% – about 82%.

Nevertheless, when coming to conclusion, we cannot fail to take into account that the band shift is determined not only by concrete interaction but also by dielectric permeability of the medium which can be calculated by formula (8.4.1).

The dependence can be built for the intensity of fluorescence as well, for example, for water-alcohol mixtures: $I_0 - I_i$ dependence (I_0 – intensity of fluorescence of the molecule in alcohol, I_i – intensity of fluorescence of the molecule at various concentrations of water) on concentration of water.

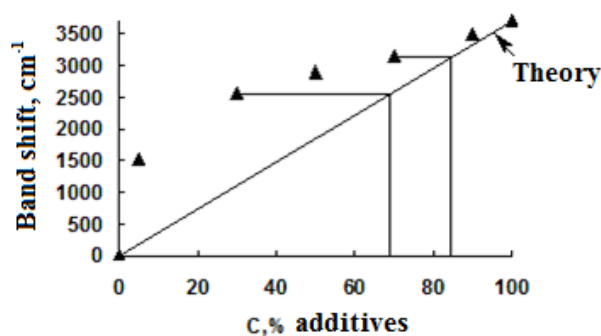


Figure 9.1.2. Dependence of the fluorescence bands shift on the concentration of isopropanol for the prodan mixture: isooctane+isopropanol

IMIs between solute and solvent serve as a driving force of solvation. However, it must be noted that more often solvation is determined by hydrogen bonds. Recently, a lot of attention has been paid to the possibility of equalising photochemical and chemical processes by including molecules (reagents) into ordered formations (micelles) [25]. Therefore, let us consider the types of specific interactions in more detail.

Task

For the molecule of aniline, demonstrate which IMIs form the solvation shell of the molecule in such solvents as water, alcohol, and acetone; how will they appear in electronic and vibrational spectra?

9.2 Hydrogen bond

9.2.1 Nature and essence of the hydrogen bond

Hydrogen bond is one of the types of specific intermolecular interactions in gases, liquids and solid bodies. Hydrogen bond is widely spread in nature and due to its strength it can be studied experimentally. The studies play an important role in physics, chemistry and biology. It defines the

structure of many biological objects and the technology of some industrial processes (adsorption, dyeing and processing of other polymeric fibers), plays a significant role in forming the spectral-luminescent properties of molecules, photochemistry, laws of the effect of pharmaceuticals, and providing vital activity of living organisms.

Let us name the molecule of proton-donor as X-H (when it is necessary to state the nature of atom covalently bound to hydrogen – R-X-H), and proton-acceptor – B (or :B-R'). Hydrogen bonds affect the redistribution of the electronic density in molecules which reflect the properties of substances. In a weak hydrogen bond changes in the electronic density are slow and lie mainly within the X–H...B fragment. When the energy of hydrogen bond increases, redistribution of the electronic density concerns all the atoms of molecules belonging to the molecular complex. As a result, there are deep changes in physical and chemical properties of substances. The hydrogen bond can appear at the interaction of acid and base groups which belong to one or different molecules. If there is an association of similar molecules, *n*-mers are formed. These interactions are widely spread and called intermolecular hydrogen bonds. They can lead to the formation of chains, rings or spatial nets.

Traditional approach to the study of hydrogen bond consists in studying the properties of complexes. Studying the dynamics of systems with the hydrogen bond is very interesting since the hydrogen bond plays a crucial role in kinetics of some processes, in particular, proton transfer and proton exchange.

The term of hydrogen bond was introduced by Huggins, in 1919. The first important work on the study of hydrogen bonds was published in 1920 by W. Latimer and W. Rodebush who worked at the laboratory of G.N. Lewis (University of California, USA), the founder of the covalent bond theory, the author of the acid-base reaction, and fruitful in organic chemistry concept of a generalised electron pair [25]. The authors explained the reason for specific physical and chemical properties of water which essentially consists in the interaction of the hydrogen atom of one molecule with electronic pairs of the oxygen atom of a different molecule. Moreover, the hydrogen atom becomes simultaneously bound to two oxygen atoms by covalent and hydrogen bonds. To date, the approach to the interpretation of the hydrogen bond has not fundamentally changed. Only the understanding of the impact of the structure of organic compounds on the formation of hydrogen bonds was clarified and methods for identifying the compounds were found. Numerous studies have been conducted to estimate the effect of hydrogen bonds on physical and chemical properties of substances.

According to modern terminology, formation of the hydrogen bond occurs at the interaction of proton-donor with proton-acceptor.



The interaction results in the formation of stable X–H...B complex with the intermolecular hydrogen bond, where the hydrogen atom serves as a bridge connecting fragments of X and B molecules [25].

Hydrogen bonds can be both intermolecular and intramolecular. If the hydrogen bond is caused by the interaction of acid and base groups inside one molecule, the bonds are called intramolecular hydrogen bonds. It is possible, if the structure of the molecule permits spatial convergence of X–H and B fragments up to the length of the hydrogen bond.

However, there are molecules which are not able to form both intra- and intermolecular hydrogen bonds, e.g. salicylaldehyde (ortho-isomer) (Fig. 9.2.1, *a*), whereas for para-isomer (Fig. 9.2.1, *b*) location of the interacting groups is so that it is possible to form the intermolecular hydrogen bonds only.

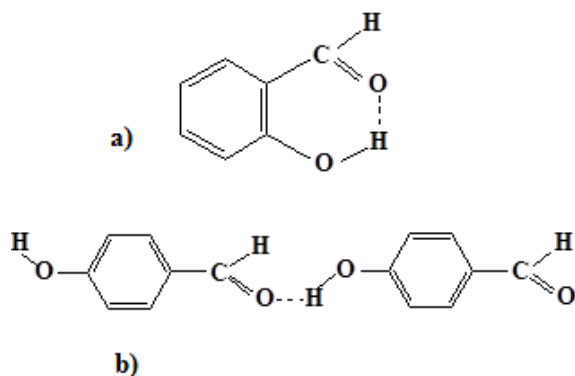


Figure 9.2.1. a) – intramolecular hydrogen bond (salicylaldehyde, ortho-isomer); b) - intermolecular hydrogen bond (salicylaldehyde, para-isomer)

It appears that the intermolecular hydrogen bond can be easily distinguished from the intramolecular one by means of experimental studies:

- there is no signs of association at the intramolecular hydrogen bond;
- spectral emergence of the intermolecular hydrogen bond disappears at low concentration of a substance in a neutral solvent, while it remains in the intramolecular interaction.

Properties of organic compounds are highly affected by both intra- and intermolecular hydrogen bonds. The influence of the latter, especially on the physical properties, is more significant, since the intermolecular interactions lead to the increase in molecular weight with all the consequences.

Comparative characteristics of the emergence of intra- and intermolecular hydrogen bonds are represented in Table 9.2.1 [38].

Table 9.2.1

Comparative characteristics of the emergence of intra- and intermolecular hydrogen bonds

Property	Compound	
	with the intramolecular hydrogen bond	with the intermolecular hydrogen bond
Dielectric permeability	Normal	Often above the norm
Dipole moment	Below the vector sum of moments of the bonds	Above the vector sum of moments of the bonds
Solubility	Normal	Higher, if formation of the H-bonds is possible with a solute
Surface tension	Lower	Higher
Reaction rate	Can both increase and decrease	
Linearity of the hydrogen bond	Usually non-linear	Linear

At early stages of studying the hydrogen bond it was supposed that the hydrogen bridge is formed only between the atoms with high electronegativity (F, O, N, C). Recently, it has been added with Cl, S, Br, I and others. The most important donors of the electronic pair (i.e. hydrogen bond acceptors) are oxygen atoms in alcohols, ethers and carbonyl compounds, and nitrogen atoms in the amine and nitrogenous heterocycles. The most important donors of protons – hydroxyl, amine, carboxyl and amide groups. Strong hydrogen bonds are established in such pairs as O – H ... O, O – H ... N and N – H ... O. Bonds of the N – H ... N type are much weaker, and Cl₂C – H ... N and Cl₂C – H ... O bonds refer to the weakest [25].

Let us enumerate the most significant experimental facts accompanying the formation of the hydrogen bond:

1. Formation of hydrogen bonds is accompanied by the heat release – thermochemical measure of the hydrogen bond energy. The parameter is used to calibrate the spectral methods for studying hydrogen bonds.

2. Distance between adjacent atoms involved into formation of the hydrogen bond is much lower than the sum of their van der Waals radiuses. Therefore, in water the distance between oxygen atoms in O–H...O configuration is 2.76 Å. If it is assumed that the length of the covalent bond of O–H is 1.0 Å, consequently, the length of the H...O bond will be 1.76 Å, i.e. it is much (approximately by 70%) longer than the covalent bonds between atoms. Nevertheless, the H...O bond appears to be much shorter than the sum of van der Waals radiuses that are equal 1.2 and 1.4 Å for hydrogen and oxygen respectively. The last consequence is one of the criteria indicating the formation of hydrogen bonds between molecules.

3. During the formation of hydrogen bonds there is an increase in the length of the X–H covalent bond (where X – atom of O, N, etc.), which leads to the shift of the relevant band of stretching vibrations in the IR spectrum towards the region of lower frequencies. The IR spectroscopy methods are one of the principal methods for studying the hydrogen bond. However, the method describes the hydrogen bond only in the ground state of the molecule. It is necessary to know the emergence of the hydrogen bond in the excited state of the molecule to study photoprocesses in the molecule. This will be further considered.

4. During the formation of hydrogen bonds polarity of the X–H bond increases, which leads to the increase in dipole moment of the molecular complex in comparison with the calculations obtained by means of the vector addition of dipoles of molecules R–X–H and B–R'.

5. Protons involved into the hydrogen bond are characterised by lower electronic density, therefore, they deshield leading to a significant shift of relevant resonant signals in spectra of the proton magnetic resonance.

6. For intermolecular hydrogen bonds there observed a shift of the acid-base equilibrium of molecular complex ↔ ion pair to the right when polarity of the solvent increases.

7. The work [39] contains some values for the lengths of hydrogen bonds N–H...O and O–H...O. The authors in [27] say that the length of the hydrogen bond N–H...O is less than 2.65 Å, O–H...O is less than 2.55 Å. The authors of [36] also indicates, according to the works by Hibbert and Emslie, other intervals of the lengths of hydrogen bonds: the length of the N–H...O bond lies within the interval from 2.49 to 2.65 Å, and O–H...O from 2.49 to 2.72 Å. According to [39], in water clusters the length of the O–H...O hydrogen bond belongs to the interval 2.43 – 2.61 Å. The spread of these values is associated with a varying strength of the hydrogen bond in systems.

Earlier, it was supposed that the nature of the hydrogen bond is reduced to the dipole-dipole (or electrostatic) interaction. However, according to the dipole-dipole interaction, it is impossible, for instance, to understand the reason why we fail to notice any law of the dependence between energy of the hydrogen bond and dipole moment or polarizability of interacting molecules. Short length of hydrogen bonds proves considerable overlapping of van der Waals radiuses. A simple electrostatic model does not take into account the wave function overlapping, redistribution of the electronic density when molecules approach each other. The questions can be solved, if we assume that the hydrogen bond is partially covalent due to donor-acceptor interactions of the electron-donor B–R' with the electron-acceptor R–X–H. The increase in the electronic density on X atom occurs through the hydrogen bridge. Thus, hydrogen bonds are formed due to simultaneous appearance of the following forces: electrostatic interaction and charge transfer.

9.2.2 Hydrogen bond energy

Hydrogen bonds can be both strong and weak. The energy of the formation of strong hydrogen bonds is 15 – 20 kJ/mol (O–H...O bonds in water, alcohols, carbon acids, O–H...N, N–H...O and N–H...N bonds in compounds containing hydroxyl, amide and amine groups, for example, in proteins), but sometimes its value can reach 60 – 80 kJ/mol and more [33]. An example of strong hydrogen bond can be the bond of the 1-naphthol molecule in water, its experimental value in the base state is 24 kJ/mol [37]. Weak hydrogen bonds have the formation energy of 4 – 15 kJ/mol (C–H...O bonds in ketones, ethers, aqueous solutions of organic compounds).

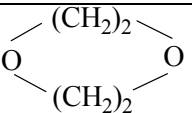
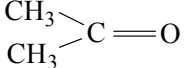
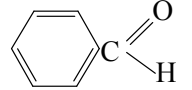
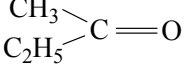
The hydrogen bond energy increases with a growing positive charge on the hydrogen atom of the X-H bond and higher proton-acceptability (basicity) of the B atom. However, in the case of hydrogen halides, acidity and tendency to form hydrogen bonds are inversely related. Big differences consist in basicity of organic compounds. Consequently, having the same ability to form hydrogen bonds, degree of basicity in amines is by five orders higher than in pyridines and 13 orders of magnitude higher than that of substituted carbonyl compounds.

Table 9.2.2 contains the values of the energy of hydrogen bonds in water for some compounds containing O and N atoms as proton-acceptors [40].

Reason for different energies of compounds containing ether and carbonyl groups (Table 9.2.2) should be referred to π -bond of the C=O group. Its presence leads to the change in the type of hybridisation of atomic orbits of oxygen from sp^3 -forms in ethers to sp^2 in ketones. Increase in the share of s -character of the bond is accompanied by the strengthening of chemical bond and leads to a change in the strength of the hydrogen bond O...H–O–H.

Table 9.2.2

Energy of the hydrogen bond of some organic compounds with water

Compound	Structural configuration	Proton-acceptor	E_H , kJ/mol
Diethyl ether	$C_2H_5-O-H_5C_2$	$C-\ddot{O}-C$	14.2
Dioxane			13.8
Acetone		$C=\ddot{O}$	11.3
Benzaldehyde			10.9
Methyl-ethyl ketone			10.5
Triethylamine	$(C_2H_5)_3N$	$\begin{matrix} \cdot\cdot \\ \vdash \\ \cdot\cdot \\ \cdot\cdot \\ \vdash \\ \cdot\cdot \\ \cdot\cdot \\ \vdash \\ \cdot\cdot \\ \cdot\cdot \end{matrix} \ddot{N}$	23.8–24.7
Diethylamine	$(C_2H_5)_2NH$		
Ethylamine	$(C_2H_5)NH_2$		
Pyridine			
Acetonitrile	$CH_3C\equiv N$	$C\equiv\ddot{N}$	9.6

There is a similar phenomenon for nitrogen-containing compounds. For trimethyl-, diethyl- and ethylamines the water absorption of OH groups is significantly shifted towards the region of low frequencies, which proves the formation of a strong hydrogen bond of the H – O – H...N type. Values of the hydrogen bond energy approximately belong to the same range (Table 9.2.2). The transition from ethylamines to pyridine caused by the coupling of the nitrogen atom with aromatic ring results in changes in hybridisation of orbits of the nitrogen atom N (from sp^3 in alkylamines to sp^2 in pyridine). During sp^2 -hybridisation a lone electron pair of the heteroatom, i.e. nitrogen atom, has 33.3% of s -nature accompanied by the strengthening of the chemical bond. During the transition from pyridine to acetonitrile there is a maximum overlapping of orbitals, i.e. further increase in the contribution of s -nature bond and change in the type of hybridisation to sp , which leads to declining energy of the hydrogen bonding with water.

In [41] authors conclude on the power of hydrogen bonds in complexes phenol-water and indole-water: oxygen atom in the phenol form attracts the hydrogen atom more strongly than nitrogen atom in the indole molecule. For these complexes relevant lengths of H...O bond in case of phenol are equal to 1.97 Å (S_0) and 1.93 Å (S_1), and for indole - 2.935 Å (S_0) and 2.933 Å (S_1). It is demonstrated that the energy of the indole-water bond is weaker than the energy of water with OH group in phenol-water complex. The same is applied to the water-naphthol complex.

Let us consider the influence of changes in enthalpy of the hydrogen bond formation $-\Delta H$ on the increment of dipole moment $\Delta\mu$. The resultant increment of dipole moment essentially is vector difference

$$\Delta\mu \equiv \mu_{H...B} - \mu_{RXH} - \mu_{BR'}, \quad (9.2.2)$$

where $\mu_{H...B}$, μ_{RXH} and μ_{BR} – relevant dipole momenta of the complex and its components.

The curve in Figure 9.2.2 was built using the data from various groups of complexes with O–H...N bonds (amines+phenols, pyridines+phenols) in benzene, toluene and sometimes in CCl_4 . As it seen from the figure, there are three possible regions of $-\Delta H$ values:

1. Region of values from 0 to 30 kJ/mol corresponding to the complexes with low polarity.
2. Transition region from 30 to ≈ 70 kJ/mol where $\Delta\mu$ dramatically increases with higher $-\Delta H$.
3. Enthalpy region corresponding to the complexes with high polarity which is characterised by the moderate growth of $\Delta\mu$ at growing $-\Delta H$.

The graph illustrates that if $-\Delta H$ exceeds 50 kJ/mol (in C_6H_6 or CCl_4), most of the hydrogen bonds will refer to the type of bonds with transfer. At $-\Delta H > 80$ kJ/mol it is probable that the majority of hydrogen bonds will be characterised by the proton transfer.

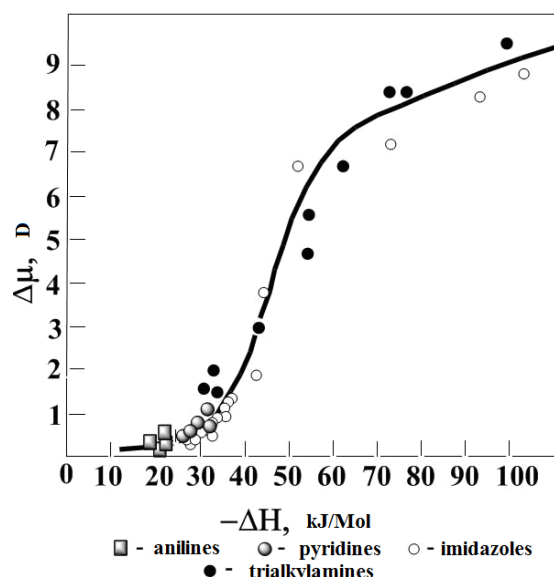


Figure 9.2.2. Dependence of the increment of dipole moment $\Delta\mu$ on enthalpy $-\Delta H$ of hydrogen bonds $O-H\cdots N$. Solvents: benzene, toluene or CCl_4 . Proton-donors – phenols. Bases: anilines, pyridines, imidazoles, trialkylamines.

9.2.3 Hydrogen bond in ground and excited states

It is well-known that the hydrogen bond formation causes shifting of maxima of electronic bands and blurring of vibrational structure. Since the hydrogen bond formation is a weak excitation, in comparison with the energy of electronic transition, consequently, the spectrum of a complex with the hydrogen bond usually represents a slightly excited spectrum of a free molecule. The same will be for the fluorescence spectrum. However, the band shift can be considered valid only for bands with pronounced vibrational structure.

Let us consider the effects occurring during formation (strengthening) of the hydrogen bond in the excited state of the molecule and emerging in the emission spectra [26]. These effects can be divided into three types: 1) inversion of excited electronic levels of $(n\pi^*)$ - and $(\pi\pi^*)$ -types; 2) quenching of luminescence; 3) phototransfer of proton in the complex with the hydrogen bond. Luminescence quenching during the formation of the complex with the hydrogen bond occurs, if two conditions are satisfied: 1) both molecules forming the complex with the hydrogen bond have developed π -electronic systems and 2) functional groups forming the hydrogen bond are coupled with π -electronic systems.

Fluorescence quenching during the hydrogen bond formation is typical of not only such systems as aromatic hydroxyl-compound – nitrogen-containing heterocycle, but of many other systems of the type aromatic amine – nitrogen-containing heterocycle [31].

Using the scheme of a relative position of single and triplet levels of $(n\pi^*)$ - and $(\pi\pi^*)$ -types and data on various influence of the intermolecular hydrogen bond on $(n\pi^*)$ - and $(\pi\pi^*)$ -transitions, we can qualitatively explain such effects as change in radiative properties and the type of glow at the hydrogen bond formation. Quenching of fluorescence and proton transfer will be thoroughly considered below.

It is a commonplace that interaction leading to the hydrogen bond formation between some aromatic hydroxyl- or amino-derivatives such as naphthols, naphthylamines and carbazoles, on the one hand, and various acceptors of proton – on the other, is stronger in state S_1 than in S_0 [42]. Furthermore, distance between donor and acceptor, position of proton in the hydrogen bond, configuration of surrounding molecules of the solvent in states S_1 and S_0 can be different.

Relaxation from the Franck-Condon into the equilibrium state includes rearrangement of nuclear configurations of the solvent molecules along with the rearrangement of the hydrogen bond.

For example, some systems with the hydrogen bond, such as 2-naphthol – triethylamine in benzene form ion pairs caused by proton transfer into state S_1 , where fluorescence emits (Fig. 9.2.3) [43]:

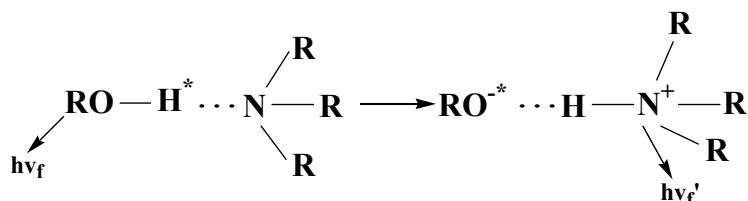


Figure 9.2.3. Formation of ion pairs caused by proton transfer

Shift of the absorption band $S_1 \leftarrow S_0$ caused by the hydrogen bond formation in the system is 370 cm^{-1} , and relevant shift of the fluorescence band determined by the formation of ion pair reaches 4000 cm^{-1} . The increase in polarity of the solvent leads to the growth of the fluorescence shift, since it defines the stabilisation of ion pair in the equilibrium state S_1 and destabilisation of the Franck-Condon state S_0 .

However, other example must be also considered. If the acceptor of proton and solvent for 2-naphthol is monobutylamin (MBA), which is not a strong polar solvent, the fluorescence shift increases and makes up 5700 cm^{-1} [43]. The result can be explained by the fact that proton transfer from the excited naphthol to MBA is accompanied by the proton transfer between the MBA molecules, which leads to separation of charges by a greater distance.

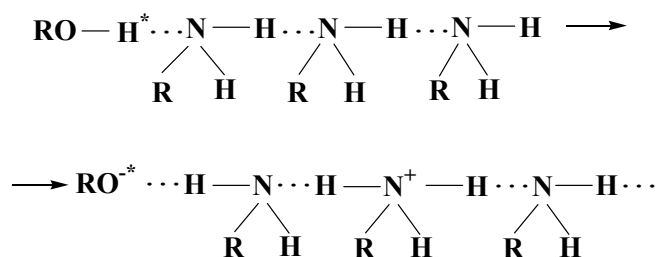


Figure 9.2.4. Proton transfer from the excited MBA molecule accompanied by proton transfer between MBA molecules

In some cases, the hydrogen bond formation extremely affects the fluorescence yield. If two conjugated π -electronic systems interact with each other forming the hydrogen bond which interacts with the conjugated π -electronic system, as it occurs in such systems as naphthol-pyridine, naphthylamine-pyridine, carbazol-pyridine and acridine dye-phenol or acridine dye- naphthol, there is an almost complete quenching of fluorescence.

For the system of carbazol-pyridine located in the low-temperature solid matrix characteristic fluorescence quenching is caused by the hydrogen bond formation and indicates an extremely great increase in the rate of non-radiative deactivation of the state S_1 , which, however, does not lead to the formation of the triplet state. Charge transfer between two conjugated π -electronic systems through the hydrogen bond was proposed as a mechanism of the fluorescence quenching [43].

Task

Explain the shift of absorption bands (Tab. 9.2.3) corresponding to transitions $S_0 \rightarrow S_1$ and $S_0 \rightarrow S_2$ for mesityl oxide (Fig. 9.2.5) at transition from water to hexane. Is the inversion of states $\pi\pi^*$ and $n\pi^*$ possible for the molecule (see below)?

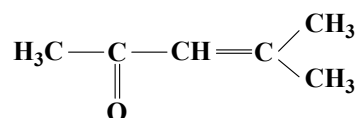


Table 9.2.3

Maxima of the absorption bands of mesityl oxide corresponding to transitions $S_0 \rightarrow S_1$ and $S_0 \rightarrow S_2$ and molar absorption coefficients in solvents of various polarity

Solvent	ϵ	$\lambda_{\max}(S_0 \rightarrow S_1)$, nm	$\lambda_{\max}(S_0 \rightarrow S_2)$, nm
n-hexane	1.89	327	230
diethyl ether	4.34	326	230
ethanol	24.3	315	237
methanol	38.6	312	238
water	78.5	305	244

9.3 Micellar solvation

9.3.1 Surface activity of substances

In the Gibbs adsorption equation

$$G = - \left(\frac{c}{RT} \right) \left(\frac{\partial \sigma}{\partial c} \right), \quad (9.3.1)$$

where G – Gibbs adsorption; c – concentration of the solute; R – gas constant; T – absolute temperature; σ – surface tension, influence of the nature of a substance on the adsorption is expressed by derivative. To exclude the influence of the concentration on the derivative $\frac{\partial \sigma}{\partial c}$, its limit value at $c \rightarrow 0$ is taken. Rebinde called this value the surface activity

$$g = - \left(\frac{\partial \sigma}{\partial c} \right)_{c \rightarrow 0} = RT \left(\frac{\Gamma}{c} \right)_{c \rightarrow 0}. \quad (9.3.2)$$

Absolute value and sign of the surface activity depend on the nature of an adsorbed substance and a medium (solvent). If the surface tension at the interface decreases with a growing concentration of a substance, the substance is called surfactant. For this $g > 0$, $\frac{\partial \sigma}{\partial c} < 0$, $G > 0$. Substances reducing the surface tension at the interface with a growing concentration are called surface-inactive. For them $g < 0$, $\frac{\partial \sigma}{\partial c} > 0$, $G < 0$. The Gibbs adsorption (G_i) implies a surface excess of i component in the surface layer in comparison with its equilibrium concentration in the bulk phase. Therefore, $G < 0$ means that the concentration of the adsorbed substance in the bulk phase is more than in the surface layer.

A principal characteristic of surfactants is their diphility. Molecules of surfactants consist of two parts that are extremely different in their molecular nature and properties: non-polar (hydrophobic) part – hydrocarbon radical and polar (hydrophilic) part represented by functional groups – COOH, -NH₂, -OH, -O-, -SO₂, etc. Diphilic molecules tend to gather on the surface of the interface where hydrophobic groups are isolated from water, while the hydrophilic ones remain immersed into water. The ability explains their surface activity.

Most of the organic substances have surface tension less than water; consequently, they are surfactant with respect to water, for example, non-organic salts which are highly hydrated.

According to P.A. Rebinder, surfactants fall into two groups: water-soluble and colloidal (soap-like). The former includes substances with insufficient hydrophilic group (alcohols, amines) or insufficiently branched hydrocarbon radical (lower fatty acids, their salts). Substances of this type remain in the solution in the molecular-dispersion state up to the concentration corresponding to their intrinsic solubility and the separation of the system into two solid phases. Molecules of colloidal surfactants have branched hydrocarbon radicals (the number of hydrocarbon atoms is more than 7) reducing the solubility in water. They also have a quite strong polar group enabling the solubility. If there are such conditions, molecules acquire specific feature – exceeding a certain concentration they form micellar structures in the solution which results in formation of the colloidal solution along with the true one.

9.3.2 Classification of colloidal surfactants

General classification of surfactants is based on the properties of a polar part of molecule [25]. According to the dissociation in aqueous solutions, surfactants are divided into ionic and non-ionic. The ionic are subdivided into anionic, cationic and ampholytic (amphoteric).

1. Anionic surfactants dissociate in water generating a surfactant anion, for example:



2. Cationic surfactants, when dissociate in water, generate positively charged surfactant ions (cations):



3. Ampholytic surfactants contain two functional groups, one of which has acid and another one – base nature, for example, carboxyl and amino groups. Depending on the conditions these substances demonstrate both cation-active and anion-active properties.

4. Non-ionic surfactants do not dissociate into ions in solutions. Diphilic molecules of surfactants usually consist of a long hydrocarbon chain with several polar but non-ionic groups at the end determining the solubility of substances. These groups are presented by hydroxyl and ether groups.

9.3.3 Micelle formation. Critical micelle concentration

The main feature of colloidal surfactants is their ability to spontaneously form thermodynamically stable heterogeneous disperse systems (associative or micellar colloids). In these aggregates molecules are so close that the total contact area of hydrophobic groups of the dissolved molecule with water is reduced. Ionic surfactants will form systems on the surface of which emerges an electrical double layer. A particle of the disperse phase in a micro-heterogeneous system together with the electrical double layer is called micelle. Micelles of surfactants serve as constructing blocks for the majority of self-organised structures. Micelles are the aggregates of long-chain diphilic molecules of ions of surfactants spontaneously formed in their solution at a certain concentration depending on the nature of a polar group and, especially, on the length of molecule chain. In aqueous solutions the association of some molecules (ions) occurs as a result of coupling of hydrocarbon chains; in non-aqueous media – due to polar functional groups. For anion-active surfactants in water each micelle is a kind of an ultra-micro-drop of hydrocarbon encased in a shell formed by hydrated polar groups. For the surfactants with a flexible hydrophobic part of the molecule self-association in aqueous solutions leads to the formation of micelles with the structure illustrated by Figure 9.3.1.

The main cause of aggregates of hydrocarbon chains in aqueous solutions is cohesive forces between water molecules which are bigger than the mutual attraction of water molecules and hydrocarbon chains. Water molecules “squeeze” hydrocarbon chains out of the solution, which is accompanied by a decrease in enthalpy of the system. Micelles of surfactants do not change until the external factors cause the shift of the equilibrium, where the system was. Stability of micelles is characterised by the dissociation rate, i.e. the average residence time of a molecule in the micelle.

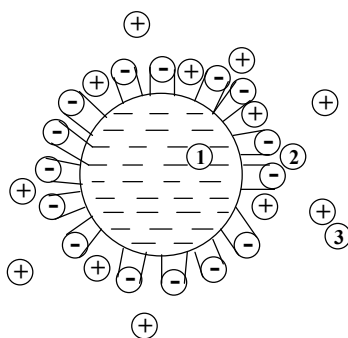


Figure 9.3.1. Scheme of the ionic micelle in water: 1 – nucleus of the micelle; 2 – Stern layer (charged head groups and some counterions); 3 – Gouy-Chapman layer (other counterions)

There is no a unanimous opinion on the look and shape of micelle. It is generally accepted that the critical micelle concentration in a micelle formed by individual molecules of the surfactant produce the so-called Hartley micelles. The micelles represent spherical aggregates, their internal part consists of hydrocarbon radicals, and the polar group of the molecules of the surfactants is turned into the aqueous phase. The diameter of micelles is equal to the double length of the surfactant molecule (Fig. 9.3.2).

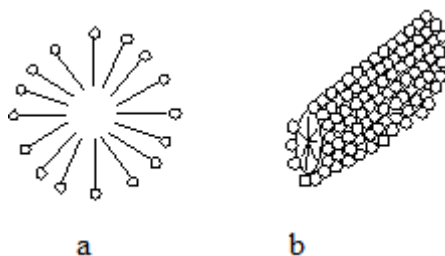


Figure 9.3.2. Micelles: a – spherical; b – cylindrical.

Spherical micelles can contain from 20 to 100 molecules. The aggregation number is raised by adding electrolytes to the surfactant solution, since electrolytes reduce the forces of electrical repulsion in the surface of micelles. The size of micelles of non-ionic surfactants is typically greater than ionic.

As the surfactant concentration in the solution increases, the size of micelles grows and hydrocarbon chains become located in them more and more parallel with respect to each other. Micelles tend to take a cylindrical, plate-like shape (Fig. 9.3.2). Such micelles are thermodynamically stable. They are called McBain micelles.

The formation of micelles starts or becomes apparent above some region of the concentration called the critical micelle concentration (CMC) [13]. Thus, the CMC is determined by the concentration of a surfactant at which in its solution a big number of micelles in the thermodynamic equilibrium with molecules (ions) emerge, and some properties of the solution dramatically change. The micelles themselves – thermodynamically stable reversible formations which emerge at the CMC and break up when the solution is diluted.

This is the reversibility of micellar systems. Isotherms of the surface tension of the colloidal surfactants are characterised by sharp decrease in the surface tension (σ) with increasing concentration and break on the isotherm at the region of the concentration corresponding to the true solubility. Concentration of a break point corresponds to the CMC. Above the CMC the true solution passes into the ultra-micro-heterogeneous system. The break point is more pronounced on the curve built in the coordinates σ , $\lg C$ (Fig. 9.3.3).

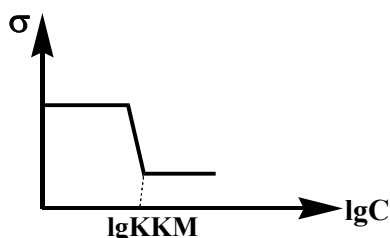


Figure 9.3.3. Isotherm of the surface tension of colloidal surfactants

The surface activity of colloidal surfactants can be approximately expressed through the CMC with the help of the relation:

$$g \approx \frac{\sigma_0 - \sigma_{CMC}}{CMC}, \quad (9.3.5)$$

where σ_0 – surface tension of the solvent. The relation defines the connection between surface and bulk properties of the surfactant.

It states that micelle formation is preceded by the association of the surfactant molecules into dimer, trimers, and so on. However, the behavior of the curve in Figure 9.3.3 is a sufficient basis to take into account only two states of surfactants in the solution at concentrations above the CMC: monomeric and micellar. The CMC is a quite definite value to build the two-phase model of a micellar solution based on it. At the same time it is possible to describe micelle formation as a chemical reaction of the association:



where K^+ – counterions; R^- – surfactant ions; M – micelle; n – number of surfactant ions, m – number of counterions in the micelle.

Some surfactants are used as an example in Table 9.3.1. The table contains relevant CMCs and number of molecules associated in the micelle.

Table 9.3.1

Some causes of surfactants, their CMC and number of molecules associated in the micelle in aqueous solutions at 25°C

Surfactant	CMC, mol·l ⁻¹	Number of molecules associated in the micelle
n-Sodium dodecyl sulfate CH ₃ (CH ₂) ₁₁ OSO ₃ ⁻ Na ⁺	0.0081	62
n-cetrimonium bromide CH ₃ (CH ₂) ₁₅ N ⁺ (CH ₃) ₃ Br ⁻	0.0013	78
Hexa-oxyethylene dodecanol CH ₃ (CH ₂) ₁₁ (OCH ₂ CH ₂) ₆ OH	0.00009	400
3-(N-n-Dodecyl -N,N-Dimethyl)- ammonio-1-propanesulfonate CH ₃ (CH ₂) ₁₁ N ⁺ (CH ₃) ₂ (CH ₂) ₃ SO ₃ ⁻	0.003	55

The CMC is the most important physical and chemical constant defining various properties of surfactants. According to the CMC values it is possible to evaluate:

- changes in thermodynamic functions at micelle formation;
- concentration-dependence of the surface tension;
- equilibrium distribution of surfactants between the bulk and the surface;
- calculation of concentrations of micelle and monomers in the solution. The concentration of micelles in the solution is calculated by the following formula:

$$C_{mic} = \frac{C_{SUR} - C_{CMC}}{A}, \quad (9.3.7)$$

where C_{SUR} and C_{CMC} – concentration of surfactant and CMC respectively, A – number of molecules in the micelle;

- influence of additives on the surface activity of surfactants.

One of the major factors defining the CMC is the length of the hydrocarbon radical. In the process of micelle formation the longer the hydrocarbon chain is, the greater is the decrease in the Gibbs energy. It was demonstrated, that the CMC magnitude declines by logarithmic law with a growing number of hydrocarbon atoms n and is associated with the relation

$$\lg C = A - Bn, \quad (9.3.8)$$

where A and B – constants typical of various homologous series and temperatures. As a rule, the ability for micelle formation is characteristic for the surfactant molecules with the length of the hydrocarbon radical more than 7-8 atoms of carbon. In the molecules with a shorter length of the hydrocarbon chain the aggregation energy is insufficient to keep the molecules from random thermal motion. When the CMC chain grows the solubility of surfactants increases and decreases. Branching and cyclisation of the hydrocarbon radical reduce the tendency to micelle formation and increase the CMC.

The nature of the polar group plays an important role in the micelle formation. Its influence on the CMC reflects the A parameter in the equation (9.3.8). The presence of ionic end groups provides good solubility of surfactants in water; therefore, transition of the ionic molecules in the micelle requires much more energy than non-ionic molecules. As the result, the CMC of ionic surfactants is much higher (approximately by 2 orders) than that of non-ionic at the same length of the hydrocarbon chain of molecule.

Viscosity of micellar solutions is an important parameter. For the surfactants able to form large micelles the viscosity rapidly grows with the increasing concentration, and in comparison with the water viscosity can exceed 10^7 .

9.3.4 Methods for CMC determination

Methods for the CMC determination are based on a dramatic change in physical and chemical properties of surfactant solution at the micelle formation. On the dependence curve “the surfactant property – content” a break usually appears in the region of the CMC (Fig. 9.3.4).

One of the branches of the curves (at $C_{SUR} < CMC$) describes the properties of the system in the molecular state, and another – in colloidal (at $C_{SUR} > CMC$). The abscissa of the break point is considered as corresponding to the micelle formation, i.e. CMC. The CMC is determined by the conduct metric method, by measuring the surface tension of the solution, by a change in the light scattering at the micelle formation, and by a change in the refractive index.

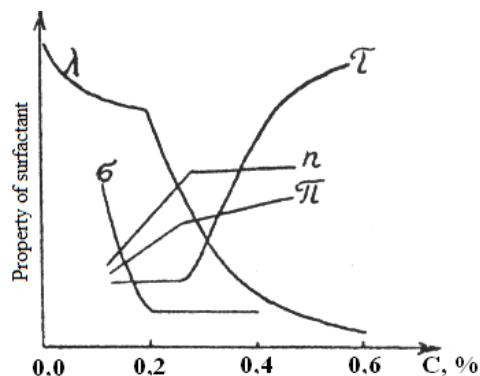


Figure 9.3.4. Concentration-dependence of turbidity τ , equivalent conductivity λ , surface tension σ , refractive index n , osmotic pressure π of the solution of sodium dodecyl sulfate in water

Determination of the CMC by the solubility of dyes and hydrocarbons in micelles can be used for ionic and non-ionic surfactants both in aqueous and non-aqueous solutions. When the concentration of surfactants in solution is equal to the CMC, the solubility of hydrocarbons and dyes dramatically increases. It is convenient to use fat-soluble dyes intensively staining the solution of surfactants above the CMC.

Spectral characteristics of solutions of water-soluble dyes can be also used to determine the CMC. In aqueous solutions organic dyes are prone to form dimers and higher aggregates which are characterised by their own absorption spectra. Dimers of dyes have a strong absorption band in a shorter wave regions of the spectrum than monomers (Fig. 9.3.5).

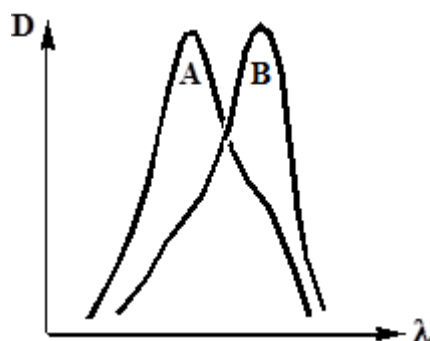


Figure 9.3.5. Absorption spectra of dimers (A) and monomers (B) of the organic dye

Dimers either fluoresce weakly or do not fluoresce at all at room temperature. It is known that there is a destruction of the association of dyes on the micelles of surfactants, i.e. on the micelles the dye is in form of a monomer. Changes observed in the spectra of absorption and fluorescence of dyes in aqueous solutions of surfactants can be used to determine the CMC by the electronic spectra. Curves of the dependence of I/I_0 and $\varepsilon/\varepsilon_0$ on the concentration of surfactants are built, where I and I_0 – intensity of fluorescence of the dye with and without added surfactant respectively; ε and ε_0 – decimal molar absorption coefficient of the dye with and without added surfactant respectively. Curves of the concentration-dependencies I/I_0 and $\varepsilon/\varepsilon_0$ of surfactants can be divided into three regions (Fig. 9.3.6):



Figure 9.3.6. General view of the curve of the fluorescence rise of the dye in the water-surfactant mixture

1. *Concentrations of surfactants far from the CMC (I).*

The region is characterised by stability of the fluorescence intensity and decimal molar adsorption coefficient of the dye.

2. *Concentration of surfactants close to the CMC (pre-micellar region) (II).*

The region for anionic and cationic surfactants is characterised by the absence of fluorescence of the dye or its decline. For the majority of non-ionic surfactants, I and ϵ of the dye do not change in the region. This is associated with the formation of non-luminescent complex aggregates of molecules of the dye with each other and surfactant molecules. Half-widths of the long-wave absorption band of dyes in the region increase by 3 and more times. The surface tension of the solution dramatically decreases in the region.

3. *Concentration of surfactants exceeding the CMC (III).*

The region is a region of the micellar solution. It is characterised by a dramatic increase in the fluorescence intensity of the dye and ϵ of the monomer maximum and narrowing of the absorption band associated with the destruction of associates of the dye on or inside the formed micelles of surfactants.

The CMC values obtained by the above method agree well with the CMC values obtained from the measurements of the surface tension of solutions.

9.3.5 Solubilisation

The phenomenon of dissolution of substances in the micelles of surfactants is called solubilisation [25]. In aqueous micellar systems water-insoluble substances (benzene, dyes, and fats) dissolve in water. According to the modern theory, dissolution of substances occurs in the internal (hydrocarbon) part of the micelle. Non-polar hydrocarbons are situated in the hydrocarbon nuclei of the micelle. Polar organic substances build in between the molecules of surfactants in the way that their polar groups face water, while non-polar parts are oriented parallel to the hydrocarbon radical of surfactants. There is one more way to include the solubiliser in the micelle, which is typical of non-ionic surfactants, - fixing on the surface of the micelle. Figure 9.3.7 demonstrates some possible centres for coupling in aqueous micellar systems.

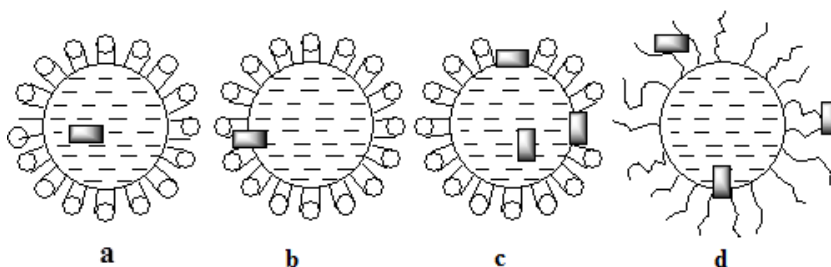


Figure 9.3.7. Scheme of solubilisation in aqueous micelles (anion-active surfactants): a – non-polar solubiliser; b – diphilic solubiliser; c – weakly polar solubiliser; d – polar solubiliser in the non-ionic micelle where the centre of solubilisation is the polyoxyethylene shell

It is obvious that solubilisation leads to the increase in size of micelle. Ability to solubilise grows with the increasing concentration of surfactants. When plate-like micelles appear in the solution, the ability increases intermittently.

Themes for independent work: Fluorescent methods in medicine

Use the additional literature [44 – 47] devoted to the subject.

PART 4. RAMAN SPECTROSCOPY FOR ANALYTICAL DIAGNOSTICS

LECTURE 10. PHYSICAL FOUNDATION OF RAMAN SPECTROSCOPY

Raman scattering of light is one of the processes of interaction of light with substance characterised by the change in frequency of the scattered radiation in comparison with the frequency of the exciting radiation [48-53]. The phenomenon was discovered in 1928 by G.S. Landsberg and L.I. Mandelstam during the studies of light scattering in crystals, and simultaneously by C.V. Raman and K.S. Krishnan during their studies of light scattering in liquids. However, as it is known, the 1930 Nobel Prize was awarded to the Indian scientist Raman along with the world's recognition. That is why the phenomenon is called "Raman effect" or "Raman scattering".

10.1 Classical theory of Raman scattering

The classical theory of Raman scattering is based on the following physical principles:

1. Molecular scattering of light is caused by forced vibrations of the dipole moment induced by the field of incident wave.

2. Light mainly scatters in the electron shell of the molecule, since the nuclei of the molecule are slightly shifted under the influence of a high-frequency field.

3. Raman scattering is caused by the fact that ability of the electronic cloud of the molecule to deform under the influence of an electric field of the light wave depends on configuration of nuclei at a definite moment of time. At vibrations of nuclei close to the equilibrium the ability of the electronic cloud to deform changes with the vibrational frequency of nuclei. Therefore, Raman scattering can be considered as the result of modulation of the induced dipole moment of molecules caused by vibrations of nuclei.

The physical mechanism of Raman scattering from the classical perspective can be thoroughly presented as follows. Imagine that light wave $\mathbf{E}(\mathbf{r}, t) = \mathbf{E}_0(\mathbf{r}) \cos(2\pi\nu t)$ falls on a molecule. In the long-wave approximation, which is well performed in optics, within the size of a molecule the \mathbf{r} -dependence of the field tension can be neglected. Then, in the context of the approximation the induced dipole moment of the molecule is equal to

$$\mathbf{p}(t) = \alpha \mathbf{E}(t), \quad (10.1)$$

where α – polarizability of the molecule. If inside the molecule there are some movements periodically affecting its polarizability, the induced dipole moment will experience additional oscillation. As an example, let us consider the vibrational movement of nuclei of the molecule with $\alpha \equiv \alpha(q_i)$, where vibrational coordinate q_i defining the vibrational movement changes by the harmonic law $q_i = q_{i0} \cos(2\pi\nu_i t + \delta)$. Since q_i is small, polarizability of the molecule can be decomposed into the Taylor series close to the equilibrium value of the coordinate, i.e. at the point $q_i = 0$

$$\alpha(q_i) = \alpha(0) + \left(\frac{\partial \alpha}{\partial q_i} \right)_{q_i=0} q_i + \dots \quad (10.2)$$

Limited in (10.2) by the linear by q_i term, the expression for the induced dipole moment of the molecule can be written as

$$\mathbf{p}(t) = \left[\alpha(0) + \left(\frac{\partial \alpha}{\partial q_i} \right)_{q_i=0} q_{i0} \cos(2\pi\nu_i t + \delta) \right] \mathbf{E}_0 \cos(2\pi\nu t) =$$

$$\begin{aligned}
&= \alpha(0)\mathbf{E}_0 \cos(2\pi\nu t) + \frac{1}{2} \left(\frac{\partial \alpha}{\partial q_i} \right)_{q_i=0} q_{i0} \mathbf{E}_0 \cos[2\pi(\nu - \nu_i)t - \delta] + \\
&\quad + \frac{1}{2} \left(\frac{\partial \alpha}{\partial q_i} \right)_{q_i=0} q_{i0} \mathbf{E}_0 \cos[2\pi(\nu + \nu_i)t + \delta]. \tag{10.3}
\end{aligned}$$

Since the oscillating dipole moment is a source of electromagnetic radiation, in accordance with (10.3), there appear an elastically scattered wave with the frequency ν (Rayleigh scattering) and two waves corresponding to inelastic scattering with frequencies $\nu \pm \nu_i$ (Raman scattering).

According to the classical theory of radiation, the power of the scattered radiation dI at the combination frequencies $\nu \pm \nu_i$ in a direction \mathbf{n} (in a solid angle $d\Omega$) equals

$$dI = \frac{[\mathbf{n} \times \ddot{\mathbf{p}}]^2}{4\pi c^3} d\Omega = \frac{\overline{\ddot{\mathbf{p}}^2}}{4\pi c^3} \sin^2 \theta d\Omega, \tag{10.4}$$

where $\overline{\ddot{\mathbf{p}}^2}$ – time-average of the second derivative of the dipole moment, θ – angle between vectors \mathbf{p} and \mathbf{n} . In this case

$$\begin{aligned}
\overline{\ddot{\mathbf{p}}^2} &= 4\pi^4 (\nu \pm \nu_i)^4 \left(\frac{\partial \alpha}{\partial q_i} \right)_{q_i=0}^2 q_{i0}^2 E_0^2 \overline{\cos^2[2\pi(\nu \pm \nu_i)t \pm \delta]} = \\
&= 2\pi^4 (\nu \pm \nu_i)^4 \left(\frac{\partial \alpha}{\partial q_i} \right)_{q_i=0}^2 q_{i0}^2 E_0^2 \tag{10.5}
\end{aligned}$$

and

$$dI = \frac{4\pi^4}{c^4} (\nu \pm \nu_i)^4 \left(\frac{\partial \alpha}{\partial q_i} \right)_{q_i=0}^2 q_{i0}^2 I_0 \sin^2 \theta d\Omega, \tag{10.6}$$

where

$$I_0 = \frac{c}{8\pi} E_0^2 \tag{10.7}$$

– intensity of the linearly polarised incident radiation.

Expression (10.6) describes the power of the scattered radiation from one molecule. In case of light scattering on the ensemble of similar molecules, it must be multiplied by the number of molecules in a scattering volume N , since the scattered radiation from different molecules is incoherent.

If in expression (10.2) to take into account the next terms, it results in oscillations of the induced dipole moment of the molecule with frequencies $\nu \pm 2\nu_i$ and $\nu \pm \nu_i \pm \nu_j$, corresponding to overtones and combination frequencies of vibrations of the molecule. In such a case, the power of

the scattered radiation is defined by values $\left(\frac{\partial^2 \alpha}{\partial q_i^2} \right)_{q_i=0}^2$ and $\left(\frac{\partial^2 \alpha}{\partial q_i \partial q_j} \right)_{q_i=0, q_j=0}^2$.

Thus, in the context of the classical theory the energy flow of the scattered light is proportional to the fourth degree of its frequency, intensity of the incident radiation and concentration of scattering molecules. Moreover, it must be noted that emergence of the Raman signals requires relevant vibrations to cause changes in polarizability of the molecule.

The above statement supposes that polarizability of the molecule is isotropic. In fact, scattering molecule is not isotropic, i.e. its properties depend on the orientation of the molecule with respect to the electric field of the exciting light wave. As the result, induced moment \mathbf{p} , generally

speaking, does not coincide with the electrical vector \mathbf{E} of the exciting radiation. Therefore, relation (10.1) should be

$$\mathbf{p}_\rho = \sum_{\sigma} \beta_{\rho\sigma} \mathbf{E}_\sigma, \quad (\rho, \sigma = x, y, z). \quad (10.8)$$

A sum of values of $\beta_{\rho\sigma}$ is called scattering tensor and is represented in the form of a matrix

$$\|\beta_{\rho\sigma}\| = \begin{vmatrix} \beta_{xx} & \beta_{xy} & \beta_{xz} \\ \beta_{yx} & \beta_{yy} & \beta_{yz} \\ \beta_{zx} & \beta_{zy} & \beta_{zz} \end{vmatrix}. \quad (10.9)$$

Regularly, components of the scattering tensor are complex. Correlation of the scattering tensor with properties of the scattering molecule (with its polarizability) is defined by the quantum mechanics methods and will be demonstrated in the following section. Nevertheless, in the context of the classical theory it is possible to obtain physically correct description of spatial distribution of the power of Raman signals and its polarizability features. Generally, spatial distribution of the power of the scattered light is

$$I(\theta) = I_{\perp}(\theta) + I_{\parallel}(\theta), \quad (10.10)$$

where θ – angle between the direction of observing the scattered light and plane of the oscillation of electric vector \mathbf{E} of the linearly polarised exciting radiation, $I_{\parallel}(\theta)$ – power of the scattered light whose plane of polarisation coincides with the plane of polarisation of the exciting radiation, $I_{\perp}(\theta)$ – power of the scattered light whose plane of polarisation is perpendicular to the plane of polarisation of the exciting radiation. The relation of these components

$$\rho(\theta) = \frac{I_{\perp}(\theta)}{I_{\parallel}(\theta)}, \quad (10.11)$$

is called the degree of depolarisation of the scattered light and defines spatial distribution of polarisation of the scattered light.

Polarised components of the scattered light calculated for a free oriented molecule are

$$I_{\parallel}(\theta) = \frac{16\pi^4 (\nu \pm \nu_i)^4}{15c^4} I_0 [10\beta_c \sin^2 \theta + \gamma^2 (3 + \sin^2 \theta) + 5\beta_a \cos^2 \theta] d\Omega \quad (10.12)$$

$$I_{\perp}(\theta) = \frac{16\pi^4 (\nu \pm \nu_i)^4}{15c^4} I_0 [3\gamma^2 + 5\beta_a] d\Omega \quad (10.13)$$

where β_c , γ^2 and β_a are the invariants of the scattering tensor whose pure form is presented in [9]

$$\beta_c = \frac{1}{3}(\beta_{xx} + \beta_{yy} + \beta_{zz})^2, \quad (10.14)$$

$$\begin{aligned} \gamma^2 = & \frac{1}{3}[(\beta_{xx} - \beta_{yy})^2 + (\beta_{yy} - \beta_{zz})^2 + (\beta_{zz} - \beta_{xx})^2] + \\ & + \frac{1}{2}[(\beta_{xy} + \beta_{yx})^2 + (\beta_{yz} + \beta_{zy})^2 + (\beta_{xz} + \beta_{zx})^2], \end{aligned} \quad (10.15)$$

$$\beta_a = \frac{1}{2}[(\beta_{xy} - \beta_{yx})^2 + (\beta_{xz} - \beta_{zx})^2 + (\beta_{yz} - \beta_{zy})^2]. \quad (10.16)$$

The expressions for polarised components of the scattered light also permit describing spatial distribution of the power of the scattered light and its polarizability characteristics

$$I(\theta) = \frac{16\pi^4 (\nu \pm \nu_i)^4}{15c^4} I_0 [10\beta_c \sin^2 \theta + \gamma^2 (6 + \sin^2 \theta) + 5\beta_a (1 + \cos^2 \theta)] d\Omega, \quad (10.17)$$

$$\rho(\theta) = \frac{3\gamma^2 + 5\beta_a}{10\beta_c \sin^2 \theta + \gamma^2 (3 + \sin^2 \theta) + 5\beta_a \cos^2 \theta}. \quad (10.18)$$

The data can be significantly simplified, if we introduce the power of the scattered light and the degree of its polarizability for a special case $\theta = \frac{\pi}{2}$

$$I\left(\frac{\pi}{2}\right) = \frac{16\pi^4(\nu \pm \nu_i)^4}{15c^4} I_0 [10\beta_c + 7\gamma^2 + 5\beta_a] d\Omega, \quad (10.19)$$

$$\rho\left(\frac{\pi}{2}\right) = \frac{3\gamma^2 + 5\beta_a}{10\beta_c + 4\gamma^2}. \quad (10.20)$$

Taking into account the expression, (1.17) and (1.18) can be written as

$$I(\theta) = I\left(\frac{\pi}{2}\right) \left[1 - \frac{1-\rho}{1+\rho} \cos^2 \theta \right], \quad (10.21)$$

$$\rho(\theta) = \frac{\rho}{1 - (1-\rho) \cos^2 \theta}, \quad (10.22)$$

where $\rho \equiv \rho\left(\frac{\pi}{2}\right)$. The resultant expression demonstrates that the spatial distribution of power of the scattered light and its polarizability characteristics for each line in the Raman scattering spectrum can be described with just one parameter ρ . As an example, Figure 10.1 illustrates the spatial distribution of power of the scattered light for two most important cases: $\rho = 0$ ($\gamma^2 = \beta_a = 0$) and $\rho = \frac{3}{4}$ ($\beta_c = \beta_a = 0$). The figures are made in the spherical coordinate system, and distance from the centre to the surface at observation angle θ corresponds to the value of intensity $I(\theta)$.

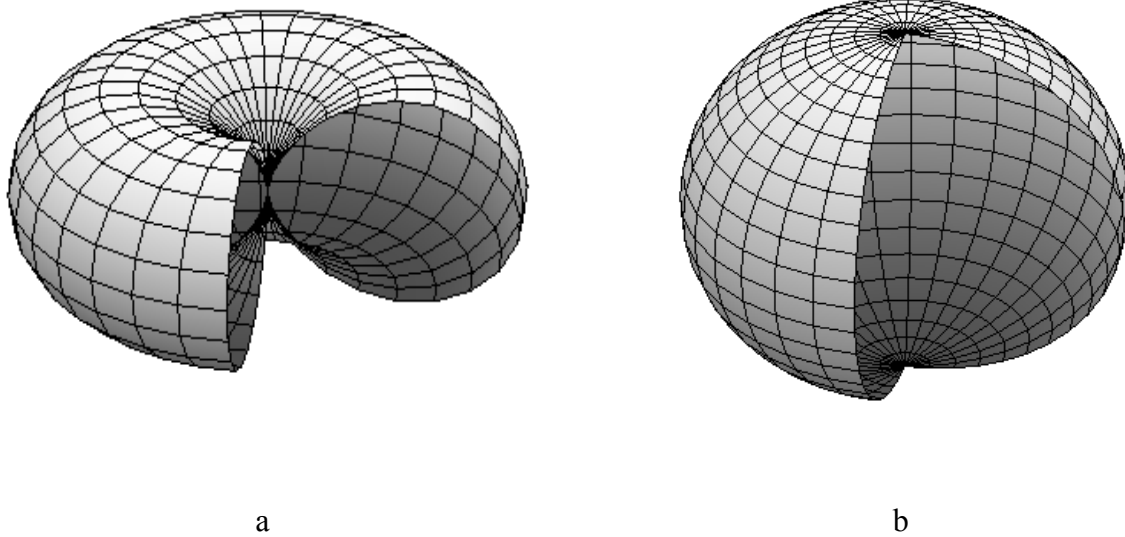


Figure 10.1. Distribution of power of the scattered light in space (a – for $\rho=0$, b – for $\rho=3/4$)

Equations (10.12), (10.13) and (10.17) express the power of the scattered radiation from one molecule. In case of the scattering of light by the ensemble of similar molecules the data of the equations must be multiplied by the number of molecules in a scattering volume.

It must be noted that in the context of approximation of the “theory of polarizability” the intensity of the scattered light and its polarizability characteristics are described by expressions (10.12) – (10.20) where the invariant of the scattering tensor is $\beta_a = 0$. In particular, according to

(10.20), the degree of depolarization of the scattered light for $\theta = \frac{\pi}{2}$

$$\rho = \frac{3\gamma^2}{10\beta_c + 4\gamma^2} \quad (10.23)$$

changes within the range $0 \leq \rho \leq \frac{3}{4}$. The scattered light is called fully polarised, if $\rho = 0$, and depolarised, if $\rho = \frac{3}{4}$. At $0 < \rho < \frac{3}{4}$ the scattered light is considered as partially polarised.

10.2 Quantum theory of Raman scattering

In quantum theory, Raman scattering arises from interaction between photon $h\nu$ and a molecule during which an exchange of energy takes place. As the result of interaction, photon $h\nu$ is absorbed and simultaneously photon $h\nu'$ is emitted, molecule passes from one energy level E_k to another one E_n (Fig. 10.2). Difference in the frequencies of absorbed and scattered photons $\nu - \nu' = (E_n - E_k)/h = \nu_{nk}$ is determined by the structure of energy levels of the molecule and is its individual characteristic. If during the interaction the molecule passes from a lower energy state to a higher energy state, then $\nu' < \nu$ and scattered radiation is called Stokes Raman scattering. Otherwise, when the molecule passes from a higher energy state to the lower one, then $\nu' > \nu$ and scattered radiation is called anti-Stokes Raman scattering. The scattering of radiation without change in the frequency $\nu' = \nu$ is called Rayleigh scattering.

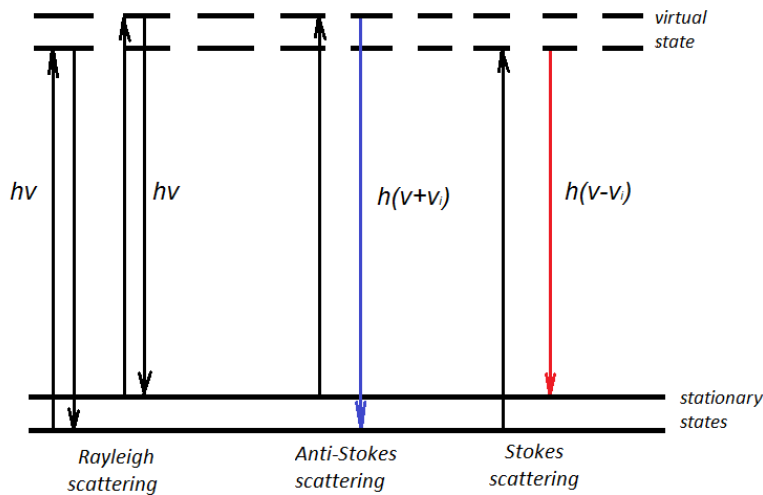


Figure 10.2. Scheme of energy levels of the molecule illustrating spontaneous Raman scattering

It must be noted that in Raman spectroscopy frequencies ν (or wavenumbers) have dimension $[\text{cm}^{-1}]$, since $\nu = 1/\lambda$. Therefore, $\Delta E = hc\bar{\nu}$, where $\bar{\nu} = \frac{1}{\lambda_{laser}} - \frac{1}{\lambda_{Raman}}$ represents the frequency shift (or Raman shift) from the laser line.

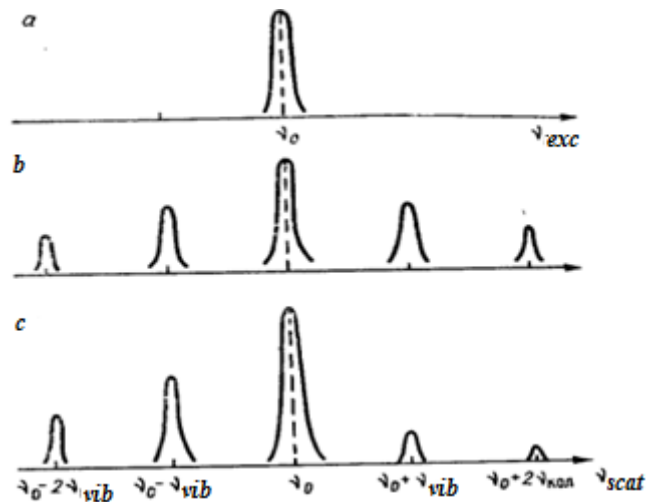


Figure 10.3. Schematic view of the spectrum of excitation source (a) and Raman spectra by the classical theory (b) and quantum theory (c)

It must be noted that a relative distribution of intensities in the Raman spectrum coming from the classical consideration (10.3) does not accurately reflect the real distribution of intensities, which may be realised only from the quantum mechanics perspective. The peculiarity consists in the fact that anti-Stokes Raman lines are always less intensive than relevant Stokes components. The reason is that the intensity of spectral bands is determined not only by probabilities of corresponding transitions (in this case Eq. 10.3 by electrooptical parameters $\left(\frac{\partial \alpha}{\partial q_i}\right)$), but by populations of levels which in relation to Stokes and anti-Stokes components are different (Fig. 10.3, Fig. 10.4).

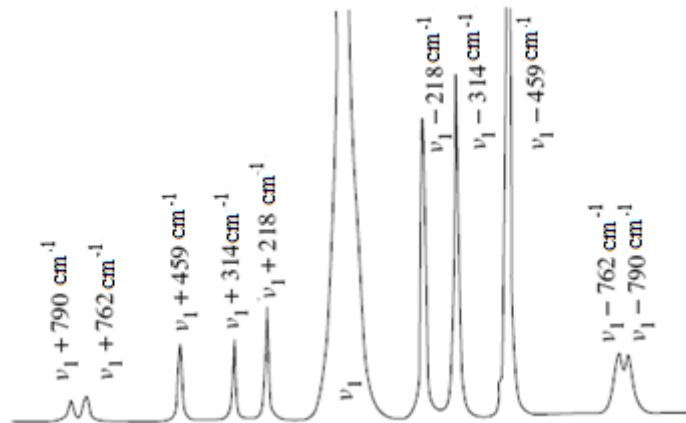


Figure 10.4. Raman spectrum of liquid CCl₄(ν_1 –Rayleigh line coinciding with the exciting radiation frequency)

Let us evaluate the relation of intensities of spectral lines of the anti-Stokes (I_a) and Stokes (I_s) scattering. We assume that in the case of spontaneous Raman scattering, intensities of lines of the transition $k \rightarrow n$ are proportional to the number of scattering particles N_k in state k . Then, since frequencies of transitions and probabilities of transition for Stokes and anti-stokes scattering are close, in case of thermodynamic equilibrium, when the Boltzmann distribution is satisfied, we have

$$\frac{I_a}{I_s} \approx \frac{(\nu + \nu_{nk})^4}{(\nu - \nu_{nk})^4} \exp\left\{-\frac{hc\nu_{nk}}{kT}\right\}. \quad (10.24)$$

The result demonstrates that the higher the temperature and the smaller the difference between energy levels of transition, the closer to each other are the values of intensities of lines of anti-Stoke and Stoke scattering.

10.3 Raman spectroscopy

In the ground electronic states under proper approximation it is possible to distinguish vibrational and rotational motion of the molecule. The vibrational motion of the molecule is the vibration of its nuclei close to their equilibrium values; it is described by a set of vibrational quantum numbers ν . The rotational motion of the molecule describes its rotation in space; it is determined by a set of rotational quantum numbers R .

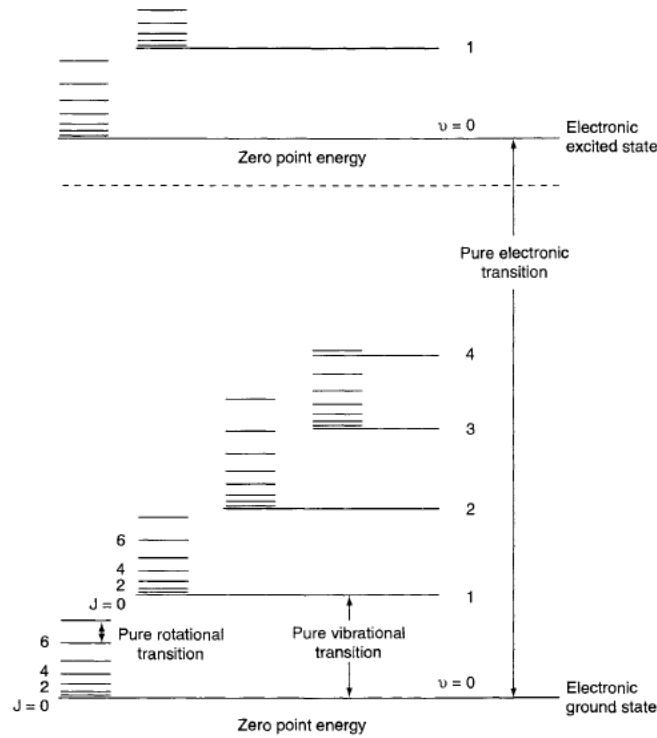


Figure 10.5. Energy levels of a diatomic molecule

In Raman spectroscopy the power of the scattered radiation from the volume V into the solid angle $d\Omega$ towards θ for an individual Raman spectrum of the vibrational-rotational line is usually defined by the expression

$$I_{\nu R \rightarrow \nu' R'}(\theta) = I_0 V n_{\nu R} \sigma_{\nu R \rightarrow \nu' R'}(\theta) d\Omega, \quad (10.25)$$

where ν, R and ν', R' – sets of quantum numbers of initial and final states of the scattering molecule, θ – angle between the direction of observation and the direction of oscillation of the electric vector of the linearly polarised laser radiation, I_0 – intensity of the exciting laser radiation, $\sigma_{\nu R \rightarrow \nu' R'}(\theta)$ – differential Raman scattering cross-section towards θ , and $n_{\nu R}$ – concentration of molecules of this type in the states with quantum numbers ν and R .

The differential Raman scattering cross-section on the approximation of the “theory of polarizability” is an individual feature of the scattering molecule and, according to (10.17), is connected with the scattering tensor by the relation

$$\sigma_{\nu R \rightarrow \nu' R'}(\theta) = \frac{16\pi^4 (\nu + \nu_{\nu R \rightarrow \nu' R'})^4}{15c^4} [10\beta_c \sin^2 \theta + \gamma^2 (6 + \sin^2 \theta)], \quad (10.26)$$

where the invariants of the scattering tensor β_c and γ^2 are determined by expressions (10.14) and (10.15).

Selection rules play an important role in Raman spectroscopy. They define possible changes in quantum numbers of the molecule during Raman scattering of light. Selection rules are associated with the symmetry of the molecule and are defined by means of methods of the group theory. In other words, selection rules help to define at which vibrational-rotational transitions of the molecule the power of the scattered light will not be zero and also allows us to identify the state of polarisation of the scattered light.

A sum of all vibrational-rotational lines permitted by the selection rules form the Raman spectrum of the molecular gas which is strictly individual for each class of scattering molecules. In spectroscopy, Raman spectra can be subdivided on pure rotational Raman spectra, vibrational-rotational Raman spectra and vibrational-rotational Raman spectra of overtones and combination frequencies. Characteristics and physical nature of these spectra vary greatly; therefore, they should be considered separately.

Pure rotational Raman spectra. The spectra are formed when during Raman scattering the molecule makes the transition $v, R \rightarrow v, R'$, i.e. when only the vibrational motion of the molecule changes. By their nature the spectra are caused by the rotation of the molecule as a whole in space; therefore, its properties are described with the help of the moment of inertia tensor. The values of three main moments of inertia (I_A, I_B, I_C) completely describe the properties of the rotating molecule. Depending on the main moments of inertia, molecules fall into four classes:

1. Linear molecules ($I_A = 0, I_B = I_C$);
2. Symmetric-top molecules $I_A \neq I_B = I_C$ or $I_A = I_B \neq I_C$;
3. Spherical top molecules $I_A = I_B = I_C$;
4. Asymmetric-top molecules $I_A \neq I_B \neq I_C$,

which are different in sets of rotational quantum numbers. Therefore, states of linear molecules, spherical top molecules and asymmetric-top molecules are described by the same quantum number of the momentum J ($R \equiv J$), and states of symmetric-top molecules are described by two quantum numbers J and K ($R \rightarrow J, K$), where K – quantum number determining the projection of the momentum on the symmetry axis of the molecule.

Selection rules for pure rotational Raman spectra of different molecules are expressed as

1. Linear molecules: $-\Delta J = 0, \pm 2$;
2. Symmetric-top molecules: $-\Delta J = 0, \pm 1, \pm 2$ и $\Delta K = 0$;
3. Spherical top molecules: $-\Delta J = 0$;
4. Asymmetric-top molecules: $-\Delta J = 0, \pm 1, \pm 2$.

Here, $\Delta J = J' - J$ and $\Delta K = K' - K$, where the initial state of the scattering molecule is determined by quantum numbers J and K , and the final state – quantum numbers J' and K' . All cases must also satisfy the condition of $J' + J \geq 0$.

In spectroscopy, lines of pure rotational Raman spectra are normally grouped into O -, P -, Q -, R -, S - branches in accordance with conditions $\Delta J = -2, -1, 0, +1, +2$. All the lines of the pure rotational Raman spectrum are located near the Rayleigh line; moreover, lines of O - and P -branches belong to the anti-Stokes part of the spectrum, lines of R - and S -branches – to the Stokes part of the spectrum, and lines of Q -branch coincide with the Rayleigh line in frequency.

By their physical nature all the lines in pure rotational Raman spectra are caused by the anisotropy of the tensor of electronic polarizability $\alpha_{\rho\sigma}^{(g)}(x)$ in scattering molecules. Consequently, the scattering light in pure rotational Raman spectra is always depolarised. The absence of the anisotropy of the electronic polarizability in the spherical top molecules leads to the fact that molecules do not produce pure rotational Raman spectra.

Vibrational-rotational Raman spectra. These spectra are formed during Raman scattering when the molecule makes transition $v, R \rightarrow v', R'$, i.e. when both vibrational and rotational motions of the molecule change simultaneously.

The vibrational motion of a polyatomic molecule is a simultaneous motion of all the nuclei of the molecule close to their equilibrium position.

In the context of the theory of molecules such a motion of nuclei can be represented as a superposition of normal modes of vibrations of nuclei, where each normal mode is characterised by its own frequency and vibrational quantum number v_i . If the frequencies of several normal modes coincide, they are called degenerate. The number of degenerate normal modes and the degree of their degeneracy are determined by the symmetry of molecule and can be found by the methods of the theory of groups. A whole number of normal modes of vibrations of N -atomic molecule is equal to $3N - 6$ (for linear molecules – $3N - 5$). Thus, each vibrational state of the molecule is defined by a set of vibrational quantum numbers v_i

This section is devoted to that part of Stokes vibrational-rotational Raman spectra which emerges during Raman scattering when the molecule makes transition $v_i, R \rightarrow v_i + 1, R'$ (other vibrational quantum numbers that do not change during transition are not presented). The anti-Stokes part of vibrational-rotational Raman spectra is not considered here, since its intensity is considerably low and it is not of a great interest in gas-analysis.

The selection rules for vibrational-rotational Raman spectra look quite complicated, since they depend on the type of normal modes and the type of top of the scattering molecule. The set of selection rules for vibrational-rotational lines of various types is presented in [1]. The most important are the selection rules for quantum number J . As well as in pure rotational spectra, vibrational-rotational spectra are subdivided into O -, P -, Q -, R -, S -branches in accordance with conditions $\Delta J = -2, -1, 0, +1, +2$.

According to the selection rules for totally symmetric vibrations, lines of Q -branches of vibrational-rotational bands are polarised in spherical top molecules and partially polarised in linear molecules and symmetric- and asymmetric-top molecules. In other cases, vibrational-rotational lines are depolarised.

Generally, the intensities of lines of the rotational-vibrational spectrum (transition $v_i, R \rightarrow v_i + 1, R'$) are significantly lower than the intensities of relevant lines in a pure rotational spectrum (transition $v_i, R \rightarrow v_i, R'$).

Vibrational-rotational Raman spectra of overtones and combination bands. Spectra are formed during Raman scattering when the molecule makes transition $v_i, R \rightarrow v_i + 2, R'$ (first overtone) or transition $v_i, v_j, R \rightarrow v_i + 1, v_j + 1, R'$ (combination frequency). Raman spectra of overtones and combination frequencies of higher orders are not considered due to their extremely low intensity.

The origin of these spectra is defined by two reasons [3]: firstly, non-linear change in polarizability of molecules under the change of its inter-nuclear distances (presence of non-zero

values $\left(\frac{\partial^2 \alpha}{\partial q_i^2}\right)_{q_i=0}$ and $\left(\frac{\partial^2 \alpha}{\partial q_i \partial q_j}\right)_{q_i=0, q_j=0}$), secondly, break in harmonicity of vibrations of the

molecule nuclei which results in the interaction of its normal modes.

The selection rules and polarizability characteristics for vibrational-rotational Raman spectra of overtones and combination frequencies can differ from the set of selection rules and polarizability characteristics for vibrational-rotational Raman spectra of fundamental tones and can be obtained by means of the theory of groups.

It must be noted that the intensities of lines of the Raman spectrum of overtones and combination bands are significantly lower than the intensities of lines of vibrational-rotational

Raman spectra of fundamental tones. Except for the cases, when the frequency of the overtone (or combination tone) is close to the frequency of the fundamental tone of a different vibration of the same molecule. Resonant interaction between these vibrations causes re-distribution of intensities of the scattered light between these bands leading to an increase in the intensity of overtone lines.

10.4 Differences between IR spectroscopy and Raman spectroscopy

Despite the fact that absorption spectroscopy in the IR range (hereinafter, IR spectroscopy) and Raman spectroscopy are similar in providing the information about vibrational frequencies, each approach has numerous advantages and disadvantages (Fig. 10.6).

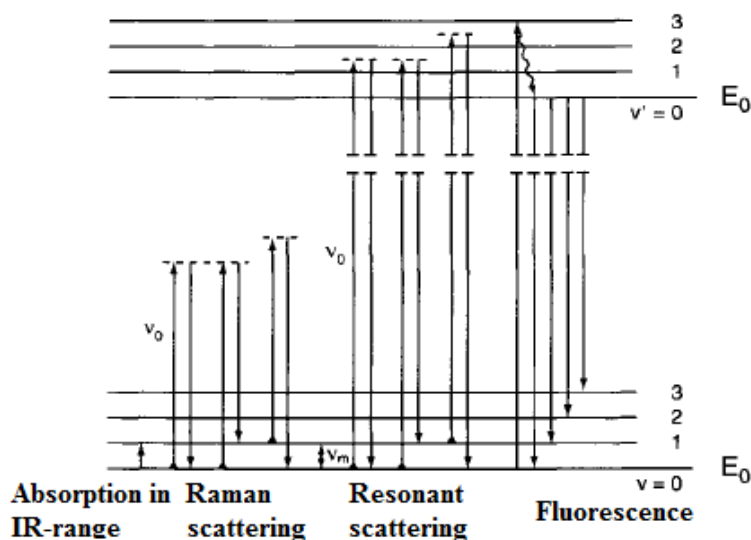


Figure 10.6. Comparison of transition in IR, Raman scattering, resonant scattering and fluorescence

1. Selection rules are different for IR and Raman scattering. As the result, some vibrations are active not only in Raman spectrum, other only in IR. Typical examples can be found in molecules with a centre of symmetry for which the selection rules are mutually exclusive. As a rule, vibration can be active in IR or Raman scattering, or both, however, it must be noted that totally symmetric vibrations are always active in Raman scattering.
2. Some vibrations are weak in IR and strong in Raman scattering. For example, stretching vibrations corresponding to the types of bonds: $C \equiv C$, $C = C$, $P = S$, $S - S$, $C - S$. As a rule, vibrations are strong in Raman scattering, if the bond is covalent; they are strong in IR, if there is ionic bond (O-H, N-H). It should be noted that in Raman scattering the deformation vibrations are normally weaker than the stretching ones.
3. In Raman scattering it is possible to measure polarizability, which provides reliable information about the symmetry of normal modes of vibrations. The information cannot be obtained from the IR spectrum.
4. It is possible to use resonant scattering to strengthen particular vibrations.
5. Obtaining the Raman spectrum, as a rule, requires a smaller volume of a sample.
6. In Raman scattering water has its typical spectrum representing one band, which allows us to analyse aqueous solutions or gas media containing water vapours by means of Raman scattering. In IR spectroscopy water has strong absorption bands; therefore, it is difficult to identify required spectral components on its background.
7. The Raman spectrum within the range 0-4200 cm^{-1} contains main bands of any molecule. The spectrum can be simultaneously recorded by one device with the help of a laser with non-tunable wavelength. It permits obtaining the information about all molecular

compounds of the sample, the content of which exceeds the sensitivity threshold of the equipment. In IR spectroscopy, when working in various spectral regions, it is necessary to use optimal diffraction elements, filter and detectors.

Raman scattering has the following disadvantages.

1. Extremely low intensity of Raman scattering signals. This circumstance is particularly evident when dealing with gas media.
2. When working with some samples exposed to laser radiation, fluorescence occurs and complicates the identification of the Raman spectrum on its background.
3. It is more difficult than in IR to obtain pure rotational or vibrational-rotational spectrum with high resolution in Raman scattering.
4. Raman spectroscopy permits obtaining only molecular spectra.

To sum up, Raman spectroscopy is a more universal analytical tool. However, IR spectroscopy permits obtaining more reliable results. Nevertheless, in general, both methods must be considered as complementary.

LECTURE 11. RAMAN INSTRUMENTATION

Since the discovery of Raman scattering, equipment required for its registration has been continuously improved. To date, as radiation sources mercury lamps were replaced by small-sized lasers, scanning double and triple monochromators with photoelectronic multipliers were replaced by single spectrometers with holographic notch-filters at the entrance and high-sensitivity multichannel photodetectors at the exit.

11.1 General scheme of registration of Raman spectra

Generally, recording Raman spectra requires the following components:

- source of monochromatic radiation (laser),
- optics for light collection,
- spectral device (spectrometer),
- photodetector,
- computer.

The principle operation of a Raman spectrometer consists in the following (Fig. 11.1). Monochromatic radiation falls on the sample, where it scatters on the molecules of a sample. The emerged scattered radiation containing Rayleigh and Raman scatterings is gathered in optical system and directed to the entrance of a spectral device. Inside the spectral device the radiation is decomposed into spectrum, after which it is registered by photodetector. Computer, in this case, is necessary to visualise the results of processing.

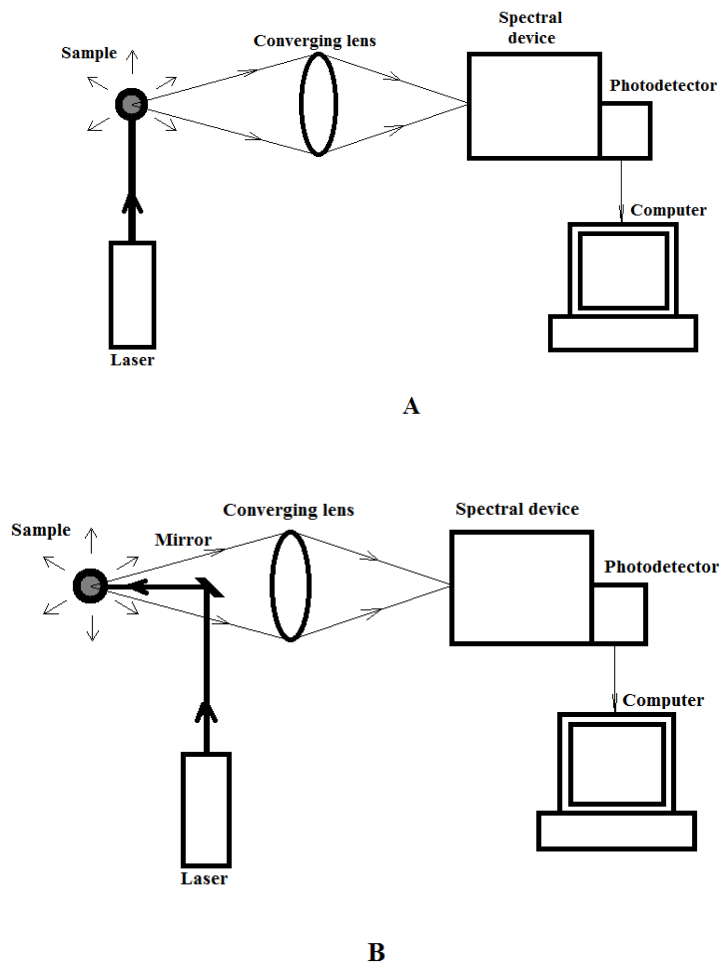


Figure 11.1. Configurations for recording Raman spectra: a – 90°-geometry, b – 180°-geometry

Depending on the angle of observation of the scattered light in relation to the exciting laser radiation, there are two possible configurations: 90°-geometry and 180°-geometry (Fig. 11.1). Table 11.1 demonstrates the main advantages of each configuration. It must be noted that 180°-geometry is the most used in modern Raman spectrometers. However, there are cases, when 90°-geometry is the best option (for example, registration of Raman spectra of gas media in a cell).

Table 11.1.

Comparison of advantages of 90°-geometry and 180°-geometry.

90°-geometry	180°-geometry
Permits gathering more scattered radiation when projecting a laser beam waist on the input slit of a spectral device	
	Permits working with solid bodies and non-transparent liquids
	More convenient to use, less sensitive to maladjustment
Lower level of background and fluorescence	
Realisation takes less optical elements	

11.2 Laser

A source of Raman excitation – laser – is the most important component of a Raman spectrometer. It defines such parameters of Raman spectrometer as size, cost, stability, reliability, and sensitivity. Moreover, wavelength of the laser radiation will define the value of cross-section of the scattering of the molecule and the value of emerging background in the spectrum. Let us study the circumstances of the registration of Raman spectra with various excitation wavelengths in more detail.

The cross-section of the scattering included into the dependence for the intensity of the Raman signal (see relation (1.25)) of any molecular component depends on the frequency of the exciting light, whose simplified formula is

$$\sigma = c \cdot (\nu_0 - \Delta\nu)^4, \quad (11.1)$$

where ν_0 – frequency of the exciting light, $\Delta\nu$ – frequency shift, c – constant taking into account the degeneracy of a normal mode of vibrations, amplitude of zero vibrations and value of the polarizability tensor of molecule.

Therefore, it is highly beneficial to use the intensive short-wave exciting radiation to obtain maximum analytical signal (for example, from UV range). Furthermore, short-wave radiation due to high level of the quantum energy can be registered by detector with higher quantum effectiveness and lower noise, consequently, total sensitivity of spectrometer will worsen. However, the practice of using short-wave sources of radiation, unfortunately, proved that they have some disadvantages. Here belong, firstly, high level of fluorescence, since more electronic transitions occur in UV and visible ranges than in IR. Therefore, since the intensity of fluorescence can be by several orders higher than intensities of Raman signals, which can significantly complicate the identification of Raman signals in the registered spectrum. Besides the emerging fluorescence, the application of the short-wave source raises the requirements for resolution of a spectral device due to decrease in distance between lines in the Raman spectrum. The problems can be resolved by decreasing the

aperture ratio of the device; however, it also leads to declining analytical signal. Transition to IR range determined by the absence of listed disadvantages threatens with a significant decrease in the cross-section of the scattering, consequently, in the intensity of Raman signals. As seen from the above peculiarities, radiation from each range has both advantages and disadvantages. Therefore, each task requires reasonable choice of a specific laser with optimal wavelength. It must be noted that currently the most widely spread are the lasers of visible wavelength range (~400-800 nm) where “a golden mean” of the “fluorescence/Raman signal” ratio lies.

In addition, it must be noted that the optimality of laser source depends not only on its wavelength, but directly on its characteristics. Laser for Raman spectroscopy must meet the following requirements: to ensure the stability of the wavelength, to provide an opportunity for generating a narrow spectral line at high power radiation, and to be small-sized and relatively inexpensive.

Lasers that mostly meet the criteria are gas, solid-state and semiconductor. Among gas lasers He-Ne laser draws attention. Despite its advantages (relatively low cost and high reliability (~100 000 hours), a major limitation of its use is the low power per unit length, consequently, low total output power. Potentially, semiconductor laser can be used to excite Raman spectra, however, these lasers work, as a rule, in multimode or simultaneously, or change the wavelength of generation (depending on the dominant mode), which complicates their use for this purpose, since they do not meet criteria of “stability of the wavelength” and “width of generation band”. Another option is the use of solid-state lasers. Recently, rapidly developed technologies have significantly affected their cost and availability. Moreover, solid-state lasers, as a rule, small-sized, cover a wide spectral range and are capable of providing high output power in continuous mode. An important advantage is that the lasers have emerged on the market in their portable variant – “laser pointers” working continuously in a visible wavelength range and providing power output up to 1 W.

Note that due to a small density of molecules in the gas phase, registration of their Raman spectra requires laser with the output power at the level of unit W, and for liquids (since their density is several orders higher) – the power at the level of mW is sufficient.

11.3 Light collection

Paying attention to the relation (10.25) we can see that the intensity of Raman signals depends on the solid angle of light collection $d\Omega$. Therefore, it is reasonable to use optics providing a larger angle of light collection to obtain a maximum analytical signal. The most popular option in modern Raman spectrometers is the use of lenses or lens objectives (Fig. 11.1). It must be noted that the angle of scattering by a point source is equal to 4π sr. None of the lens objectives due to their specifics is able to provide a collection angle more than 1 sr. When it is necessary to enlarge the angle of light collection, it is reasonable to use mirror optics. The simplest option is adding a spherical mirror on the optical axis to collect the light scattered “backward” (Fig. 11.2a). The configuration permits enlarging the angle of light collection (and, respectively, Raman signal) almost by two times. Other option is using the mirror only to collect the scattered light. It is reasonable to use an elliptical mirror for the latter (Fig. 11.2). The mirror has two focal points, one of which can be combined with the analyte, and another with the input slit of a spectral device. In this case, it is possible to see that the angle of light collection will be significantly larger than 1 sr and can reach 2π sr.

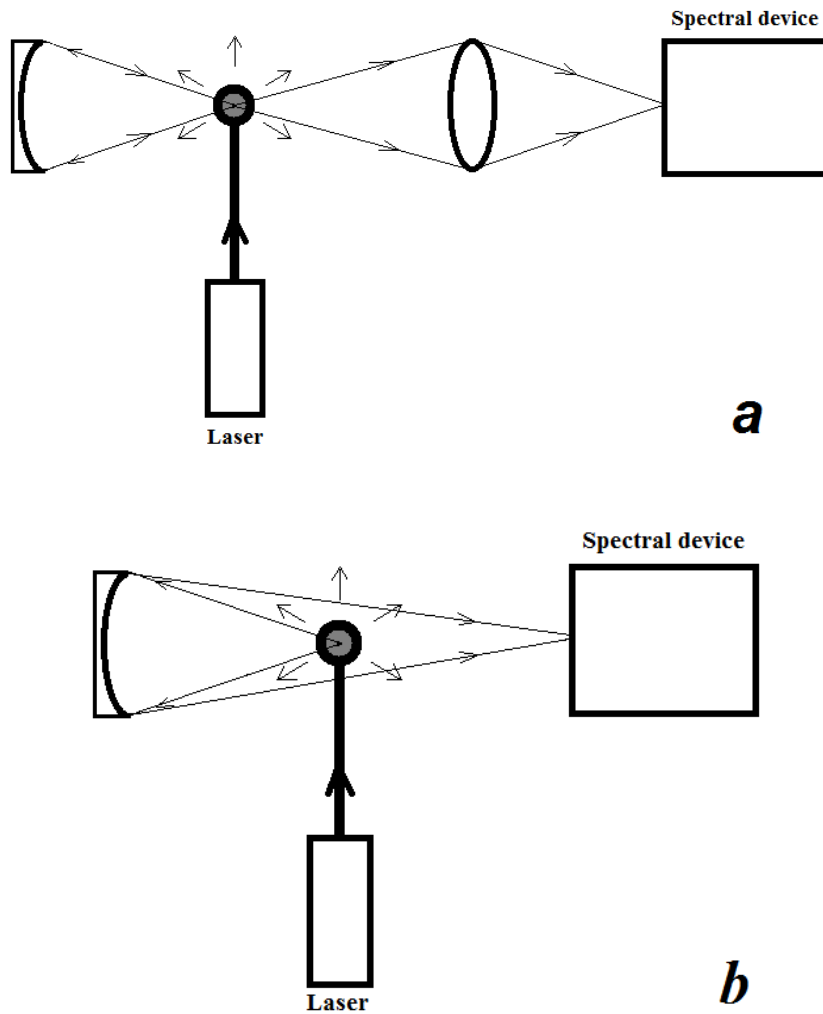


Figure 11.2. Options for the scattered light collection: a – by means of the lens objective combined with a spherical mirror; b – by means of elliptical mirror

The above systems for collecting the scattered light is suitable for laboratory Raman spectrometers. In case of industrial application of Raman spectroscopy, where there is no possibility of placing the analyte into a Raman spectrometer, special fibers for remote excitation and collection of Raman scattering are used (Fig. 11.3).

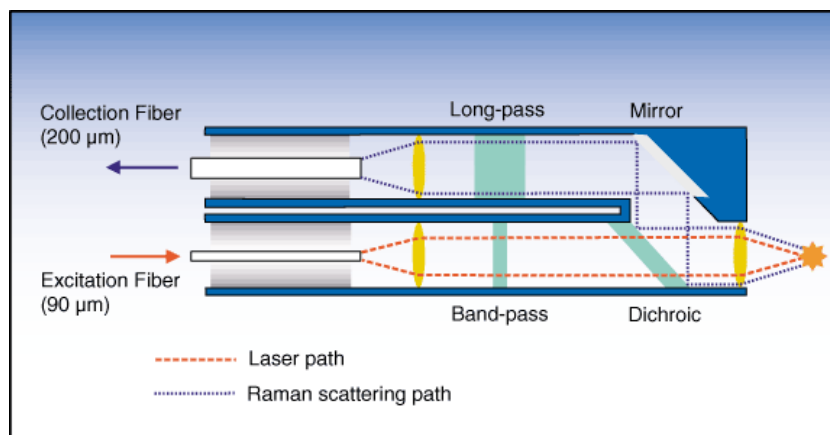


Figure 11.3. Optical system “Raman Probe” for exciting and collecting Raman scattering by means of the fiber

11.4 Spectral device

The scattered light collected from the analyte must be decomposed in the spectrum for further identification of characteristic Raman bands and evaluation of their intensities. This function in Raman spectrometer is performed by a spectral device. Let us consider the types of spectral devices suitable for Raman spectroscopy.

Monochromator – spectral device designed to detect monochromatic radiation. This device is designed so that it blocks all the incoming radiation except for a narrow spectral region.

Monochromator consists of the following parts: input slit, collimator lens, dispersing element (prism or grating), chamber lens, and output slit which selects the radiation belonging to a narrow interval of wavelengths. The scanning of the spectrum (to obtain a required spectral range at the output) is provided by means of rotation of dispersing element.

It must be noted that, to date, in modern Raman spectrometers diffraction gratings have almost replaced prisms. The main reason is that diffraction gratings provide much better combination of optical transmission and spectral resolution than prisms.

Among various optical schemes for decomposing the light into the spectrum the most widely used is the monochromator designed according to the Čzerny-Turner scheme (Fig. 11.4). Its principle of operation consists in the fact that the light coming from the input slit is collimated by the first concave mirror, decomposed into the spectrum of plane diffraction grating and is focused by the second concave mirror on the plane of the output slit.

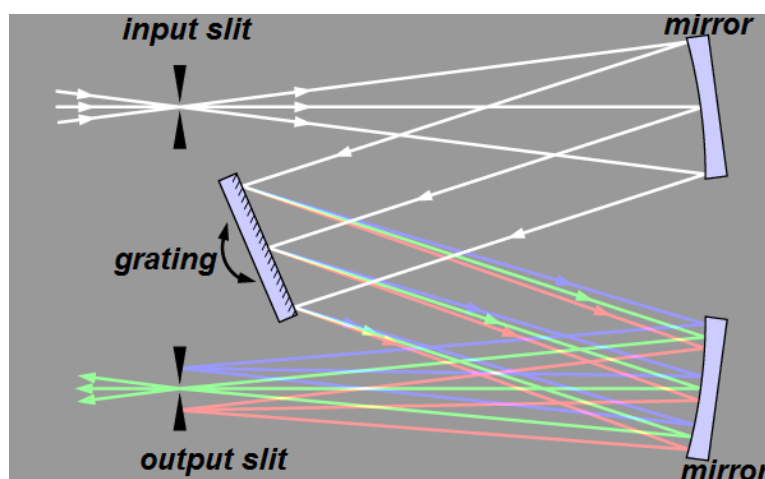


Figure 11.4. Scheme of the Čzerny-Turner monochromator

It is also worth paying attention to the monochromator designed according to the Rowland scheme. It consists only of input slit, concave diffraction grating, and output slit (Fig. 11.5). Due to the lower number of optical components the monochromator permits minimising losses of the collected Raman radiation. Moreover, the monochromator designed according to the scheme is small-sized and relatively inexpensive. However, it should be noted that the quality of the spectrum in this case is worse than in the above scheme.

It is worth noting that Raman spectrometer based on monochromator is single channel (i.e. at the exit there is a single channel radiation detector, for example photoelectronic multiplier), and for recording the required spectral range it is necessary to perform the scanning of the spectrum (by rotating the grating). Therefore, recording the entire Raman spectrum takes certain time, which often limits the use of similar devices.

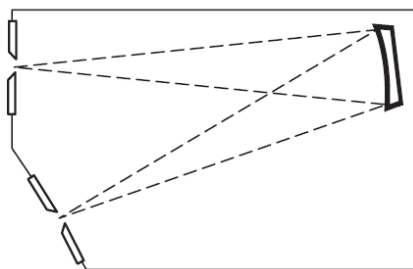


Figure 11.5. Monochromator with the concave diffraction grating

At present, Raman spectrometers based on *polychromator* are getting more popular. Their main difference consists in the absence of output slit. Instead of it there is a multi-channel photodetector. Therefore, it is possible to simultaneously record the entire Raman spectrum. Figure 11.6 demonstrates the most used in Raman spectroscopy optical schemes of polychromators.

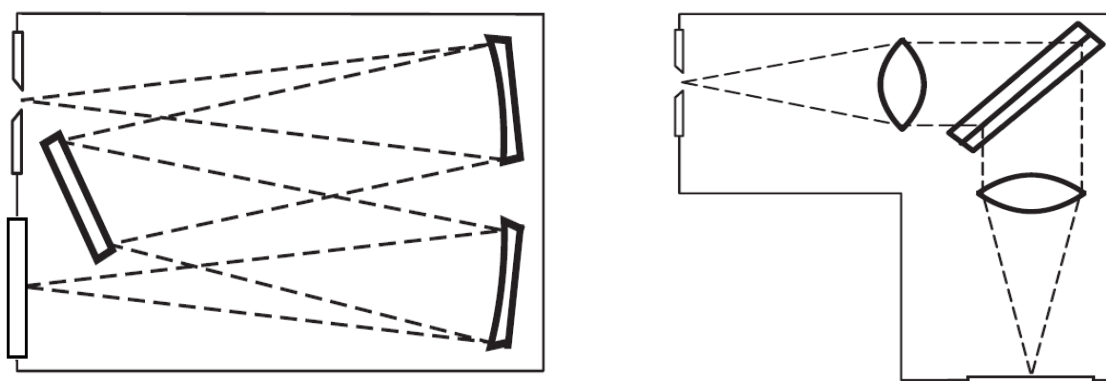


Figure 11.6. Optical systems of polychromators for Raman spectrometers

The main characteristics of spectral devices are:

1) *Dispersion.*

It indicates which spectral range is per unit length in the focal plane of device. As a rule, manufacturers indicate the value of the inverse linear dispersion ($d\lambda/dl$, [nm/mm]). The main component detecting dispersion is the diffraction grating: the more the number of grooves per 1 mm of the grating is, the lower the inverse linear dispersion will be provided and, respectively, the resolution of the device will grow.

2) *Aperture ratio.*

It is the ratio of the focal distance of collimator to its aperture. The device with higher lens speed provides a larger collection angle of the scattered radiation, and, consequently, Raman spectrometer works more effectively.

3) *Transmittance coefficient.*

It indicates which share of the light passing through the input slit of a device will reach the detector. As a rule, this parameter varies from 5 to 50%; the larger losses occur on diffraction grating.

4) *Suppression of the scattered light.*

It represents the relation of the value of the “parasitic” scattered light (emerged inside the spectral device) to the total amount of light. As a rule, the value is 10^{-5} and less.

It must be noted that there is no configuration with the record values of all listed parameters. For example, the best suppression of the scattered light is provided in configurations with low emission coefficient and low aperture ratio. Thus, optimal configuration of a spectral device must be selected in accordance with the task.

11.5 Photodetectors

Due to the fact that Raman signals are low-intensive, obviously, photodetector must, first of all, have high sensitivity and low noise level. For a long time the absence of detectors with the required parameters has limited the use of Raman spectroscopy in solving the applied tasks, particularly in chemical analysis. However, modern microelectronic technologies brought it to a new technological level.

Historically, photographic plates were used as first “photodetectors” to register Raman spectra. Photographic plates were placed in the focal plane of spectrograph and permitted simultaneous recording of the required spectral range. In addition, among the advantages of photographic plates were their low cost and absence of dark noise. The main disadvantages that predetermined their fate and displacement with photoelectronic detectors are the impossibility of automation of a Raman spectrometer (associated with the need to develop photographic plates and to make photometry) and relatively small dynamic range.

Photoelectronic multiplier tube (PMT) replaced photographic plates due to its high sensitivity. PMT is an electro-vacuum device which converts the energy of optical radiation into electrical signals due to multistage amplification (Fig. 11.7a) and contains photocathode, secondary-electronic multiplier, and anode.

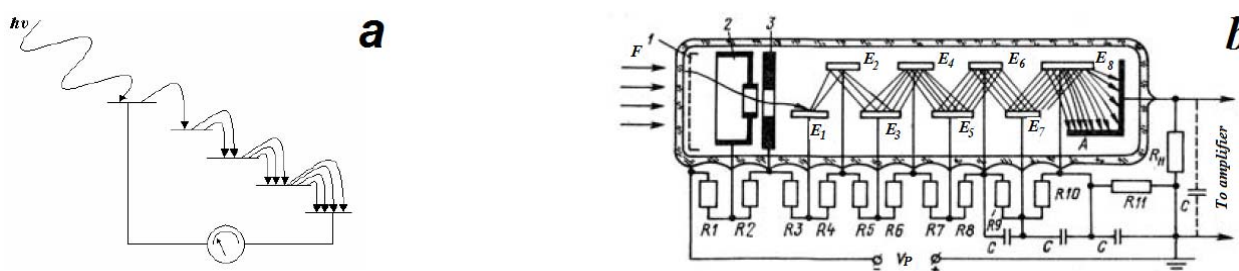


Figure 11.7. Photoelectronic multiplier tube (PMT): a – principle of multistage amplification, b – PMT device

When illuminated the photocathode 1 (Fig. 11.7b) emits primary photoelectrons, which are accelerated by the electric field and focused by the electronic optical system 2 on the first dynode $E1$ causing its enhanced secondary electron emission. Secondary electrons emitted from the first dynode are accelerated by the field and directed on the second dynode $E2$, the enhanced electron flow from the second dynode goes to the third and so on. The electric field accelerating the electrons is generated by a voltage divider which provides high positive potential for each succeeding stage relative to the previous one $R1 - R11$. When working in “transmission” mode, semi-transparent photocathode is applied to a flat output window of the flask in form of a circle with 10-50 mm in diameter.

Such a principle ensures high-sensitivity of PMT. This type of photodetectors has been dominant in Raman spectroscopy and has been used in combination with monochromator for a long time. However, as it can be seen, PMT is a single channel detector and recording the spectral range with the monochromator-PMT system requires scanning of the Raman spectrum. The main problem in scanning is that during the time required for the procedure a registered Raman spectrum can undergo changes associated with fluctuations of the power of the exciting radiation or fluctuations of components of the analyte.

Despite the fact that today multichannel PMTs are available, they represent a set of miniature single channel PMTs, they are not widely spread in Raman spectroscopy due to their low resolution.

To date, the most widely spread photodetectors used in Raman spectrometers are *CCD image sensor* or *linear CCD arrays*.

Charge-coupled device (CCD) is an integrated circuit (Fig. 11.8) consisting of the so-called MOS structures (metal-oxide-semiconductor). MOS structures are formed on a common semiconductor substrate (1) so that bands of electrodes (2) form a regular linear structure (linear CCD) or matrix (CCD *image sensor*). Electrodes are isolated from the substrate by the thinnest dielectric layer – silicon dioxide.

Applying electrical potentials to electrodes causes formation of potential wells in the volume of the substrate (3). A charge trapped in a well cannot leave it independently due to the inhibitory action of the electrode potential. The number of wells is equal to the number of electrodes and defines the number of CCD pixels.

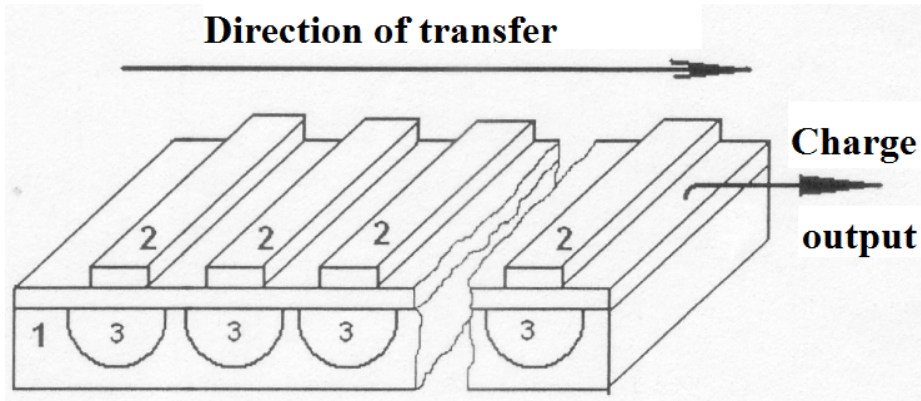


Figure 11.8. Charge-coupled device (CCD)

CCD is mostly used to measure spatial distribution of the intensity of light, for example, in digital cameras. Therefore, CCD consists of the transparent window, and CCD itself is placed in the focal plane of the lens of camera or chamber of a spectral device. The absorption of quanta of the incident light by silicon is accompanied by the release of electrons weakly bound in the crystal grating of semiconductor (internal photoelectric effect). These electrons fall in the closest potential wells. In a period of time called the exposition time, the wells are filled with photoelectrons. Moreover, the distribution of the number of electrons accumulated in the wells corresponds to the distribution of the intensity of the incident light over the surface of the CCD crystal.

The problem consists in measuring accumulated charges. Physically, it is impossible to connect each potential well with a charge meter by semiconductor, because modern CCD pixels make up millions and tens of millions.

In 1969, W. Boyle and G. Smith invented the charge transfer principle. For the first time, the inventors made the distance between neighbouring electrons so small (0.2-1 micron) that their mutual influence became significant due to the overlapping of regions of a spatial charge close to the edges of adjacent electrodes. Such a mutual influence enables a direct transfer of charge packages from electrode to electrode by manipulating electric tensions on these electrodes. A concrete form of impulses is not considered here, since the form significantly varies in various types of CCD. The succession of impulses leading to the charge transfer is called timed or shifted.

Figure 11.9 demonstrates a part of the CCD in five succeeding timed impulses T1-T5. It is clear, that all charge packages are simultaneously shifted towards the charge meter. It is also obvious that during the reading, potential wells of CCD become free from the accumulated charge, i.e. they become ready for next exposition. After reading the CCD and measuring the distribution of charges it is possible to measure the distribution of the light intensity on the surface of CCD.

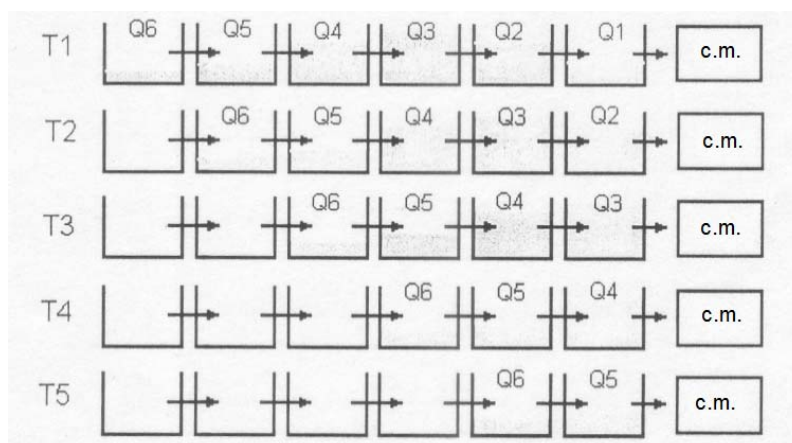


Figure 11.9. Charge transfer principle in CCD

It must be noted that due to this fact, modern Raman spectrometers (using polychromators with photodetector of the CCD type) have become multichannel, i.e. each pixel in a linear CCD or each column of a CCD matrix registers Raman radiation on its own wavelength.

It is worth noting that the main characteristics of photodetectors are:

1. Quantum efficiency. The probability that photon fallen on the detector will generate a photoelectron. The value depends on the wavelength and defines the spectral region of sensitivity of a detector.
2. Size of photosensitive area.
3. The number of sensitive channels and their size.
4. Dark signal. The average number of electrons generated at the moment when the detector is not illuminated.
5. Read noise. It indicates a standard deviation of succeeding measurements of a stable number of electrons.

11.6 Suppression of Rayleigh scattering

To reduce the stray light inside spectral device, it is necessary to make filtration of radiation on the wavelength of a laser. Rayleigh scattering, as a rule, is at least by 4 orders stronger than Raman scattering; therefore, to avoid overlapping of the Raman signal with Rayleigh scattering, spectral device must suppress the scattered light better than 10^{-4} . However, Rayleigh scattering from solid samples, optics, dust and so on may easily exceed Raman scattering by several orders and entirely overlap the useful Raman signal.

Earlier, two methods were used to eliminate the drawbacks: multistage monochromators (double or triple) or absorption filters. However, multistage monochromators are complex large-sized expensive optical constructions with low transmittance.

Absorption filters (or colored glass) is the simplest type of light-filters which has a spectral selectivity defined by different absorption of various portions of the electromagnetic spectrum. Filters, by installing them in front of the input slit of a spectral device, can be used to block (absorb) Rayleigh radiation and transmit Raman scattering. Absorption filters are not sensitive to the angle of incident light; therefore, they can be installed in a non-collimated light beam. The absorbing thickness may be raised, if necessary, to obtain the required optical density on the laser wavelength. The main drawbacks of these filters are that their absorption spectra are too sloping, which may lead to the loss of the Raman spectrum up to 1000 cm^{-1} caused by the Rayleigh line. Furthermore, filters can serve as a source of fluorescence, which will be a disturbing factor in a registered Raman spectrum.

Holographic *notch* and *edge filter* represent a more effective option for filtering the laser radiation in Raman spectroscopy. *Edge filter* is characterised by the fact that all wavelengths higher or lower than a definite frequency are blocked (by reflection) and other part is transmitted. *Notch filter* blocks only a narrow spectral range, while the rest spectrum is transmitted. Figure 11.10 illustrates the transmission spectra of these filters.

Holographic filters are designed by creating an interference image generated by a laser beam in the layer of dichromated gelatin placed between two glass plates. Commercially available holographic filters can weaken the Rayleigh radiation in amplitude by 4 or 6 orders while transmitting at least 90% of the radiation in the rest range. Thus, holographic notch filters allow single diffraction spectral devices provide acceptable performance for the scattered light while maintaining their high efficiency.

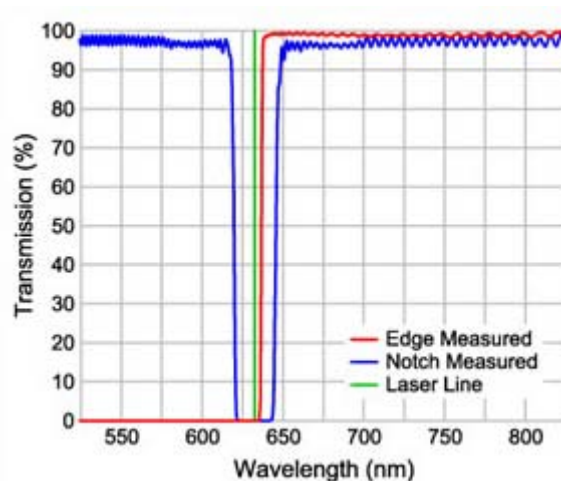


Figure 11.10. Transmission spectra of notch and edge filters on the background of the laser line

11.7 Fluorescence suppression

Each sample (or its impurities) can absorb the laser radiation and re-radiate it as fluorescence. In this case, the Raman spectrum will be covered by a large and strong fluorescence band; moreover, its intensity may be 10^4 times higher than the Raman signal.

There are a few methods for solving the problem. If impurities in the sample cause fluorescence, the sample must be purified. If the sample itself generates fluorescence, the first thing to do is to change the wavelength of the exciting laser. Shifting towards a long-wave part of the spectrum may significantly reduce fluorescence. Excitation with the IR wavelength range, in this case, is ideal, since within this range electronic transitions are very rare and probability of observing fluorescence is extremely small. In some cases, addition of quenching agents may be effective such as potassium iodide or mercury halides. Furthermore, the influence of fluorescence on the Raman spectrum can be minimised by using pulsed lasers coupled with photodetectors equipped with electronic shutters. Since the lifetime of Raman scattering is $10^{-12} - 10^{-13}$ sec, which is significantly smaller than the lifetime of fluorescence ($10^{-7} - 10^{-9}$ sec), in this case, registration of a difference spectrum is an effective approach (i.e. subtract the fluorescence spectrum from the spectrum registered at the initial moment of time representing the Raman spectrum and fluorescence). Other option is transition to the anti-Stokes region where fluorescence is absent. However, it must be taken into account that in the anti-Stokes region Raman signals are by several orders weaker than in the Stokes one.

PART 5. PRACTICUM MANUAL

LABORATORY WORK 1

QUALITATIVE ELEMENTAL ANALYSIS OF SUBSTANCE

Objective. To study the basis of the visual method for spectral analysis by means of steeloscope with photoelectric registration of the spectrum.



Figure 1. Exterior view of a steeloscope with photoelectric registration

Procedure

Part 1. Determination of dispersion in steeloscope.

1. Place copper electrodes on the table, the lowest – copper disc. Distance between the electrodes (working space) is 1 mm, it is set according to the template.

2. Select required spectral region. Select a green region of the spectrum where three bright copper lines are visible, whose wavelengths are 5105.54 Å, 51583.24Å, 5218.20Å respectively.

3. Arc between electrodes starts burning; spectrum can be observed by means of the eyepiece.

4. Switch the eyepiece into the projector mode moving it from the focal plane of device.

5. Start SL-13 software on the computer. While the arc is burning check the quality of the spectrum in the test mode of measurements. Test spectra are observed on the computer screen. Add neutral light-filters in case of the saturated pixels.

6. Record noise signal and spectrum. Save the spectrum in computer memory using SL-13 software.

Use the spectrum of copper (Cu). Find dispersion in the green region. Dispersion of the device is determined by the relation:

$$D = \frac{\Delta\lambda}{\Delta l},$$

where $\Delta\lambda$ – difference between wavelengths; Δl – distance between pixels.

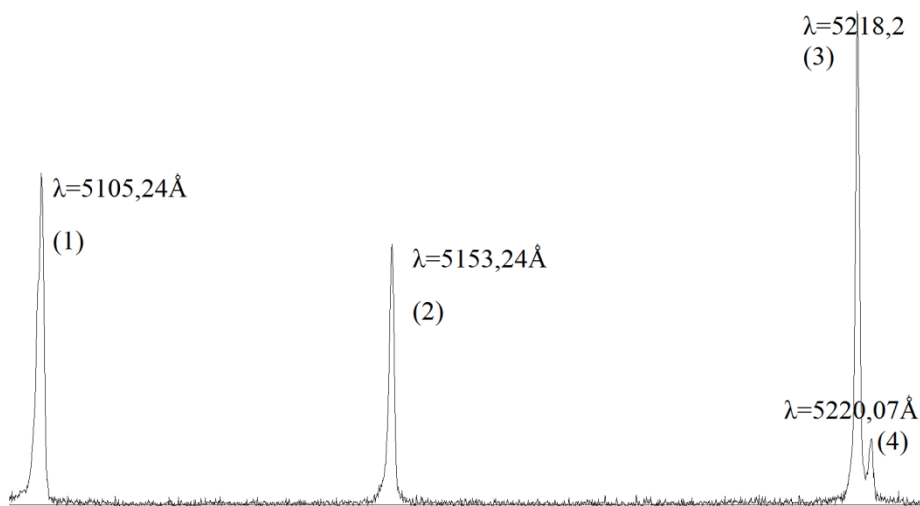


Figure 2. Spectrum of copper

Part 2. Elemental analysis of unknown sample.

1. Keep the previous setting of the steeloscope. Change the upper electrode only. The upper electrode is represented by the electrode with unknown elements.

2. Burn the arc between electrodes. 4A Current. Choose light-filter in the test mode of measurements.

3. Record the spectrum. Do not forget to check the purity of the disc electrode. If it darkens, turn it to the unburned area.

4. Save the spectrum.

5. Use the software to determine the wavelengths. Use the known copper line as a reference line.

It is necessary to know dispersion, wavelength and number of a pixel of the reference line in order to identify the unknown lines. Calculate their values in SL-13 software which automatically calculates the wavelengths of other lines of the spectrum.

6. Write down the values of the wavelengths for these lines. Identify the elements using the tables [6].

7. Make a conclusion about the composition of the sample.

LABORATORY WORK 2

STUDYING THE SPECTROSCOPY DATABASES. MODELLING CH₄ GAS-ANALYSER IN EXHALED AIR

Objectives. To study in practice the IR gas absorption spectra; to model the absorption spectrum by means of the computer information system.

Methodological instructions. Modelling of the IR absorption spectra is carried out by means of specially developed information system Atmospheric spectroscopy "SPECTRA" designed for the Internet access to the information about parameters of spectral lines of atmospheric gases and small impurities required for solving the problems of optics of atmosphere, modelling and imaging the molecular absorption spectra.

The database of the system relies on commonly distributed data banks HITRAN and GEISA. In general, they cover relatively well-studied IR region of the spectrum and encompass a wide spectral range from microwave to ultraviolet. Besides these databases, fundamental information about properties of molecules and other databases are used.

Modelling of spectra is based on the methods of line-by-line counting of the absorption spectrum of substances in gas phase, which is a sum of standard absorption profiles of isolated lines. When modelling high-resolution spectra, data sampling is carried out in the *given frequency range* for a *gas mixture* chosen or proposed by user. To perform the simulation of the spectrum observed in devices of lower resolution, the laboratory provides an opportunity to make a convolution of high-resolution spectra with the instrumental function of device.

TASKS

Registration in the information system. Using the URL address <http://spectra.iao.ru> enter the information system for modelling the IR absorption spectra. Register in the system using your personal information.

I. Study SPECTRA software

1.1 Obtain the atmospheric spectrum (Diagram of intensities)

Perform operations by means of Menu of the information system:

Operation	Range
a. Separate molecules	
b. Natural scale	
c. Logarithmic scale	
d. Change the range of wavenumbers	1000...10000 cm ⁻¹
e. Change the interval of wavenumbers	10...2000 cm ⁻¹
f. Change minimal intensity of lines	10-20...10 ⁻²⁸ cm ² /mol
g. Change temperature of mixture	(77K...2000K)

1.2 Obtain the atmosphere transmission spectrum in the narrow spectral range

Perform operations by means of Menu of the information system:

Operation	Range
a. Change the shape of spectral line profile	Lorentzian, Doppler
b. Change the instrumental function of spectrometer	Triangle, Gaussian
c. Change the wing	
d. Minimal intensities of lines	10...50 cm ⁻¹
e. Spectral range	10 ⁻²³ (cm ² /mol) 2000 -5000 cm ⁻¹

II. Selection of spectral lines for controlling CO₂ in atmosphere

1. Make gas mixture (CO₂ – 100%). Obtain Diagram of intensities of CO₂.
2. Select the part of a strong band.
3. Obtain CO₂ transmission spectrum at changing temperature (77K ...2000K).
4. Obtain CO₂ transmission spectrum at changing path length (1 mm, 1 cm, 1 m, 1 km).
5. Obtain CO₂ transmission spectrum at changing pressure (0.1, 1, 20 atm).
6. Obtain CO₂ transmission spectrum at changing spectral resolution (0.01, 1, 30 cm⁻¹).
7. Select lines promising for development of gas-analyser for concentration of 300 ppm (0.03% in atmosphere)

Parameters of spectrometer	Range
a. spectral resolution	0.1 cm ⁻¹
b. pressure	1 atm
c. temperature	293K
d. transmission	10-90%,
e. reasonable path length	1-100 m

8. Make atmospheric gas mixture (N₂, O₂, CO₂, H₂O – 1%, CH₄- 0.0001%). Standard atmosphere of the Institute of Atmospheric Optics or the USA included into the database can be used.
Obtain the transmission spectrum of the modelled atmosphere in the region of selected lines.
9. Make final selection of measuring lines.
The main selection criterion – CO₂ lines must be strong enough in comparison with the absorption by other lines of atmospheric air and must not overlap with lines of atmospheric air.
10. Describe and explain the results.

III. Modelling of CH₄ gas-analyser in atmosphere

1. Make gas mixture (CH₄ – 100%). Obtain Diagram of intensities of CH₄.
Select the part of a strong band.
2. Select lines promising for development of gas-analyser.
for concentration of 1 ppm (0.000001 parts in atmosphere)
(Parameters of spectrometer: Spectral resolution - 0.1 cm⁻¹, pressure – 1 atm, transmission – 10-90%, reasonable path length – 1-100 m).
3. Make atmospheric gas mixture (N₂, O₂, CO₂, H₂O – 1%, CH₄- 0.0001%). Standard atmosphere of the Institute of Atmospheric Optics or the USA included into the database can be used.
Obtain transmission spectrum of the modelled atmosphere in the region of selected lines.
4. Select parts.
Make final selection of measuring lines.
The main selection criterion – CH₄ lines must be strong enough in comparison with the absorption by other lines of atmospheric air and must not overlap with lines of atmospheric air.
5. Make optimal selection of parameters of spectrometer (p. III.2) at their variations.
6. Describe and explain the results.

LABORATORY WORK 3

STUDYING WATER ABSORPTION SPECTRA IN NANOPORES

Objectives. To study in practice a Fourier transform spectrometer; to register the IR absorption spectra of liquid water and water in nano-sized pores.

Methodological instructions. Experimental scheme (Fig. 3.1) is used in the work. Source radiation focuses in a working volume of the cell, after that it enters the operating part of spectrometer. The cell is connected with the vacuum post and thermoregulation unit of the studied sample. The Fourier transform spectrometer FT-801 is designed for obtaining the IR spectra of substances within the range of $550 \dots 10000 \text{ cm}^{-1}$ with spectral resolution up to 0.5 cm^{-1} .

According to the principle of operation, FT-801 belongs to the class of modulating spectral devices where splitting of the studied radiation into spectral constituents is carried out by special modulation of the radiation flow with an optical movable element and further electro-magnetic processing of the signal of detector recording the interferogram.

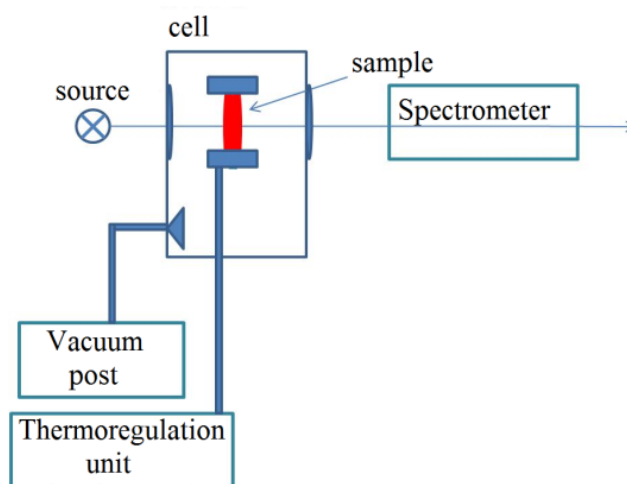


Figure 3.1. Bloch-scheme of the experimental equipment

Interferogram is recorded as a final number of values of the signal taken from photodetector and transformed by the analog-digital transducer into digital code. During further transmission of the code into PC the inverse Fourier transform occurs. Recorded signal is visualised by means of Zair software.

The recorded signal represents the intensity of the light passed through the absorbing path and containing optical system and studied sample itself. According to the Beer–Lambert–Bouguer law, the intensity is expressed by:

$$I = I_0 e^{-\tau}, \quad (3.1)$$

where I_0 – source radiation intensity, I – intensity registered by detector, τ – optical depth. Since optical depth includes both studied sample and air environment inside the device, registration of the absorption spectrum of a sample requires preliminary registration of the absorption spectrum of the background.

Procedure

1. Study experimental equipment.
2. Model the absorption spectrum of water monomer with spectral resolution of 10 cm^{-1} using the SPECTRA software
3. Register spectrum of the background signal.
4. Register spectrum of liquid water with spectral resolution of 10 cm^{-1} .
5. Register spectrum of water placed in nanopores with spectral resolution of 10 cm^{-1} .
6. Study the environment of digital data processing “Origin”.
7. Process obtained absorption spectra. Define principal parameters of the absorption spectrum. Decompose the absorption spectrum into constituent modes.
8. Compare absorption spectra of water monomer, liquid water and water in nanopores. Interpret their difference.

LABORATORY WORK 4

DETERMINATION OF CHARACTERISTICS OF THE ELECTRONIC BANDS OF ABSORPTION AND ELECTRONIC STATES AS EXEMPLIFIED FOR AMINO-ACID RESIDUES CONTAINED IN PROTEINS (PHENYLALANINE, TRYPTOPHAN, TYROSINE)

Objectives:

1. To define the characteristics of the electronic absorption bands for the molecule:
 - a) wavelength and wavenumber at the maximum of the absorption band λ_{\max} , ν_{\max} ;
 - b) decimal molar absorption coefficient ϵ_{\max} ;
 - c) half-width of the band $\Delta\nu_{1/2}$;
 - d) integral intensity of the band;
 - e) power of the oscillator of electronic transition (see (7.2)).
2. To define the characteristics of electronic states:
 - a) type of the state $S_1(\pi, \pi^*)$ or $S_1(n, \pi^*)$;
 - b) lifetime of the excited state $\tau^f = \frac{3.5 \cdot 10^8}{\nu_{if}^2 \int \epsilon_{\nu} d\nu}$.
3. Make a scheme of the energy levels of the molecule in polar and non-polar solvents.

Procedure

1. Measure the absorption spectra of the molecule in offered solvents.
2. Validate the feasibility of the law of light absorption.
3. Define the characteristics of electronic states and electronic transitions of the molecule stated in **Objectives**.

LABORATORY WORK 5

SOLVATOFLUOROCHROMISM OF FLUORESCENT PROBES IN BIOPHYSICS AND MEDICINE

Objectives:

1. To study the role of solvation in forming the absorption spectrum of probes;
2. To study the role of solvation in forming the fluorescence spectra.

Procedure

1. Prepare solutions of the fluorescence probe in solvents of various polarities (proton-donor, inert, base) with the concentrations of the probe about 10 micromoles.
2. Measure the spectra of absorption and fluorescence in selected solvents.
3. Assess the shift of the band of absorption and fluorescence due to universal interactions and hydrogen bond.
4. Study the dependence of position of the fluorescence band on dielectric permeability, parameters of acidity and basicity.

Questions

1. Types of electronic transitions for the probe.
2. Hydrogen bond.
3. Dipole-dipole interactions.
4. Selection of the wavelength of excitation to produce fluorescence spectra.

LABORATORY WORK 6

APPLICATION OF UV AND VISIBLE REGIONS IN THE ANALYSIS OF VITAMINS

Objectives:

1. To check the identity of vitamins of the B group (B6, B12, B1) and vitamin C of different manufacturers;
2. To analyse the mixtures of vitamins B6, B12, B1 using the method of mathematical decomposition of the spectrum of a mixture by the spectra of constituents with known concentrations.

Procedure

1. Prepare solutions of vitamins B6, B12, B1, C of different manufacturers with the concentration about some mmol.
2. Fit the concentration of each vitamin to generate the adsorption spectrum with the optical density within the interval 0.1 – 0.5.
3. Register the absorption spectra of selected solutions.
4. Calculate the decimal molar absorption coefficient for each vitamin of the region and check the identity of vitamins of different manufacturers.
5. Register the absorption spectra of vitamins B6, B12, B1 of definite concentration and their mixtures.
6. Assess the concentration of each vitamin in the mixture using RAZLOG software.

Questions

1. Requirements for the solvents in spectrophotometry.
2. Validation of the law of the light absorption.
3. Evaluation of error in determination of the decimal molar absorption coefficient.

Notes

All the works shall be done using the spectrophotometer CARY 5000, automated spectrophotometer SF-26, equipment for studying the luminescence spectra SDL-2.

Before starting work, study procedures and equipment being used.

LABORATORY WORK 7

FUNDAMENTALS OF THE QUALITATIVE ANALYSIS BY MEANS OF RAMAN SPECTROSCOPY

Description of experimental equipment for recording Raman spectra

Typical equipment for recording Raman spectra is presented in Figure L7.1. Excitation of Raman spectra is caused by the linearly polarised laser radiation (1) with the wavelength $\lambda = 473$ nm. The power of the laser radiation is modified by adjusting the pumping current generated by a power supply unit (2). With the help of a rotary prism (3), the laser beam is directed through the analyte contained in the cell (4) parallel to the input slit of the monochromator. Observation of the scattered light is held perpendicularly to the distribution of the laser radiation and the vibration of its electric vector (90°-geometry). The scattered light is collected and focused by the lens (5) on the input slit of a monochromator (6). Registration of the scattered light is realised by the PEM (7) operating in the mode of counting individual photons. Setting of the equipment and processing of the information are made with computer (8) with special software. The results of measurements are displayed on the screen (9).

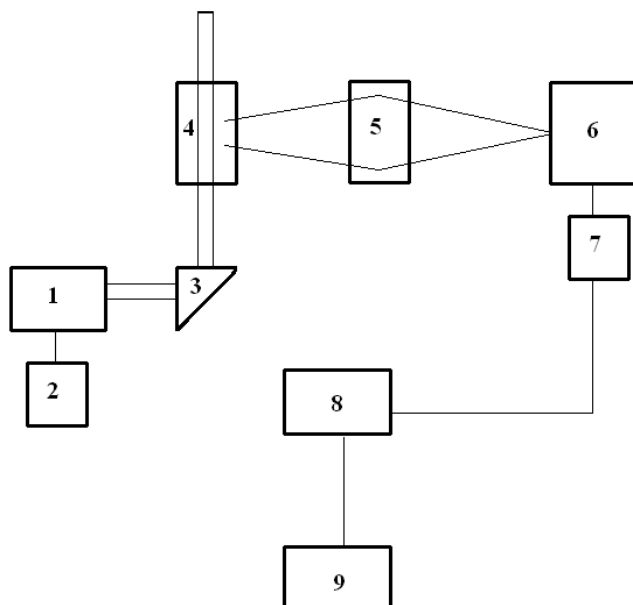


Figure L7.1. Scheme of a laboratory modification of Raman spectrometer

It should be noted that by its characteristics the above configuration of the equipment belongs to the category of Raman spectrometers having high-sensitivity at relatively low spectral resolution.

Objectives:

1. To master the methodology of recording the Raman spectra
2. To understand the methodology of the qualitative analysis by the Raman spectrum.

Procedure

Study the experimental equipment and make adjustment.

1. Since the software permits defining the boundaries of scanning of monochromator in nm, calculate the required spectral range for recording the frequency shifts from -1000 cm^{-1} to 1000 cm^{-1} . Take into account that the wavelength of the laser is $\lambda = 473 \text{ nm}$ and it represents the frequency shift of 0 cm^{-1} .

2. Receive two cells with unknown liquids from the lecturer and record their Raman spectra.
3. Using the generated spectra identify which cell contained CCl_4 . To do it, use a well-known fact that CCl_4 has in its Raman spectrum four characteristic vibrational bands with the frequency shifts: 218 cm^{-1} , 314 cm^{-1} , 459 cm^{-1} , 762 cm^{-1} .
4. Determine the temperature of CCl_4 using relation 10.24.

Questions

1. Identify Stokes lines, anti-Stokes lines and Rayleigh line in the Raman spectrum of CCl_4 .
2. Explain the distribution of intensities of the fundamental vibrational bands in the Stokes and the anti-Stokes parts of the Raman spectrum in the CCl_4 molecule.
3. Which factors define inaccuracies in temperature determination?

LABORATORY WORK 8

FUNDAMENTALS OF THE QUALITATIVE ANALYSIS BY MEANS OF RAMAN SPECTROSCOPY

Objectives: to master the methodology of the qualitative analysis of liquid or gaseous media by means of Raman spectroscopy using the decomposition by basis spectra.

Methodological instructions

Qualitative analysis of a substance by its Raman spectrum can be made by using the tables with relative differential cross-sections of the scattering of individual molecules. However, using this method requires that bands (with known cross-sections of the scattering) of individual components in the Raman spectrum are not overlapped. It is worth taking into account the spectral sensitivity of the equipment as well.

When there is a significant overlapping of the spectra of components of a mixture and, at the same time, there is an opportunity to obtain them in their pure form, it is reasonable to use the method of mathematical decomposition of the registered spectrum of the mixture by the spectra of individual components.

Imagine that there are l substances for which the Raman spectra have been obtained. Each spectrum is a set of points (values of the intensity) at given wavelengths: $I_1(\lambda_1), I_2(\lambda_2), \dots, I_n(\lambda_n)$. Studying the Raman spectrum of the mixture of substances, let us assume, that the principle of superposition is satisfied for the mixture:

$$I(\lambda) = \sum_{i=1}^l k_i I_i(\lambda), \quad (1)$$

where $I(\lambda)$ – Raman spectrum of the mixture, $I_i(\lambda)$ – spectrum of i -th component, k_i – contribution of i -th component to the mixture. Taking into account that $I_i(\lambda)$ represents the sets of readings on various wavelengths, re-write (1) as a system of equations:

$$I(\lambda_m) = \sum_{i=1}^l k_i I_i(\lambda_m), m = 1, \dots, n. \quad (2)$$

The system can be solved, if $l = n$ (n – number of points in each spectrum). However, in practice, $n \gg l$, i.e. the number of experimental points significantly exceeds the number of analysed components. In such a case, system (2) is indefinite and its solution can be easily found using the least squares method.

It must be noted that the method is applicable only when components do not enter into chemical reactions, since it leads to changes in the Raman spectrum of the mixture.

Procedure

Study the experimental equipment and make adjustment.

1. Since the software permits defining the boundaries of scanning of monochromator in nm, calculate the required spectral range for recording the frequency shifts from -100 cm^{-1} to 3500 cm^{-1} . Take into account that the wavelength of the laser is $\lambda = 473 \text{ nm}$ and it represents the frequency shift 0 cm^{-1} .
2. Register and save in the PC memory the Raman spectra of pure acetone, ethyl acetate and 1,4-dioxane.
3. Receive a mixture of components from the lecturer and register its Raman spectrum.
4. Using Origin software, subtract the Raman spectra of individual components from the Raman spectrum of the mixture and determine coefficients k_1, k_2, k_3 , if

$$I_{\text{mix}}(\lambda) - k_1 I_{\text{acetone}}(\lambda) - k_2 I_{\text{dioxane}}(\lambda) - k_3 I_{\text{ethylacetate}}(\lambda) = 0.$$

5. Determine the concentration of components in the mixture using the relation

$$N_i = \frac{k_i}{\sum_{i=1}^3 k_i} \cdot 100\%.$$

Questions

1. Explain in which cases it is reasonable to use the method of decomposition into basis spectra in Raman spectroscopy to determine the quantitative content of the analyte. What are the limits of applicability of this method?
2. Suggest, why is it impossible to get a perfect difference spectrum?

References

1. Walter R. Johnson, Lectures on Atomic Physics. – Department of Physics, University of Notre Dame, Notre Dame, U.S.A., 2006. – 262 p.
2. G. Herzberg, Atomic Spectra and Atomic Structure (2nd ed.), New York: Dover Publications, 1944. – 288 p.
3. J. M. Hollas, Modern spectroscopy. – J. Wiley&Sons, Ltd, 2004. – 452 p.
4. Jan Smit, Introduction to Relativistic Quantum Fields. – Institute for Theoretical Physics, University of Amsterdam, The Netherlands, Lecture notes, 2007. – 249 p.
5. J.D. Bjorken and S.D. Drell, I: Relativistic Quantum Mechanics, McGraw Hill, 1964.
6. Zaidel A.N. Tablitsy spectralnykh liniy [Tables of spectral lines] /A.N. Zaidel, V.K. Prokofiev, S.M. Raiskiy, E.Ya. Shreider – M.: Phismatlit, 1962. – 607 p.
7. W. Demtröder, Laser Spectroscopy. Experimental Techniques, 5th ed., Springer, Heidelberg, New York, Dordrecht, London, 2015. – 757 p.
8. Born M., Wolf E. Principles of Optics: Electromagnetic Theory of Propagation, Interference and Diffraction of Light, 7th Edition. - Cambridge University Press, 1999. - 987 p.
9. Bell R.J. Introductory Fourier Transform Spectroscopy. Academic Press, 1972. 382 p.
10. Serdyukov V. I., Sinita L. N., Vasil'chenko S. S. Highly Sensitive Fourier Transform Spectroscopy With Led Sources. J.Mol.Spectrosc. 290, pp.13-17, 2013.
11. Sinita L.N., Lugovskoy A.A. Dynamic registration of the absorption spectrum of water in the SiO₂ nanopores in high frequency range. J.Chem.Phys. 133, 204506(1-5) 2010.
12. Gaidash A.A., Sinita L.N., Babenko O.A., Lugovskoy A.A. Nanoporous structure of bone matrix at osteoporosis from data of atomic force microscopy and IR spectroscopy. Journal of Osteoporosis, 2011, ID 162041, 2011.
13. A. van der Avoird, P.E.S. Wormer, R. Moszynski, From intermolecular potentials to the spectra of van der Waals molecules, and vice versa. Chem. Rev. 94, pp. 1931-1974, 1994.
14. P. E. S. Wormer, A. van der Avoird, Internuclear potentials, internal motions, and spectra of van der Waals and hydrogen-bonded complexes. Chem. Rev. 100, pp. 4109-4143, 2000.
15. G. Chalasin'ski, M. M. Szczes'niak, State of the art and challenges of the ab initio theory of intermolecular interactions. Chem. Rev., 100, N 1, 4227-4252, 2000.
16. K. Müller-Dethlefs and P. Hobza, Noncovalent interactions: a Challenge for experiment and theory. Chem. Rev., 100, N11, 143-167, 2000.
17. Molecular Associations in Biology, B. Pullman, Ed., Academic Press: New York, 1968.
18. A.D. Buckingham, in Intermolecular Interaction: From Diatomic to Biopolymers, edited by B. Pullman (Wiley, New York, 1978), pp. 1-68.
19. S. Kielich, Molekularna Optyka Nieliniowa (Nonlinear Molecular Optics), Naukowe, Warszawa-Poznan, 1977.
20. D. Pugh, Electric multipoles, polarizabilities and hyperpolarizabilities. Chemical Modelling: Applications and Theory, Volume I. The Royal Society of Chemistry, P.1-37, 2000.
21. W. Klemperer and V. Vaida, Molecular complexes in close and far away. Proceedings of the National Academy of Sciences of the United States of America (PNAS), V 103, N 28, p. 10584-10588, 2006.
22. G. Maroulis, Interaction-induced electric properties. Chemical Modelling: Applications and Theory, V.9. Ed. by M. Springborg, The Royal Society of Chemistry, P. 25-60, 2012.
23. J. Stone, The Theory of Intermolecular Forces, Clarendon Press, Oxford, 2002.
24. I.G. Kaplan, Intermolecular Interactions: Physical Picture, Computational Methods and Model Potentials, John Wiley & Sons, Ltd, 2006.
25. Christian Reichardt, Thomas Welton. Solvents and Solvent Effects in Organic Chemistry. John Wiley & Sons., 2011. – 718 p.
26. Nicholas J. Turro. Modern Molecular Chemistry. Columbia University, 1991.
27. James Guillet. Polymer Photophysics and Photochemistry: An Introduction to the Study of Photoprocesses in Macromolecules, Cambridge University Press, 1985. – 391 p.
28. Kamlet M.J., Abboud J.L.M., Abraham M.H., Taft R.W. Linear solvation energy relationships. A comprehensive collection of the solvatochromic parameters, σ^* , α , and β , and some methods for simplifying the generalized solvatochromic equation // J. Org. Chem. – 1983. – V.48, № 17 – P. 2877-2887.
29. Swain C.G., Swain M.S., Powell A.L., Alunni S. Solvent effects on chemical reactivity. Evaluation of anion- and cation-solvation components // J. Am. Chem. Soc. – 1983. – V. 105, № 3 – P. 502-513.
30. Solntsev K.M., Huppert D., Agmon N. Solvatochromism π -naphthol // J. Phys. Chem. A. – 1998. – V. 102, № 46. – P. 9599-9606.
31. Lakowicz J.R. Principles of fluorescence spectroscopy. – New York: 2nd ed. 1999. – 698 p.
32. Nad S., Pal H. Unusual Photophysical Properties of Coumarin-151 // J. Phys. Chem. A. – 2001. – V. 105, № 7. – P. 1097-1106.

33. .Y.Y. Akhadov. Dielectric Properties of Binary Solutions: A Data Handbook. – Pergamon Press Ltd. , Headington Hill Hall, Oxford OX 3 OBW, England, 1981.
34. Morimoto A., Yatsuhashi T., Shimada T. et al., Radiationless Deactivation of an Intramolecular Charge Transfer Excited State through Hydrogen Bonding: Effect of Molecular Structure and Hard-Soft Anionic Character in the Excited State // J. Phys. Chem. A. 2001. – V. 105, № 45. – P. 10488-10496.
35. Bakhshiev N.G., Kiselev M.V. Selective Nonspecific Solvation Under Dielectric Saturation and Fluorescence Spectra of Dye Solutions in Binary Solvents // J. Fluorescence. – 1991. – V. 1, № 3. – P. 177-182.
36. N. G. Bakhshiev, Yu. G. Siretskii, and M. B. Kiselev, Primary Transsolvation of Excited Molecules and Fluorescence Spectra of Dye Solutions in Binary Solvents // Russian Journal of Physical Chemistry A. – 1996. Vol. 70, No. 9. – P. 1497.
37. Yatsuhashi T., Inoue H. Molecular mechanism of radiationless deactivation of aminoanthraquinones through intermolecular hydrogen-bonding interaction with alcohols and hydroperoxides // J. Phys. Chem. A. – 1997. – V. 101, № 41. – P. 8166-8173.
38. George C. Pimentel, A.L. McClellan, Hydrogen bonds. Francisco and London, Publisher W. H. Freeman And Company, 1960 (<https://archive.org/details/hydrogenbond031051mbp>).
39. Short H-bonds and spontaneous self-dissociation in (H₂O)₂₀: Effects of H-bond topology / Kuo J., Ciobanu C. V., Ojamae L. and oth. // J. Chem. Phys. – 2003. – V. 118, № 8. – P. 3583-3588.
40. Karyakin A.V. n-electrons of heteroatoms in the hydrogen bond and luminescence. – M.: Nauka, 1985. – 136 p. (in Russian).
41. Helm R. M., Clara M., Grebner Th. L., Neusser H. J. Hydrogen bonding in the indol – water complex: a high resolution UV study of the Hydrogen donor conformer // J. Phys. Chem. A. – 1998. – V. 102, № 23. – P. 3268-3272.
42. Terenin, A.N. Photonics of Dye Molecules and Related Organic Compounds, Nauka, Leningrad (in Russian), 1967.
43. Molecular interactions, Том 3. Ed. by H. Ratajczak, W. J. Orville-Thomas, J. Wiley, 1982. – 584 p.
44. W. Schmidt, Optical spectroscopy in chemistry and life science. Wiley-VCH Verlag, 2005.
45. Y. Bekker, Spectroscopie. Instrumentelle analytische mit atom und molekülspektrometrie. Vogel Buchverlag, 1997.
46. H.-D. Holtje, W. Sippl, D. Rognan, G. Folkers. Molecular modeling. Basic principles and applications. Wiley-VCH Verlag, 2008.
47. I. Tinoco, K. Sauer, J.C. Wang, J.D. Puglisi. Physical Chemistry. Principles and applications in biological sciences. Prentice Hall, New Jersey, 2002.
48. Weber A. *Raman Spectroscopy of Gases and Liquids*. Springer: Berlin. 1979. 320 p.
49. McCreery R.L. *Raman spectroscopy for chemical analysis*. Wiley. 2000. 437 p.
50. Ferraro J.R., Nakamoto K., Brown C.W. *Introductory Raman spectroscopy*. Elsevier. 2003. 435 p.
51. Lewis I.R., Edwards H.G.M. *Handbook of Raman spectroscopy*. From research laboratory to the process line. Marcel Dekker. 2001. 1049 p.
52. Smith E., Dent G., Modern Raman Spectroscopy – A Practical Approach. – John Wiley & Sons Ltd, 2005. – 225 p.
53. McCreery R.L, Raman Spectroscopy for Chemical Analysis. – A JOHN WILEY & SONS, INC., PUBLICATION, New York - Chichester - Weinheim - Brisbane - Singapore - Toronto, 2000. – 437 p.

Отпечатано на участке оперативной полиграфии
Издательского Дома Томского государственного университета

Заказ № 1919 от «16» июня 2016 г. Тираж 8 экз.